Indoor optical network technologies for multiple services provisioning

Forni, F.

Published: 26/06/2018

Document Version
Publisher's PDF, also known as Version of Record (includes final page, issue and volume numbers)

Indoor Optical Network Technologies for Multiple Services Provisioning

PROEFSCHRIFT

ter verkrijging van de graad van doctor aan de
Technische Universiteit Eindhoven, op gezag van de
rector magnificus, prof.dr.ir. F.P.T. Baaijens, voor een
commissie aangewezen door het College voor
Promoties in het openbaar te verdedigen
op dinsdag 26 juni 2018 om 16.00 uur

door

Federico Forni

geboren te Bologna, Italië

Dit proefschrift is goedgekeurd door de promotoren en de samenstelling van de promotiecommissie is als volgt:

Voorzitter:	prof.dr.ir. J.H. Blom
Promotor:	prof.ir. A.M.J. Koonen
Co-promotor:	dr.ir. E. Tangdiongga
	N.C. Tran PhD (Genexis BV)
Leden:	dr. G. Tartarini (Università di Bologna)
	prof.dr. B. Ortega Tamarit (Universidad Politècnica de València)
	prof.dr.ir. S.M. Heemstra - de Groot
	prof.dr. M. Matters - Kammerer

Het onderzoek of ontwerp dat in dit proefschrift wordt beschreven is uitgevoerd in overeenstemming met de TU/e Gedragscode Wetenschapsbeoefening.

A catalogue record is available from the Eindhoven University of Technology Library.

ISBN: 978-90-386-4537-7
NUR: 959
Title: Indoor Optical Network Technologies for Multiple Services Provisioning
Author: Federico Forni
Eindhoven University of Technology, 2018.

Typeset using LaTeX, printed in the Netherlands.

Success depends on how many
experiments you can fit into 24 hours.

Thomas A. Edison

Summary

Currently, in each house and building there are a multitude of connected devices and a range of separate networks. Moreover, the growth of the indoor data traffic is largely carried by wireless access networks, such as Wi-Fi, mobile networks, and wireless sensor networks (WSNs). Looking to the indoor wireless local area network (WLAN) and WSNs, they typically rely on the residential gateway. The residential gateway provides the connectivity between the outdoor and the in-home network, network routing, network switching, and also the wireless connectivity. The residential gateway is usually located in a sub-optimal position to deliver the wireless connectivity (e.g. inside meter cabinets and utility rooms). This leads to weak received signals and high interference between the wireless devices and networks in densely populated areas.
Together with WLAN and WSN devices, also mobile devices may suffer by the poor indoor coverage, since smartphones and tablets located indoor still may rely on the outdoor macrocells.
In all the cases, the penetration through walls and windows attenuates the radio signals, which may result in poor coverage and low throughput. The wireless networks can take advantage from multi radio access technology (M-RAT), for which the connectivity is provided by both mobile networks and WLANs, and from the spatial densification. The spatial densification is defined as the deployment of various types of nodes (i.e. macrocell, microcell, picocell, and femtocell), which are equipped with different transmission powers and data processing capabilities. The macrocell architecture based on high power outdoor base stations is the fundamental layer providing the coverage over large areas. Wherever higher capacity or improved coverage is needed (such as outdoor urban areas, malls, and stadiums), microcells are installed. For a home area network, the microcell indoor deployment is unsuitable with the low-cost requirement because they are

installed by operators. Instead, particularly interesting for in-home deployment is the picocell/femtocell node, which is defined as a low-power, indoor deployed, small range (i.e. few tens of meter), and low-cost base station. The femtocell is able to convert the data provided by the mobile core network into the radio signal. The femtocell is co-located with the residential gateway, hence the baseband signal processing and most of the radio signal processing are centralized. The radio signal filters, amplifiers and antenna of the femtocell are remotely deployed in the radio resource unit (RRU) in each room and connected through a point-to-point distributed antenna system (DAS). Thus, the RRU antenna is able to cover an entire room and is brought closer to the user devices. The deployment of a single network that is able to support wireline, mobile, WLAN, and WSN services (i.e. network convergence) reduces installation and operational costs and is easy to upgrade to future services and applications. Different media have been studied for the single backbone network, both wireless (i.e. mm-wave or free-space optical based) and wired (i.e. based on copper cables or on silica optical fibers) backbones have been proposed. However, these solutions can have major problems if applied for in-home networks. For instance, the mm-wave wireless propagation through the walls limits its indoor coverage. Moving to the wired backbone solutions, none of them is completely satisfactory from installation cost (glass optical fiber) and complexity of the remote unit (Cat 5 cable) perspectives. In particular, the widely available Cat 5 links have a limited bandwidth, which makes the transmission of multiband radio signal less practical. Hence, the data are transmitted by digital baseband signal over the Cat 5 link and modulated on the radio signal at the remote units. Thus, part of the signal processing is moved from the centralized residential gateway to the remote units, which increases their complexity.

Creating this network convergence scenario by allocating all the wireless and the wired services in a single network composed of low-cost links is the target of this research. Plastic optical fiber (POF) is a prominent option to achieve the network convergence. The visible light transmission by POF makes easier the troubleshooting of faulty links as faults can be detected by human eye. Furthermore, the connectorless technology and the large core diameter make the deployment easier. Thus, for these reasons POF links can be installed by not-skilled persons (do-it-yourself technology) and potentially decrease the installation cost. POF can bring the multi-standard (i.e. LTE-A, WLAN, and WSN) radio signals to each RRU, by acting as an optical backbone for both wired (e.g. Ethernet protocol) and wireless-based in-home services with the additional advantage of POF's do-

it-yourself technology. POF has been studied for many years, its application for in-home gigabit/s transmission based on 16-PAM coding scheme has reached the standardization and commercialization stages.

In this thesis, firstly the POF link for wired service delivery is designed by exploring different types of POF transceivers. In particular, two POF links are studied, the first is based on a 680 nm wavelength 0.8 dBm emitted power VCSEL and p-i-n photodiode receiver. This has limited reach and bandwidth (340 MHz) due to the low emitted optical power of the VCSEL and the limited bandwidth of the optical receiver, respectively. The second POF link has a bandwidth of 1.16 GHz and higher launched power, which is achieved by using a broadband p-i-n photodiode and Fabry-Pérot edge emitting laser diode (EE-LD) with 5.7 dBm of emitted power at a wavelength of 650 nm. Different modulation formats, such as NRZ, 4-PAM, CAP, and DMT, were considered. Thus, 4-PAM was chosen as a suitable trade-off between complexity and spectral efficiency to deliver a gigabit/s throughput. This thesis work resulted in a baseband throughput up to 2 Gb/s over 50 m PMMA 1 mm core diameter GI-POF using the EE-LD transmitter and the broadband p-i-n optical receiver.

Secondly, a radio-over-POF transmission system is designed, which also carries the services for wired delivery. A frequency division multiplexing (FDM) scheme combining the baseband and bandpass radio signals spectrum is proposed. While awaiting 5G radio access network specifications, a 64-QAM OFDM LTE-A compliant signal was used. The design focused on transmitting the 4G bands in the frequency spectrum between 700 and 1800 MHz without frequency down shifting. The GI-POF link based on the EE-LD and broadband p-i-n photodiode has a bandwidth of 1.16 GHz, therefore, a pre-equalization technique is necessary. The pre-equalization is realized by amplifying each LTE-A band by a digital amplifier having a gain that is equal to the frequency response of the POF link in that LTE-A band, before being combined with the remaining LTE-A bands. Hence, the low-pass behavior of the POF link is balanced (i.e. equalized) and the LTE-A bands have the same EVM at the POF link output. The gains training can be performed during the set up time of the link due to the time-invariant frequency response of the POF link. Each gain is trained on the received error vector magnitude (EVM) calculated at the RRU. The EVM values can be sent from the RRU to the residential gateway, where the pre-equalization is performed, once the bidirectional link is established. Thus, up to ten LTE-A bands with 64-QAM coding were transmitted with good performance (i.e. EVM lower than the defined thresh-

old equal to 8%). Moreover, after the optical transmission, the radio signals are filtered to remove the baseband signal, amplified, and wirelessly transmitted over another 12 m. The wireless transmission is performed in a Faraday cage by using 3 dBi gain antennas and the radio signal emitted power is up to 6 dBm. The gain of the amplifiers of the pre-equalizer are initially trained on the received LTE-A EVM, which require the full decoding of each LTE signal in the RRU. Instead, the pre-equalizer is trained on the receiver signal-to-interference-plus-noise ratio (SINR), which does not require the calculation of the EVM and simplifies the RRU architecture. Furthermore, the transmission of a 1.7 Gb/s 4-PAM baseband signal and 7 LTE-A bands between 700 MHz and 1 GHz over 35 m SI-POF is demonstrated. The real-time bidirectional transmission of a live LTE signal over GI-POF and then wirelessly to a mobile device was realized as proof-of-concept of the proposed scheme.

Thirdly, the offline generated WLAN and WSN signals were transmitted with up to 9 LTE-A bands, and a baseband 4-PAM signal over the 50 m GI-POF unidirectional link based on EE-LD and broadband p-i-n photodiode. The first challenge was to accommodate the signal carrier frequency at 2.4 GHz, which is more than twice the link's bandwidth, without frequency-shifting in order to simplify the architecture of the RRU. The second challenge was to mitigate the intermodulation distortion between the baseband and wireless signals. The non-linearity distortion impact on the WLAN and WSN signals is reduced by clipping the LTE-A signal and reducing the peak-to-average power ratio (PAPR) of 6 dB. Thus, the total peak power to the POF transmitter is reduced, and the signal reception is improved. With marginal reduction in the baseband bitrate, the 64-QAM 4G bands from 700 to 1500 MHz, the QPSK WLAN, and OQPSK WSN signals located in the 2.4 GHz ISM band were correctly received with an EVM below the 8%, 22%, and 35% threshold, respectively. 600 Mb/s and 45 Mb/s data rates for the LTE-A and WLAN signals were achieved over the unidirectional link.

In conclusion, the 50 m GI-POF link successfully demonstrated the transmission of all the 4 standards with limited signal quality degradation, plus transmission of the radio signals over a 12 m wireless link. The 50 m POF length well suits the requirement for in-home DAS systems. Longer GI-POF link lengths can be achieved by increasing the optical power budget through high-power optical transmitter. Meanwhile, longer SI-POF link lengths will be at the expenses of a lower 4-PAM bitrate and decreased number of LTE-A bands due to the limited bandwidth-distance product (i.e 40 and 150 MHz·km for SI and GI POF,

respectively). Results presented in this work, including the system concepts and the network designs, underline the increasing importance and practicality of POF for satisfying the increasing bandwidth demand of in-home and in-building networks. Hence, the increased capacity offered by optical access networks can be made available to wired and wireless devices inside buildings and houses.

This work was done in close cooperation with Genexis B.V., within the FlexCom project funded by the Netherlands Organisation for Scientific Research (NWO) through grant 13530.

Contents

Summary **i**

1 Introduction **1**
1.1 Fiber-based distributed antenna system 3
1.2 Scope of the thesis 5

2 State of the art **9**
2.1 5G challenges and demands for in-home users 10
2.2 Radio over optical fiber transmission 12
2.3 Plastic optical fibers 15
2.4 In-home network needs: a user's perspective 19
2.5 Next generation in-home network 27
2.6 Summary 30

3 Simultaneous transmission of baseband and 4G mobile signals **33**
3.1 OFDM coding and LTE/LTE-A waveforms 34
3.2 Study and characterization of a VCSEL-based GI-POF link 44
3.3 Early multi-format transmission 47
3.4 Baseband signal filtering and LTE signal pre-equalization 52
3.5 Optical link budget and bandwidth improvement 59
3.6 Optical and wireless transmission 64
3.7 Study and characterization of the 50 m GI-POF link 68
3.8 Improved pre-equalization tuning based on the received SINR . . . 71
3.9 Summary 76

4 Live 4G transmission over POF **79**
4.1 Experimental setup 79
4.2 Experimental results 83
4.3 Summary 85

5 Network convergence of services over POF **89**
5.1 Link nonlinearity analysis 90
5.2 GI-POF link dynamic range characterization 94
5.3 WLAN IEEE 802.11ac simultaneous transmission 98
5.4 WLAN IEEE 802.11n simultaneous transmission 108
5.5 Multiband WSN transmission over the POF link 122
5.6 Summary 128

6 Conclusions and outlook **131**
6.1 Conclusions 131
6.2 Outlook 134

Bibliography **137**

Acknowledgments **157**

Chapter 1

Introduction

In current home area networks (HANs) many services are used in everyday life, such as broadband Internet, telephony, TV, and smart home applications (e.g. remotely controlled light, climate, and curtains). Each of these services is characterized by very different technical requirements. Some need a wired or a wireless broadband connection, some others need a wireless, low-power, low-throughput massive machine-to-machine (M2M) connection. The current approach of in-home networks is based on deploying multiple links, one for each service, and optimizing it for that specific purpose. This leads to high capital expenditure (CapEx) and operational expenditure (OpEx), due to the higher installation and management cost of the different links [1].

Among all the in-home networks, the broadband wireless networks are transporting an increasing amount of data traffic. According to Cisco, in 2016 tablets and smartphones connected wirelessly to mobile network and wireless local area network (WLAN) generated 24% of the total Internet traffic [2]. In 2021, they will double their part reaching almost 50%, most of it indoor, where poor signal reception (e.g. interference and spectrum congestion) is a common problem [3]. The wireless broadband in-home coverage can be divided between mobile networks and WLANs, in both cases there are major challenges to improve the connectivity. In the first case, mobile operators fail to provide the quality of service required for in-home users to 45% of their clients [4]. The indoor coverage has been seen as secondary priority and it is provided by the outdoor macrocells. As a result, the penetration through walls and windows attenuates the signal, which leads

to poor cell-edge indoor coverage and low throughput. In addition, the increasing awareness on energy-efficient construction techniques and materials led to a better thermal insulation of houses. This led to the side effect of a stronger electromagnetic shielding, resulting in even worsened indoor signal reception. Furthermore, in residential areas, this also translates in capacity issues, due to the high number of users connected to the same macrocell.

Furthermore, mobile networks are not the only ones suffering from a poor indoor coverage, the WLANs are also facing coverage and throughput problems. In-home WLAN generally is based on a single access point (AP), which convert the digital baseband signal in the radio signal and it is integrated in the residential gateway. This is located most of the times in a sub-optimal position (e.g. in meter cabinets and utility rooms) to deliver the wireless signal. This often leads to weak received signals and interference when multiple devices share the same spectrum, which typically happens in highly populated areas (i.e. residential areas) [5]. According to Nokia, WLAN connectivity is a major concern for the operators. It is the most common reason for customer support calls to the Internet service providers, which might require the on-site assistance of a technician, resulting in costs of millions of dollars per year for a single provider [6].

Together with smartphones and tablets, wireless sensor devices are becoming very popular for smart home applications and Internet of Things (IoT). Additionally, in few years the majority of the network devices will be battery-powered wireless sensors. Wireless sensor networks (WSNs) are based on M2M communication, which defines the use of wireless sensors, actuators, physical objects and other devices that are not directly operated by humans. The use cases for M2M communication involve a wide range of areas, such as automation of buildings and homes (e.g. lighting, heating, ventilation, and energy consumption control). These wireless sensors are low-cost and low-energy devices with small size data payload and sporadic communications. In-home WSNs are based on a single gateway collecting the information from the nodes and providing the connectivity to the residential gateway. WSN nodes are generally battery powered and therefore must minimize the energy consumption in order to increase the node lifetime. Most of the energy is consumed for transmission and reception operations, different network topologies are proposed to limit the power consumption and extend the coverage, such as multi-hop transmission. This leads to higher level of interference between the nodes, which requires the data re-transmission and increases the power consumption [7]. Furthermore, different WSN standards operate in the

2.4 GHz industrial, scientific and medical (ISM) band, shared with WLAN standard and other services, further increasing the interference and hampering the WSN transmission [8].

1.1 Fiber-based distributed antenna system

To improve the indoor throughput of the mobile networks and WLANs and the coverage of the WSNs, different technologies are proposed. Firstly, the indoor coverage and capacity of the mobile network can take advantage from the spatial densification. The spatial densification is defined as the deployment of various types of nodes (i.e. macrocell, microcell, picocell, and femtocell). The macrocell architecture based on high power outdoor base stations is the fundamental layer providing the coverage over large areas. Wherever higher capacity or improved coverage is needed (such as outdoor urban areas and densely crowded buildings), microcells and picocells are installed. For HAN, the microcell and picocell indoor deployment is unsuitable with the low-cost requirement because they are installed by operators. Instead, particularly interesting for in-home deployment is the femtocell node, which is defined as a low-power, indoor deployed, small range (i.e. few tens of meter), and low-cost base station. The femtocell transceiver is co-located with the residential gateway and its filters, amplifiers, and antennas are remotely located in the radio resource unit (RRU). The RRUs are deployed in each room through a point-to-point distributed antenna system (DAS), closer to the user devices. Secondly, in order to improve the WLAN coverage a multi-AP topology, with an AP per room, provides the connectivity to the user for better coverage and higher signal strength. The shorter wireless distance between the AP antenna and the mobile device allows decreasing the transmitted power and therefore the interference on the neighboring network is reduced. The DAS technology is beneficial also to extend the WSN device lifetime by bringing the WSN gateway antenna in each room. In this way, the transmitted power of the nodes is reduced and the number of devices involved in the multi-hop transmission is decreased. Ultimately, the probability of packet collision and re-transmission are lowered, increasing the battery-powered device lifetime.

The remote units deployed in large numbers inside the houses must be low-cost in order to decrease the overall network price. Hence, the centralization in the residential gateway of the WLAN and mobile network signal processing is desirable to decrease the remote unit complexity. In this way, the radio signal is

generated at a central location and delivered to each remote unit. Consequently, a wired backbone medium being able to support the DAS network for all the wireless services and the remaining wired applications must be found. Most of the DAS configurations are based on unshielded twisted pair cables, coaxial cables, and silica optical fibers. The unshielded twisted pair cables suffer from the narrow band, which makes them unsuitable to transmit the multiband radio signal. Hence, the data are transmitted by digital baseband signals and converted to the radio signal at the RRU, which increases its complexity. Looking to the coaxial cables, they can transmit the radio signal, which simplifies the RRU architecture, but they are bulky and lossy. Hence, the optical fibers are preferred due to the broadband capability, the mature radio over fiber (RoF) technologies, and the low-losses, which make them the favored solution for large residential and corporate buildings. This thesis mainly focuses on small residential buildings and detached houses. In these cases, the link lengths are shorter (up to 50 m) and the installation and network management efforts are performed by the building owners, which then require these efforts to be user-friendly and low-cost. The optical fiber link in HAN must have:

- sufficient bandwidth to deliver both wired and wireless services.
- easy coupling and connectorization between the optical fiber and transceivers.
- easy troubleshooting even by not skilled persons.
- centralization in the residential gateway of most of the wireless signal processing.
- high tolerance to fiber bending and deformation during the installation.
- easy network maintenance and upgrading.

Instead, silica optical fibers are less suited due to their high cost of installation and troubleshooting. Plastic optical fibers (POFs) can meet these requirements, bringing the multi-format radio signals to each remote unit by providing an optical backbone for both wired and wireless based in-home services. Furthermore, the visible light transmission over POF makes the troubleshooting of faulty links easier. The connectorless technology and the large core diameter make the deployment easier. Ultimately, these features lead to the possibility of installing the POF network by the end-user itself (i.e. do-it-yourself technology). The thesis focuses

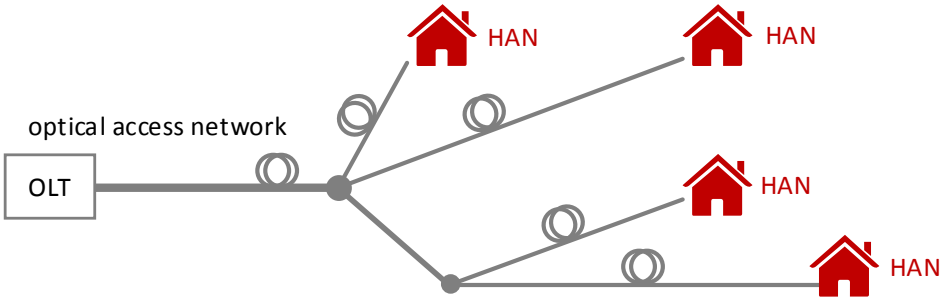

Figure 1.1. Scope of the FlexCom project, in red the scope of this thesis, in gray the scope of the other PhD student [11].

on point-to-point POF link. Point-to-multipoint POF topologies are studied in literature [9], nevertheless advanced optical components such as optical circulator, (de)muxers, and splitters/combiners which are common for silica fibers, are not available for POFs or they are available but too bulky and lossy [10], which limits further studies of these topologies. Furthermore, the current installation of POF in the already deployed electrical ducts prefers point-to-point link.

1.2 Scope of the thesis

The research reported in this thesis has been carried out by the "Flexible Broadband Communication" (FlexCom) project, a part of the research programme NWO-TTW Perspectief MEMPHIS II (Merging Electronics and Micro and nano-Photonics in Integrated Systems), which is partly financed by the Netherlands Organization for Scientific Research (NWO). The research work has been done at the Eindhoven University of Technology and Genexis B.V. The scientific goals of the FlexCom project are the following:

- Improvement of the aggregated throughput in the access network. Fiber-to-the-Home (FTTH) by a passive optical network (PON) is a future-proof solution that can facilitate the projected increase in data rate by end users in a reliable and cost-efficient manner. Current PONs use a single static modulation format throughout the network and matching the signal parameters

to the channel properties is not commonly used in a PON. Adapting modulation and coding to this channel state provides increased capacity in the network. Hence, the use of adaptive modulation in PONs is investigated in FlexCom and is carried out by another PhD student (Robbert van Linden).

- Realization of a single in-home network backbone for wireless and wired services based on large core diameter POF. POF is an emerging short reach transmission technology, which can bring the multi-standard radio signals to each remote antenna unit, by acting as an optical backbone for both wired and wireless-based in-home services. In addition, POFs have the advantage of a do-it-yourself technology, yielding low-cost installation. This POF-based fiber in the home realization forms the core of this thesis work.

The key contributions of this thesis are:

- System demonstration and network design of a multi-service and multistandard POF link for indoor deployment.

- Use of simple baseband format such as pulse amplitude modulation (PAM) and multiband radio signal format, such as long-term evolution (LTE).

- Investigation and realization of a digital signal processing (DSP) algorithm to improve the limited POF link bandwidth. In particular, the POF link bandwidth is stretch by a time-invariant pre-equalization that is able to compensate the POF frequency response in each radio band in order to have the same error vector magnitude (EVM) at the POF link output.

- Inclusion of IoT signals in the POF system.

- Investigation of the POF transceivers nonlinearity and the realization of a DSP method to reduce its impairment on the transmitted radio signals.

- Investigation of the popularity of POF technology compared to other transmission technologies.

- Compared with previous works on POF link for in-home network convergence, here the optical receiver is based on p-i-n photodiodes instead of avalanche photodiode (APD) [12]. Furthermore, 4 level pulse amplitude modulation (4-PAM) coding is chosen instead of discrete multitone (DMT) in order to simplify the baseband transceiver architecture. The analog radio over fiber (A-RoF) technology is extensively used. Thus, the POF link frequency response is stretch by a pre-equalization technique and a technique to reduce the POF transceivers nonlinearity is demonstrated.

The rest of the thesis is organized as follows:

- in chapter 2, a brief overview of the indoor wireless network requirements, RoF and POF technology, and the in-home network constraints are given. The fifth generation mobile network (5G) and WLAN demand an increase of the indoor wireless network throughput, capacity, and coverage. Consequently, the most important 5G use cases for HAN are discussed and the advantages of using DAS are analyzed. Hence, DAS based on optical network RoF transmission is considered and the available technologies are reviewed. Next, the POF system building blocks such as polymer optical fiber, transmitter, and receiver types are explored. A peculiarity of HAN compared with other access networks is the preference to be installed by the end-users. Then, their perspective on the next-generation HAN is analyzed by studying the results of a survey conducted within the FlexCom project. Finally, the main specifications for the HAN, which makes able to accommodate the operators and end-users requirements are defined. Different copper-based and optical fiber-based solutions are compared in terms of broadband and radio signal delivery capabilities and cost perspective and POF emerges as one of the most promising solution.

- In chapter 3, the simultaneous transmission of a baseband 4-PAM signal and a multiband long-term evolution - advanced (LTE-A) signal over a large core Poly(methyl methacrylate) (PMMA) POF link is discussed. Different POF types, optical receivers, and transmitters are studied and characterized in order to identify the most suitable optical link. A frequency division multiplexing (FDM) scheme is demonstrated for simultaneously transmitting a digital baseband and multiband radio signals on the same POF link. A-RoF technique is used to simplify the receiver architecture. Nevertheless, most of

the LTE-A bands have a carrier frequency higher than the optical link bandwidth. Hence, a time-invariant pre-equalization method is demonstrated to stretch the frequency response of the POF link.

- In chapter 4, the transmission of a live LTE signal on a bidirectional 35 m graded index (GI)-POF link and further wireless transmission to a smartphone is discussed. Two different POF links are optimized for the downlink and uplink. Thus, the optical link is interfaced with the core and evolved universal terrestrial radio access (E-UTRA) network emulators. Hence, the transmission of multiple services at the same time toward a mobile device up to 15 m distant is demonstrated.

- In chapter 5, the network convergence is pushed to the simultaneous transmission of WLAN IEEE 802.11n/ac and WSN signals. The WLAN IEEE 802.11ac signal is transmitted with IF over fiber (IFoF) transmission. The intermediate frequency (IF) is optimized in order to minimize the intermodulation distortion, which is discussed in the chapter. Instead, the IEEE 802.11n and WSN are transmitted by A-RoF and a method based on signal clipping is proposed, tested, and discussed in order to mitigate the link nonlinearity. At the same time, the M2M services are accommodated by transmitting a multiband WSN signal and the interference with the WLAN signal is studied.

- Finally, chapter 6 summarizes the main conclusions of the reported work and outlook remarks for the future research activity.

Chapter 2

State of the art

The data traffic generated by wireless access networks is booming and predicted to further increase in the coming years. Currently, in-home wireless connectivity, is facing coverage and capacity problems, which reduce the quality of the experience for mobile and WLAN users. HANs based on different links for each service increase the cost and limit the possibility to upgrade it to match the future challenges given by the growing wireless data traffic.
Lower costs can be achieved by using a single in-home network architecture providing a backbone for all the services (i.e. in-home network convergence). POFs are considered a good candidate as wired backbone for next-generation in-home networks thanks to the do-it-yourself technology.

In the following, section 2.1 discusses the requirements of two of the most important 5G use cases for HAN, such as mobile broadband and massive M2M connectivity. Then, section 2.2 discusses the different technologies used to transmit radio signal over optical links and the most suitable technique to support the DAS is defined. In section 2.3, an overview of the POF technology is given by discussing the POF types, the optical transmitters, and receivers. Currently most of the interest about POF network is focused on the wired signal delivery. Hence, different transmission techniques for digital baseband signal transmission are analyzed and an overview on the digital modulation formats is given. In section 2.4, the results of a survey conducted in order to understand the end-user perspectives on HAN, DAS, and POF are discussed.
In section 2.5, the main specifications for the HAN, which are able to accommodate

the technical and end-users requirements, are defined. Different copper-based and optical fiber-based solutions are compared and POF emerges as one of the most promising solutions.

2.1 5G challenges and demands for in-home users

The upcoming 5G mobile network is expected to serve many use cases, which will deeply affect the indoor networks. In particular, 5G envisions boosting the indoor coverage and throughput together with the support for M2M communications. Here briefly two of the main use cases are analyzed:

Mobile broadband connectivity: 5G is envisioned to achieve data-rate up to 100-fold increase compared with the current 4G network [13]. For this purpose, increased transmission bandwidth, multi radio access technology (M-RAT), spatial densification, and spectral efficient modulation are envisioned as possible solutions to deliver the required performance.
Firstly, the increase of the transmission bandwidth requires exploring bands at higher frequencies, such as mmWave[i] band. According with the international telecommunication union telecommunication standardization sector (ITU-T) regulation, in the 28 GHz and 60 GHz bands there are 900 MHz and 7 GHz of spectrum available, which can provide the needed peak data rate. Nevertheless, together with the peak throughput, the improvement of the average data-rate in all the covered areas is equally important. Hence, an average bit rate between 50 and 100 Mb/s in all the covered areas can be ensured by reducing the black spots. For this purpose, mmWave technology is not a suitable candidate due to the high path loss. Instead, lower frequency between 700 MHz and 6 GHz is a better candidate due to the lower path loss [15]. To achieve a truly broadband connectivity the two aspects (i.e. coverage and capacity) must cooperate, therefore 5G is expected to support flexible spectrum allocation within lower and mmWave frequencies.

Secondly, 5G is envisioned as an architecture able to support multi-connectivity, based on M-RAT. The mobile device will be connected to different radio access technologies through carrier aggregation. It will take advantage also of the existing

[i]The spectrum between 30 GHz and 300 GHz is referred as millimeter wave (mmWave) band, for which the wavelength is between 1 and 10 mm [14], some applications at 28 GHz also refer to mmWave transmission.

RAT, supporting a closer cooperation with the existing 3rd Generation Partnership Project (3GPP) standard (e.g. LTE-A). Furthermore, tighter coordination with non-3GPP standards (e.g. IEEE 802.11) is envisioned. In this way the widely deployed Wi-Fi networks can be used to perform Internet protocol (IP) traffic offloading between the mobile network and WLAN, as already supported by LTE-A [16].

Thirdly, spatial densification by heterogeneous networks also plays an important role in 5G. Heterogeneous network refers to the deployment of various types of nodes (i.e. macrocell, microcell, picocell, and femtocell), which are equipped with different transmission powers, data processing capabilities, and RATs. The macrocell architecture based on high power outdoor base stations with coverage of more than 1 km is in use since 2G and 3G and constitutes the fundamental layer providing the coverage over large areas. Wherever higher capacity or improved coverage is needed (such as outdoor urban areas and densely crowded buildings), microcells and picocells are planned and installed by operators. For HAN, the microcell and picocell indoor deployment is unsuitable with the low-cost and do it yourself requirement of in-home networks. Instead, particularly interesting for in-home deployment is the femtocell node, which is defined as a low-power (i.e. lower than 10 dBm), indoor deployed, small range (i.e. few tens of meter), and low-cost base station. In this case, site planning or coverage studies are not conducted before the deployment. The installation of the femtocells is carried out by the end-user and the femtocell uses the available access network to provide the connectivity to the fronthaul. The first advantage of using femtocells is the increase of throughput, since the smaller radius of the cell is shared among less users (i.e. 2 to 8 users for LTE-A) and the base station is moved closer to the mobile device. Secondly, the macrocell traffic will be offloaded partially or entirely to the femtocell, improving the throughput of the femtocell but also of the macrocell that does not need to allocate the resources for those users connected the femtocell.
Finally, the use of spectral efficient modulation scheme is needed. 5G is envisioned to use different coding scheme for different applications, in this use case the popular orthogonal frequency-division multiplexing (OFDM) is the most suitable.

Massive M2M communication: Historically mobile network standards have targeted broadband service delivery. Given the growing importance of IoT, industry automation, smart home, and smart city technologies, M2M communication is supported since 4G [17,18]. 5G is expected to scale it to massive M2M communi-

cation, which is an evolution of the M2M concept and involves many more sensors. The large number of deployed devices leads to the impracticality or impossibility to recharge their battery, therefore the low-energy requirements is needed to ensure long lifetime, particularly energy-consuming operations should be located on the infrastructure side.

2.2 Radio over optical fiber transmission

The transmission of radio signals over optical fiber links (i.e. RoF) has been studied since the earliest mobile network generations in order to feed the mobile network cells [19]. Since 2000, the RoF technology has been deployed in indoor locations, where augmented capacity and coverage are needed (e.g. sport venues and underground metro stations) [20].
RoF combines the advantage of optical and wireless communications by transmitting the radio signal over the low-loss and electromagnetic interference (EMI) immune optical fiber to the remotely deployed RRU [21]. The generation and transmission of an analog radio signal require few fundamental steps. As shown in Figure 2.1a, the digital data is precoded and processed in the digital domain by the baseband transmitter. Then, the bits are coded in the analog radio waveform according with the chosen modulation and shifted to the carrier frequency f_c by the radio frequency (RF) transmitter. Then the signal is further processed (e.g. filtering and amplifying) and then wirelessly transmitted.
When the radio signal is transmitted over an optical fiber instead of being directly transmitted over wireless, this is called RoF transmission. The RoF technology requires splitting the blocks showed in Figure 2.1a between the base station located in the residential gateway and the RRU placed at the other side of the fiber. Four RoF techniques are defined [22, 23]: A-RoF, baseband over fiber (BBoF), IFoF, and digitized radio over fiber (D-RoF).

A-RoF: The radio signal generated at the mixer output (Pt. B in Figure 2.1a) is modulated on the optical carrier and sent over the optical fiber to the RRU, as shown in Figure 2.1b. Then, after the optical-electrical conversion, the radio signal is processed by the RF block (e.g. amplifier) and wirelessly transmitted. The main advantage of A-RoF is the simplicity of the RRU, since most of the signal processing is performed at the base station. Furthermore, the link is waveform and frequency agnostic. The main challenge of this

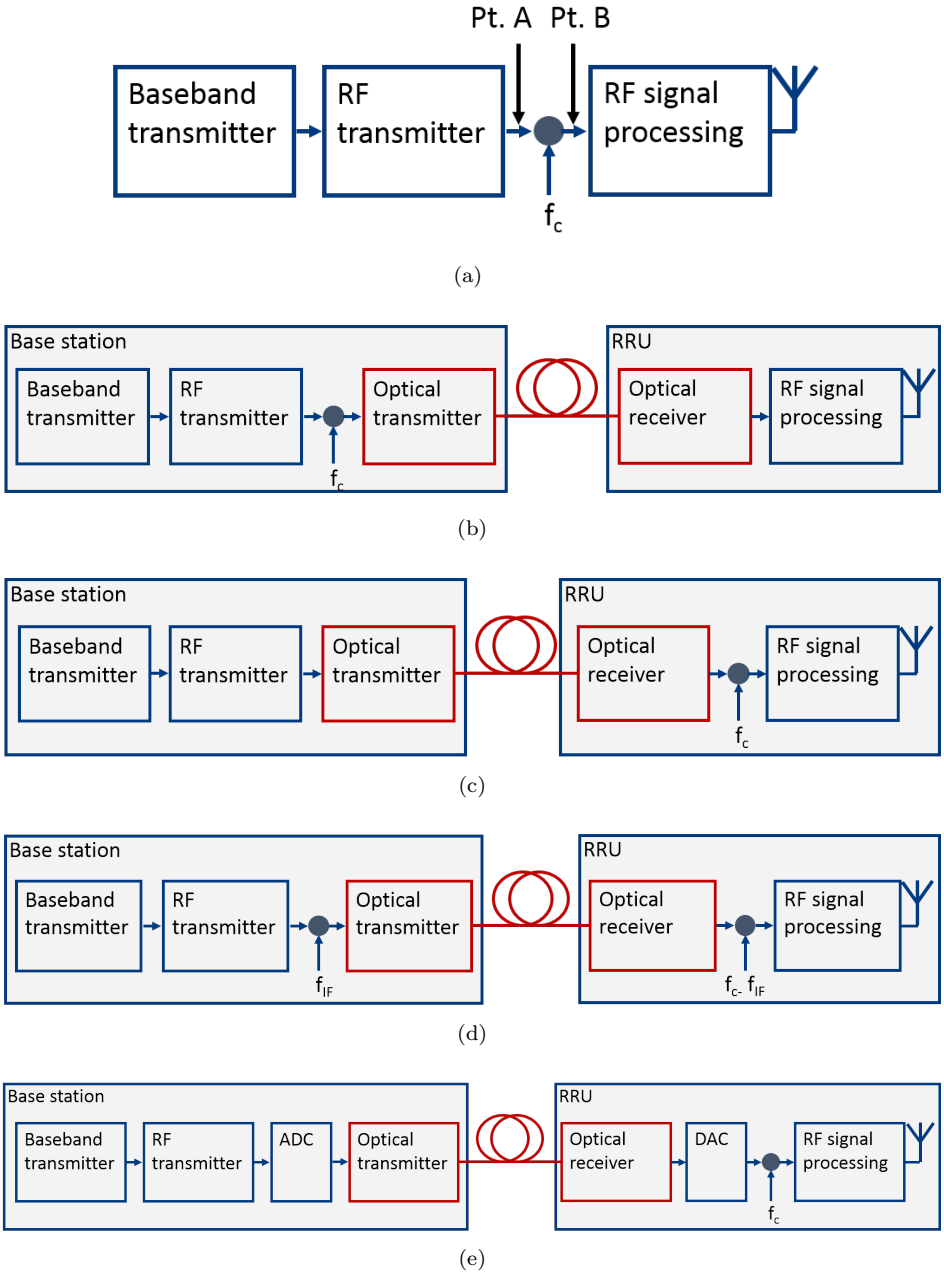

Figure 2.1. Generic block diagram of a radio frequency signal transmitter (a), A-RoF link (b), BBoF (c), IFoF (d), and D-RoF (e).

technique is the bandwidth and linearity demands for the optical link, which must match f_c, generally much higher than the modulated signal bandwidth and the linearity necessary to avoid nonlinear effect of the link [24, 25].

BB/IFoF: The analog signal generated by the transmitter (Pt. A in Figure 2.1a) is modulated on the optical carrier and transmitted over the optical link in the baseband, as shown in Figure 2.1c. At the RRU, the optical-electrical conversion is performed, the signal is shifted to f_c, processed, and wirelessly re-emitted. In this way, a single signal can be transmitted in the frequency domain but FDM and multiband transmission cannot be performed. In order to overcome this limitation, the analog signal is shifted to an IF allowing the multiplex of multiple signals in the spectrum, as shown in Figure 2.1d. In both the cases, the main advantage is the relaxed requirement on the optical link bandwidth since the occupied bandwidth is equal to the one of the analog signal or the IF in the BBoF and IFoF, respectively. The main disadvantages are the increased complexity of the RRU that performs the frequency shifting at the carrier frequency and the signal processing. Furthermore, the RRU must be tuned to shift the radio signal in the proper spectrum, therefore to the optical link is not frequency agnostic anymore [26].

D-RoF: The previous approaches are limited by the introduced nonlinear distortions, limited dynamic range, and cumulative noise [21]. Hence, an alternative solution is studied, the analog signal is digitized by analog-to-digital converter (ADC) before the transmission over the optical link. At the RRU, the signal is converted by a digital-to-analog converter (DAC) and wirelessly re-emitted, as depicted in Figure 2.1e. In this way, on the optical link is transmitted a digital signal; the system dynamic range reduction has lower impact on the signal quality [27], and the digital signal processing techniques can be applied. The main drawback is related with the required bit rate of at least $2B_{RF} \cdot N_{ADC}$ b/s, which is the product of the analog signal bandwidth B_{RF} multiplied by the resolution of the ADC N_{ADC}. Therefore, in most of the cases the analog signal is firstly down converted in frequency to IF or to baseband and then digitalized. Nevertheless, the RRU must be able to perform the digital signal processing, the digital to analog conversion, the amplification, and the frequency conversions. So, the link is not waveform and frequency agnostic anymore and the complexity is increased [27–29].

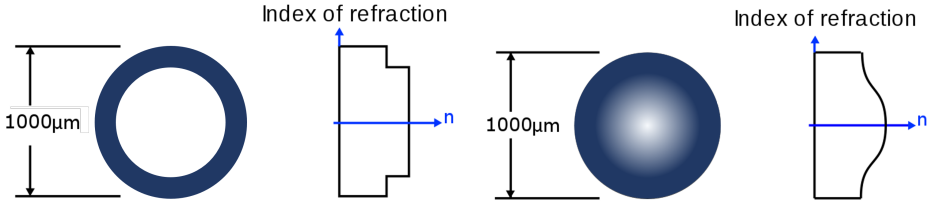

Figure 2.2. Illustrative representation of the SI (a) and GI (b) refractive index profiles for POF [30].

2.3 Plastic optical fibers

POF is an optical fiber in which its core and cladding are made from polymer or plastic materials. The use of plastic materials, instead of silica, ensure flexibility and mechanical resistance of the fiber even at large fiber diameter up to 1 mm. Different plastic materials are studied, so far the PMMA is the most popular, in particular among 1 mm core diameter POFs, defined as "large-core". This thesis focuses on large core POF. The main advantage of the large core is the easy and low-cost installation. At the same time, the main disadvantages are the narrow bandwidth due to the large modal dispersion and the high loss.
Many POF types are studied and proposed, the two most common type of POF are step index (SI) and GI, which differ by the refractive index profile, as shown in Figure 2.2. The SI-POF has refractive index profile ideally described by a step function, which leads to a bandwidth-distance product equals 40 MHz· km [31, 32]. The GI-POF has a refractive index profile which decreases from the center gradually, described by a continuous function, in most of the cases parabolic, which results in smaller modal dispersion and a higher bandwidth distance product of 150 MHz· km [33].
A major advantage of POF is the misalignment tolerance during splicing and coupling with the optical devices, which is related with the numerical aperture (NA). The NA of the standardized SI-POF is equal to 0.5, which allows easier coupling but also higher losses. Meanwhile, GI-POF has lower NA around 0.3 at the center of the core, which reduced the coupling loss but also demands tighter alignment.

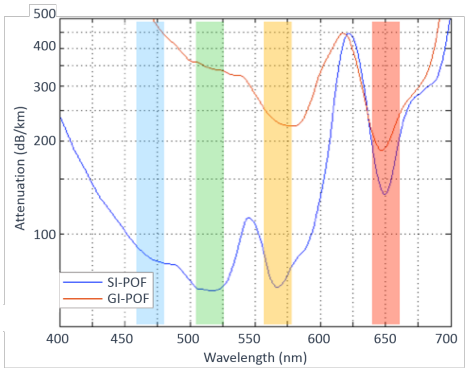

Figure 2.3. Loss vs optical spectrum for standard SI-POF and GI-POF, source: [35].

The PMMA POFs are suitable for visible light transmission. As shown in Figure 2.3, the SI-POF has low losses in four wavelength windows, hence studies on all these wavelengths are present in literature. In the recent years, the SI-POF research is moved toward the development of wavelength division multiplexing (WDM) POF link. In this way, the bandwidth of a single WDM channel is still limited but the link throughput is increased. For instance, four light-emitting diode (LEDs) working at 410, 440, 520, and 660 nm wavelengths are integrated in the same die within an area of 1×1 mm^2, hence the SI-POF can be easily coupled to the transmitter. On the other side, the WDM receiver based on planar diffraction grating is still bulky to be integrated on a single device and further study should be conducted [34].
The most common used wavelength window is around 650 nm, due to the large availability of optical sources and good responsivity of optical receivers [12]. For the GI-POF, this is the only wavelength with acceptable loss of 0.2dB/m. For SI-POF other wavelengths have lower loss, such as blue, green, and yellow light. Nevertheless, the blue and green optical transmitters have shown unequal performance regarding stability, lifetime, and bandwidth, so, 650 nm is the most used wavelength also for SI-POF links [12].

2.3.1 Devices for POF links

Optical transmitter: Up to now, three types of optical sources are used in POF links, the selection of the light source is related with the application requirements of the transmission system and the throughput. LED is the simplest POF light source and the most common optical transmitter due to its robustness and wide angle of emission. The main advantages of LEDs are low-cost, long lifetime and large operation temperature range. Meanwhile, the disadvantages are the narrow bandwidth, which limits the applications to low speed transmission systems, such as sensor applications. The angle of emission is much larger than the angle of acceptance (i.e. NA) of the POF leads to an extra power loss even for the large NA of the SI-POF. Such power loss can be decreased by collimating the beam by lenses, which in turns increase the link complexity. Nevertheless, LEDs are still limited regarding the bandwidth [36].

When higher output power, linearity, and modulation bandwidth are needed, the preferred choice is the laser diode (LD). Edge-emitting laser diode (EE-LD) emitting at 650 nm wavelength, originally designed for DVD players, has a maximum peak output power of 7 dBm and modulation bandwidth up to 2 GHz. However, most of the EE-LDs require strict operating conditions (e.g. ambient temperature and high bias current), which result in higher costs. An alternative to the EE-LDs are the vertical-cavity surface-emitting lasers (VCSELs). The VCSEL operates at lower threshold current, thus the driving current can be reduced. Furthermore, VCSELs are characterized by circular beam and low divergent patterns, ideal for efficient butt coupling to the POF. Both VCSEL and EE-LD are suitable for broadband digital and radio signal transmission thanks to the good linearity and broad bandwidth. A major disadvantage of VCSELs is the limited output power, up to 0 dBm at 650 nm, ideal only for short transmission distance ($<< 50\ m$). If the transmission distance is longer or extra lossy components are introduced (e.g. POF splitters), the EE-LD is preferred in order to meet the power budget requirement. Presently, EE-LD and VCSEL should be used with GI-POF, where the higher bandwidth distance product can take advantage of the higher transmitter bandwidth. Furthermore, the higher transmitted power of the EE-LD can compensate for the extra loss of the GI-POF.

Optical receivers: POF optical receivers are based on p-i-n photodiodes and APD.
The p-i-n devices are simple, low-cost, easy to use, and they have a relatively fast

response time. p-i-n devices with large active area (i.e. the light sensitive area of the photodiode) are usually preferred to match the POF NA and simplify the coupling. Active areas from 800 µm to 3 mm diameter are available, nevertheless, the wide active area increases the capacitance effect and reduces the device bandwidth. The responsivity of p-i-n diodes depends on the wavelength and materials and ranges from 0.4 to 0.7 A/W. The p-i-n optical receiver sensitivity and bandwidth are also depending on the architecture used for the front-end. The transimpedance amplifier (TIA) architecture is preferred when higher sensitivity is required, meanwhile the low-impedance amplifier (LIA) front-end provides wider bandwidth at expenses of a lower sensitivity [37–39].

Compared to the p-i-n, the APD has much higher sensitivity, wider bandwidth, and higher gain thanks to the multiplication gain, which can reach up to 500 for Silicon (Si) APD [40]. The main disadvantages are in the high-power consumption, temperature dependent performance, and higher noise level. Therefore, when the signal-to-noise ratio (SNR) is critical, an optical receiver based on p-i-n and TIA should be preferred.

2.3.2 Baseband digital signal transmission over POF

In the recent years, a significant interest has been given to the study of the most suitable digital baseband modulation for POF link given the standardization activity toward the gigabit Ethernet transmission over POF. Different digital baseband coding schemes are considered, among them non-return-to-zero (NRZ), PAM, carrierless amplitude phase (CAP), and DMT.
The simplest modulation scheme is the NRZ line code, in which each symbol represents a single bit and the symbol alphabet is $[\pm 1]$, hence the spectral efficiency is equal to 1 bit/Hz [41]. The limited spectral efficiency requires pre and post equalization, in order to reach satisfying throughput for broadband applications in links with narrow bandwidth, such SI-POF systems, bit rate of 1.25 Gb/s over 50 m SI-POF is reported [42].
Improvement of the spectral efficiency can be obtained by transmitting multiple bits per symbol. In case of M-PAM coding, $log_2 M$ bits are coded per symbol and the symbol alphabet is given by $[\pm 1, \pm 3, \ldots, \pm(M-1)]$, the spectral efficiency is improved by increasing M at cost of a lower sensitivity due to the noise. Most of the POF solutions use PAM in combination with pre and post equalization and could reach throughput of 3.3 and 3.8 Gb/s at 50 m SI-POF and 0 dBm of coupled

optical power by using 8-PAM and 4-PAM, respectively [43].
The previous schemes use only the in-phase modulation, here the CAP technique is based on the quadrature amplitude modulation and generates two orthogonal signals by filtering of 2 PAM signals. The spectral efficiency is the same as quadrature amplitude modulation but its implementation is simpler. Over SI-POF and 0 dBm of coupled optical power, the CAP scheme achieves 1.8 Gb/s, which is lower than the bit rate achieved by 4-PAM. This is caused by the link length, which gives a power limited rather than bandwidth limited channel condition [43].
Finally, DMT modulation belongs to the multi-carrier code, in which the incoming bits are distributed among many narrow band sub-carriers, each can use different coding in order to adapt to the channel condition. DMT is used in digital subscriber line (DSL) due to its high spectral efficiency, flexibility, and rejection of inter-symbol interference (ISI). Compared with the previous modulations, DMT offers the highest versatility to adapt to the varying channel condition and achieve high spectral efficiency. Throughput up to 10 Gb/s over 35 m GI-POF is demonstrated [44], nevertheless, the high-energy consumption of the signal processing limits its application in POF communication systems.
In conclusion, the choice of a modulation format for the digital baseband transmission over POF comes to the trade-off between available link bandwidth, noise performance, and system complexity. If the focus is on simplifying the system and reducing the power-consumption, then NRZ should be preferred up to 20 m distance, longer distances require the use of equalization techniques, hence an increase of the link complexity and power consumption. The PAM modulation is favored when the link is power-limited due to the better performance against noise compared with CAP and the lower complexity in comparison with DMT [45]. Furthermore, 16-PAM in combination with Tomlinson-Harashima precoding is chosen for the IEEE 802.3bv Gigabit Ethernet over POF standard and is further pushing the research in its direction [46, 47].

2.4 In-home network needs: a user's perspective

In the previous sections, the most significant technologies to improve the HAN and support better wireless connectivity are discussed. Here, the end-user perception about HANs is analyzed since in-home networks are generally installed and upgraded by the end-users, who needs to cover both the CapEx and OpEx. So, the key point to shape the next generation in-home networks is to grasp their

perception. Hence, a survey is performed aiming to understand:

- The users' preference about type of devices, services, and connectivity in HAN.
- The Internet connectivity satisfaction related with the user's device and services.
- The user's perception of the importance of HAN DAS networks.
- The user's perception and requirement to install a wired in-home network backbone.

The survey is conducted electronically[ii] and it is composed of up to 31 questions. The questionnaire is spread among social networks, mailing list of ECO, PHI, and EM groups of TU/e and Genexis employees between November and December 2017 and in total 110 people participated in the survey. The sample is mainly living in the Netherlands (75%), followed by Belgium, Italy (8% and 7%), and other European countries. The statistic population has mainly a technical job (79%), of which 26% related with telecommunication networks.
The survey is divided into 3 parts. In the first section, general questions are asked about the HAN connection quality and types of the most used devices and services, in order to define the current situation for HAN. Secondly, a scenario in which a DAS network is deployed to improve the WLAN quality is described and the end-users' perception is analyzed. Finally, the POF as wired backbone for the WLAN DAS system is considered and the end-user thoughts about installation types and cost are analyzed.

2.4.1 Internet connectivity satisfaction at home

In the first part of the survey, the perception of the quality of the Internet connectivity at home is analyzed. As shown in Figure 2.4a, almost all people rate the connection quality at least sufficient, a third good, and a third excellent.

The level of satisfaction is then compared with the number of users per HAN. As depicted in Figure 2.4b, the level of satisfaction decreases when the number

[ii]The questionnaire can be found at the following link: `https://goo.gl/forms/0OFwAxeC42TJF7PJ2`

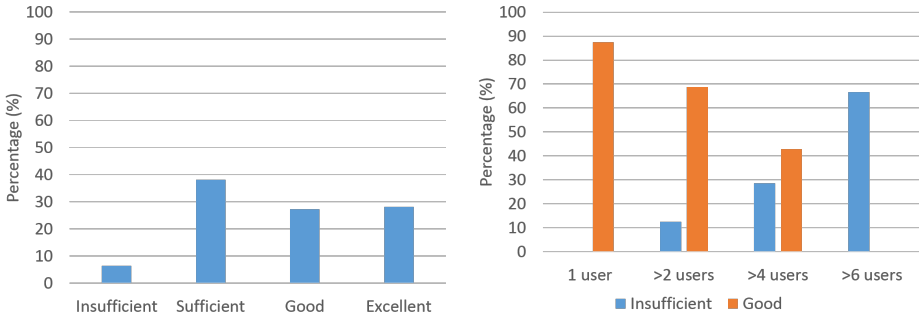

Figure 2.4. Users' level of satisfaction of the Internet connection at home (a) and level of satisfaction compared with the number of users per HAN (b).

of users increases. For instance, 90% of the people rate the Internet connection at least good when a single user is connected, which decrease to 0% when more than 6 users are connected to the HAN. The reason of this trend is that more users involve more connected devices, so a bigger aggregated throughput, which the HAN cannot handle. Furthermore, if the devices are connected by WLAN, the congestion of the wireless channel can occur. Finally, more users per HAN can be associated with a bigger house and more rooms, which might be difficult to be covered by the AP.

Next, participants are asked to identify the most used service, device, and in-home connection type. As shown in Figure 2.5a, the most used services are almost equally divided between video streaming, Internet surfing, and social application, all of them are characterized by asymmetric traffic. Meanwhile, within *other* are collected services such file transferring, online gaming, or a mix of them.

Moving to the type of device, as depicted in Figure 2.5b, half of the sample uses most of the time the mobile devices, mainly smartphones (42%) and tablets (9%). The remaining interviewees use laptop and personal computers (PCs), in accordance with the IP traffic share estimated by [48].

Clearly, WLAN Wi-Fi is the most preferred link, as shown in Figure 2.5c, in more than 80% of the cases, followed by wired connection by Cat 5e and 6, and

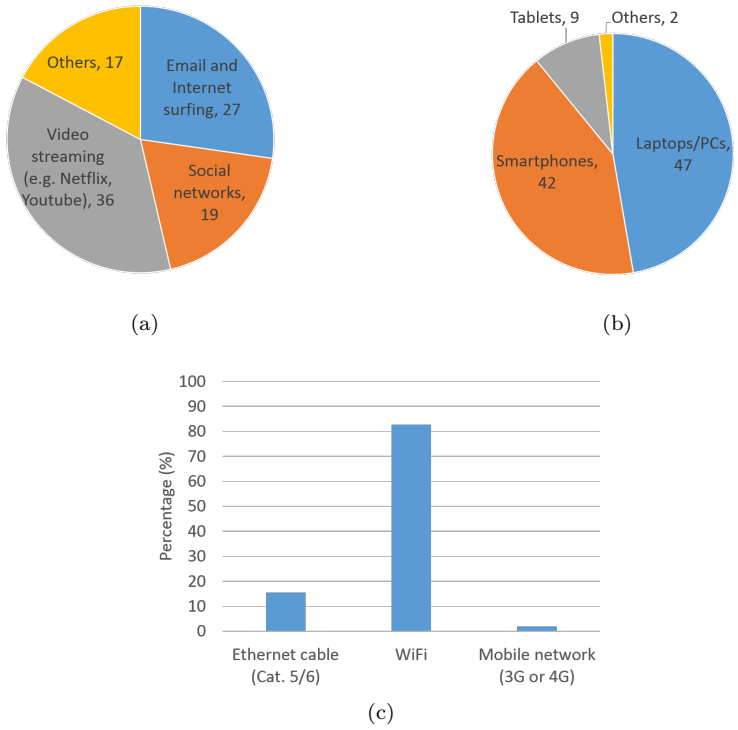

Figure 2.5. Percentage of the most used application (a), device (b), and connection type (c).

marginally by mobile network connection. Share of Wi-Fi connections around 50% would be expected from the result in Figure 2.5b, eventually, the percentage reaches a much higher value, meaning that also laptops and PCs are connected by wireless. The low share of mobile connectivity can be related by the available low-cost mobile bundle, offering in most of the cases only limited Internet traffic. This value can be expected to increase when the low-cost bundle with unlimited Internet traffic will become widespread.

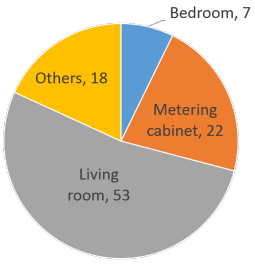

Figure 2.6. Share of the preferred AP location in home in percentage.

When comes to connectivity satisfaction over a wireless link, the location of the AP is important, then placing the AP close to the user's device improves the signal quality. As shown in Figure 2.6, more than half of the sample has the AP located in the living room, which can be expected to be the place in which the HAN connectivity is used. Notably, around 20% of the participants place the AP in the metering cabinet, most probably where the access network connection is terminated, which decreases the WLAN performance.

2.4.2 User's perception of in-home DAS networks

In this second part of the survey, the participants are asked to suppose of improving the HAN WLAN by installing an in-home DAS. The survey is meant for general audience, therefore the idea of a DAS architecture and RRU are not introduced and instead, the more familiar idea of installing multiple-APs around the house is proposed, nevertheless the results can also be used for DAS architecture and RRU deployment.
As shown in Figure 2.7a, more than half of the sample is willing to install multiple-APs to improve the WLAN connectivity. When comes to the preferred network solution, as depicted in Figure 2.7b, almost half of the sample would use the repeater mode of the AP and a third would follow the attached instructions. The same share would use a wired backbone based on Cat 5e and 6 cables and a marginal share would use power-line communication (PLC), glass optical fiber, and POF. The choice of using the WLAN repeater is arguably the less reliable and future-proof. This solution depends on the deployment scenario and further

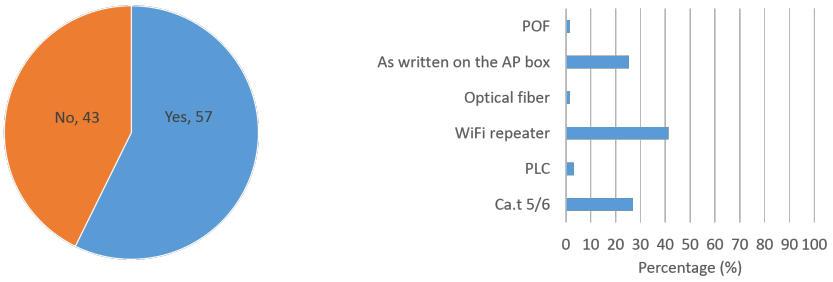

(a) (b)

Figure 2.7. Percentage of users willing to install more APs to improve the WLAN performance (a) and type of link used to connect them (b).

contributes to the generation of interference on the already overcrowded ISM band.

2.4.3 In-home DAS by wired backbone

In this section, the part of the sample who agreed with the assumption that a DAS can improve the wireless is asked about different wired installation types. In this way, the requirements of a POF in-home network from user's perspective are highlighted. Despite of the promising performance of POF as in-home network backbone, it is not yet well known among the end-users. In order to focus on the DAS installation instead of POF technology, the questions are related with Cat 5e and 6 cable deployment in order to use a familiar wired medium to the general audience.

As shown in Figure 2.8a, a pre-installed wired network is almost unanimously the reason to use the wired backbone. Next, in Figure 2.8b is assumed a brown-field installation and the cables are installed within the wall, without specifying any technique or difficulty involved. In this case, the majority of the population is still willing to install the network, but 30% of the sample would do it only by themselves and another 30% only without construction works. Next, the installation on the wall is considered since it does not require construction work and it is faster than the previous. As shown in Figure 2.8c, the main concern is aesthetic, almost half

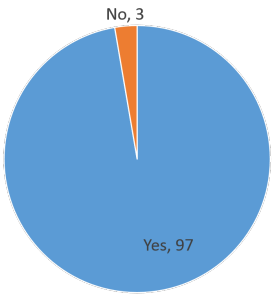

(a)

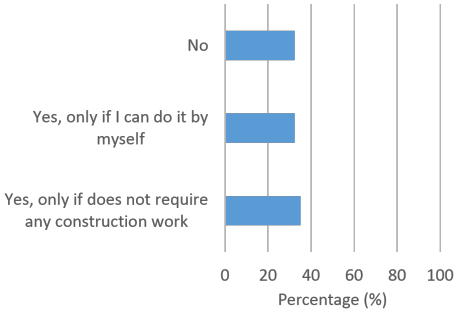

(b)

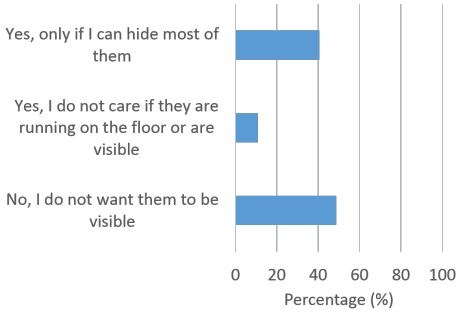

(c)

Figure 2.8. Percentage of participants willing to adopt a wired backbone if it is already installed (a), if it must be installed in and on the wall (b) and (c), respectively.

of the sample does not prefer this installation due to the chance to have cables visible. Then, nearly 40% of the persons interviewed are willing to perform the deployment only if the cable can be hidden.

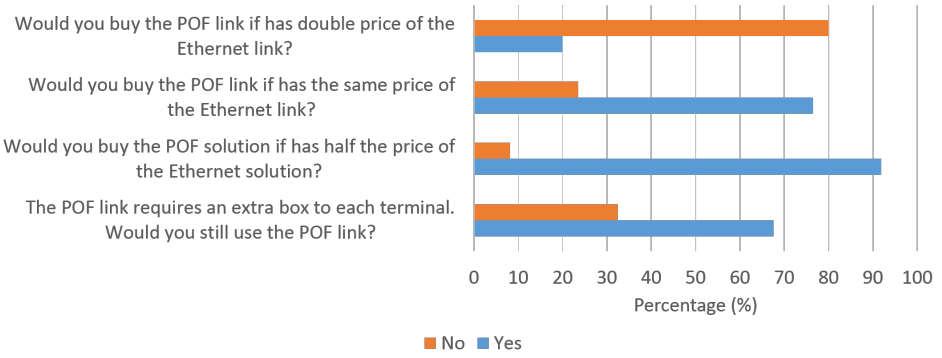

Figure 2.9. Share of the sample willing to use a POF link to a Cat 5e and 6 link.

2.4.4 In-home POF network perception

The installation cost and aesthetic aspects of a generic POF network are introduced to the participants as follows:

- The POF link ensures the same connection quality of the Ethernet Cat 5e and 6 cable.
- The POF link would be used to connect the APs and the wireless connectivity to the devices is still in place.
- The POF link does not require any connector and it is much thinner than Ethernet cable.
- The POF link can be hidden under carpet or easily pulled in ducts.

As shown in Figure 2.9, the main consideration of the participants is related with the price. Almost 80% of the persons are willing to install a POF link if it is cheaper than the Cat 5e and 6 solution. The share decreases to 25% if they have the same price, and further reduces to less than 10% if it is more expensive. Finally, the presence of the media converter needed to convert the optical signal into Ethernet and WLAN signal in almost 70% of the cases is not a limitation to the installation.

In conclusion, the survey gives an insight into different aspects of in-home networks. Firstly, the survey confirmed the importance of the mobile devices and WLANs in HANs. Secondly, a mix of services is characterizing the HAN, which strengthens the importance of a multi-standard in-home network backbone able to support all these services. Thirdly, in-home connectivity satisfaction showed to rapidly decrease with the number of users connected to the same HAN, which is related with the limited coverage of single-AP topology. Most of the end-users approve the DAS installation to improve the WLAN connectivity but this would rely on WLAN repeaters. DAS based on a wired backbone network can become more popular by decreasing the installation complexity and time. Finally, POF is appreciated for the do it yourself capability but the cost reduction down to price comparable with the Cat 5e and Cat 6 cable networks is necessary.

2.5 Next generation in-home network

In section 2.1 the necessity to improve the wireless network performance in HANs in order to support, in a future-proof manner, the homogeneous broadband coverage and massive M2M communication envisioned by 5G is highlighted.
Looking to the WLAN, the coverage can be improved by moving from a single-AP topology to a DAS solution. In this way, the wireless propagation through the walls is avoided. At the same time, better coverage and higher throughput are provided.
Looking to the current 4G and future 5G mobile networks, the coverage improvements can be achieved by heterogeneous networks and M-RAT technologies as explained in section 2.1. As discussed in section 2.4, most of the survey participants would install a wired DAS to improve the WLAN connection quality if the wired network can be installed by themselves or by installers.

Both the DAS and heterogeneous network need a broadband low-cost network that is able to provide a reliable connection between the residential gateway and the RRUs. Instead of a dedicated medium for each service, a single network supporting all the services should be pursued. Such solutions must be able to provide:

- Multiband radio transmission supporting mobile network carrier aggregation.

- Multi-standard transmission capability to support mobile signals, Wi-Fi, and WSNs.

- Gb/s baseband digital signal for wired services.

Different wired links are available, none of them is completely satisfactory from bandwidth and EMI immunity (e.g. unshielded twisted pair cables) or cost (glass optical fiber) perspectives.

Unshielded twisted pair. Cat 5e and Cat 6 are among the most common wired solutions used nowadays in-home [49]. Cat 5e supports up to 1 Gb/s over 100 m length using 1000BASE-T standard, meanwhile, Cat 6 provides up to 10 Gb/s over 55 m and 1 Gb/s over 100 m by 10GBASE-T and 1000BASE-T protocols [50, 51]. The wide diffusion of the solutions makes the cable and systems inexpensive. Nevertheless, the cable bandwidth at 100 m is limited to 100 and 200 MHz for the Cat 5e and 6 cables, respectively [52]. Hence, a DAS based on Cat 5e and 6 cables can only transmit the baseband digital signals to the remote unit, which acts as full-fledged base station. Hence, the digital signal is remotely converted to the radio waveform for the wireless transmission. Furthermore, the cables are potentially exposed to EMI. From installation point of view, the price of the cables is comparable to the optical solutions but it requires the installation of dedicated ducts, due to safety reasons, which increase the final cost. Additionally, the cable diameter (6 mm for the Cat 6 cable) is larger than the POF, which reduces the number of cables deployed in the same duct and the capability to install them on the wall without being noticed [53].

Glass optical fiber. Despite the popularity of twisted pair links, the large bandwidth of optical fiber lines can offer a more powerful set of broadband services. In this terms glass single-mode optical fiber (SMF) and multi-mode optical fiber (MMF) offer the widest bandwidth. The broad bandwidth of the SMF makes them the perfect candidate for networks where more than 10 Gb/s of throughput and A-RoF capability, also for mmWave spectrum, are required. For these reasons, SMF RoF links are mainly used for corporate and public buildings [54]. Finally, both the fibers require to be installed by trained technicians through specialized tools and delicate handling, thus incur higher installation costs [1, 49].

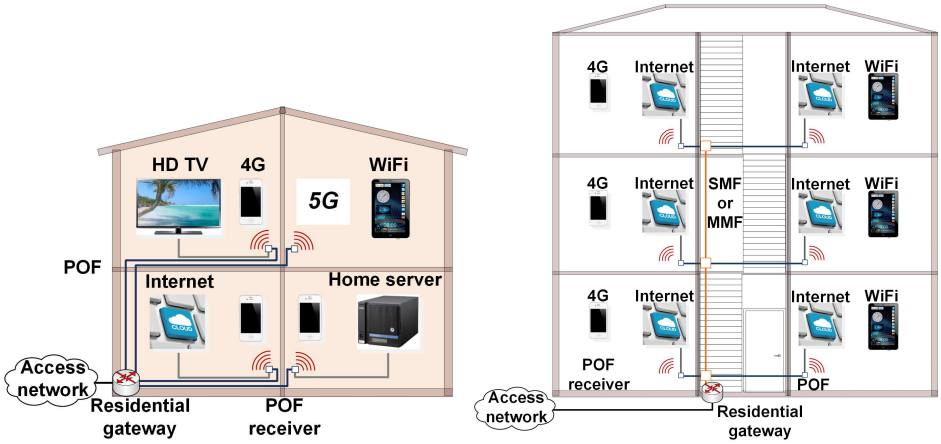

Figure 2.10. Illustrative POF network for multi-format in-home (a) and in-building (b) networks.

POF. POF is used already in automotive industry (e.g. media oriented systems transport (MOST) standard) and its application for access networks is studied for many years. Recently, gigabit Ethernet over POF standard ensures 1 Gb/s over 50 m large core PMMA SI-POF, meanwhile multi-gigabit/s transmission is demonstrated (as discussed in section 2.3.2). Preliminary studies on in-home network convergence over POF were conducted. Transmission of gigabit/s digital baseband and radio transmission over 50 m GI-POF are demonstrated by DMT and IFoF techniques and APD receiver [55]. Recently, the use of D-RoF transmission over POF is demonstrated but multistandard transmission is not supported yet [29].

Two HAN POF use cases are envisioned. Firstly, in case of a single-detached dwelling house with multiple rooms on different floors, as shown in Figure 2.10a, the access network is terminated in the residential gateway at the houses' doorstep. The POF connects the residential gateway to the remote POF transceiver in each room, and from there the last meter connectivity is made to support all the services.

Secondly, in case of a larger building (e.g. multi-dwelling unit), depending on

the size, the POF can connect the residential gateway to each apartment or, as shown in Figure 2.10b, a hybrid installation might be needed. In this case, the connection from floor-to-floor or fiber riser could be realized by SMF or MMF [56]. Connection from the fiber riser to each apartment doorstep and further in-home is performed by POF cables, which thanks to the connector-less technology require shorter installation time and easy fiber splicing, so lower costs.

From the previous comparison, POFs emerged as the most satisfactory solution in terms of both broadband and multistandard capability and low-cost installation and simplicity. POF can meet these challenges, transmitting the multi-format radio signals and providing an optical backbone for both wired and wireless based in-home services.

2.6 Summary

In this chapter a brief overview of the indoor wireless network requirements and RoF technologies is performed and the POF technology capabilities for in-home networks are highlighted. In section 2.1 the mobile broadband and massive M2M communication 5G use cases are defined. Regarding the broadband connectivity case, the importance of delivering an average data-rate of 100 Mb/s in all the covered area is shown. Such uniform coverage can be achieved by employing the low frequency band together with M-RAT and heterogeneous network. At the same time, the large number of battery powered massive M2M devices leads to the impossibility to frequently recharge them. Hence, the increase of the battery lifetime must be achieved by reducing the transmission time and power, for instance by shorten the distance between the nodes and the network gateway. In both use cases, DAS technique is clearly shown as a promising solution supporting the targeted average data-rate and reducing the WSN device energy consumption Optical fiber links are favored for DAS, the optical fiber EMI immunity, low loss, and large bandwidth make them the ideal candidate for data transmission. As shown in section 2.2, different techniques to transmit radio signals over optical fibers are discussed. Whenever the low-cost requirement and the low-complexity of the RRU are main concerns of the RoF link, the A-RoF technique is preferred. Section 2.3 describes the POF types, the optical transmitters, receivers, and the most used modulation scheme for digital baseband transmission over POF. The requirement of a simple optical link with wide bandwidth, necessary to support the A-RoF transmission, makes GI-POF together with LD and p-i-n photodiode

the most promising configuration. Regarding the digital baseband transmission, PAM scheme shows the best trade-off between complexity and spectral efficiency. The end-user perspective about in-home DAS and POF is analyzed in section 2.4. DASs emerged as an interesting solution to improve the wireless coverage and the signal quality. Nevertheless, the survey highlighted the necessity of further efforts in order to simplify their installation, since the complexity and time consumption are the main concerns. Finally, POF results an attractive technology for the in-home network backbone. Further market penetration and adoption will be achieved when the trade-off between performance and price becomes competitive with the other solutions (i.e. Cat 5e and 6).

Chapter 3

Simultaneous transmission of baseband and 4G mobile signals

Delivery of high-speed wired service and mobile network signal is an important deployment scenario for HANs. Thus, this chapter demonstrates the simultaneous transmission of a baseband 4-PAM signal and a multiband LTE-A signal over a large core PMMA POF link. The demonstration is carried out in steps to analyze system impairments and to introduce improvement techniques. The multi-service optical link consists of an electrical RF source for the LTE-A signal and electrical baseband source for the 4-PAM signal, an optical transmitter, a POF, a photodetector, and two electrical receivers, one for each signal. After being received by the POF link, the LTE-A signal is further wirelessly transmitted. Two types of POF link are investigated, which are based on 1 mm core diameter PMMA SI and GI POFs. In order to reduce the system complexity, thus cost, most of the signal processing is located at the centralized residential gateway instead of the RRU, then A-RoF transmission is preferred as discussed in section 2.2. However, most of the LTE-A bands have carrier frequency higher than the POF link bandwidth. Hence, a time-invariant pre-equalization method is proposed to stretch the frequency response of the POF link. The pre-equalization aims to balance the attenuation of the optical link in each LTE-A band. Different optical transmitters and receivers are tested, among them VCSEL and EE-LD-Fabry-Pérot (FP) for the transmitter and different p-i-n photodiodes for the receiver.

This chapter is based on the results published in [57–61]

The optical couplings between transmitter, POF, and receiver are realized with a single lens mounted in the receiver and in the transmitter, therefore no complex alignment is required. Both the GI and SI POFs are terminated without connector (i.e. connectorless).

In this chapter, section 3.1 presents OFDM and LTE-A signal waveforms and the most important parameters. In section 3.2, a first POF link based on VCSEL and p-i-n devices is characterized. In section 3.3, the first multiband LTE and 4-PAM signal transmission over 20 m GI-POF is performed by careful signal spectrum multiplexing. In section 3.4, the spectrum allocation is simplified by introducing DSP filtering, which reduces the 4-PAM and LTE mutual interference. Furthermore, the number of LTE-A bands transmitted is increased by the mentioned time-invariant pre-equalization. From section 3.5, the POF link budget is extended to increase the link length and to support the wireless re-transmission in order to meet the demand of in-home and in-building networks. Thus, section 3.5 investigates difference optical transceivers and POF types. The LTE-A and 4-PAM signals are transmitted together over the GI and SI-POF links and in section 3.6 the wireless transmission is implemented after the GI -POF link. Next, in section 3.7 the POF link length is extended to 50 m, which is considered satisfactory for most of the in-building and in-home applications. Finally, in section 3.8, the pre-equalization method is optimized based on different feedback parameters, which allows to simplify the RRU. Hence, the trade-off between the transmission of new LTE-A bands and the overall signal quality is discussed.

3.1 OFDM coding and LTE/LTE-A waveforms

OFDM is among the most used modulation format for wireless transmission because of its relatively low complexity and the reliability against inter-symbol interference by multi-path propagation. OFDM is currently used in many standards: mobile network air-interface (LTE and LTE-A), WLAN (IEEE 802.11a/g/n/ac/ah), and terrestrial digital television broadcasting (DVB-T and ISDB-T). In this section, the OFDM modulator, demodulator, and main parameters are analyzed. Then, the application of OFDM for mobile networks is briefly analyzed in section 3.1.2 by the discussion of important LTE-A RAT characteristics.

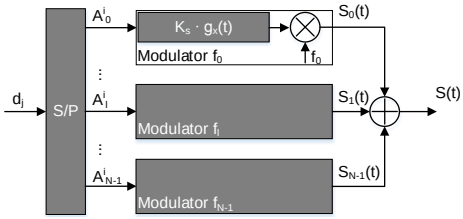

Figure 3.1. Multi-carrier transmitter scheme.

3.1.1 OFDM coding

The bits to be transmitted are mapped in the sequence of symbols d_j with symbol rate $\frac{1}{T_s}$ by a constellation of size $M = 2^m$, which occupies a bandwidth B. Then, the generated symbol sequence is serial-to-parallel (S/P) converted over N outputs, as shown in Figure 3.1. The symbol at the n^{th} output and the i^{th} symbol period is denoted by $A_n^i = d_{iN+n}$, $n \in [0, N[$, $i \in \mathbb{Z}$, and the symbol time becomes $T_{OS} = T_S \cdot N$. Next, each symbol A_n^i is modulated at the carrier frequency $f_n = f_0 + n\Delta f$, where Δf is the sub-carrier spacing. Then, the N modulated signals $s_n(t)$ are given by:

$$s_n(t) = \mathfrak{Re}\left\{ K_s \sum_{i=-\infty}^{\infty} A_n^i g_x(t_i - T_{OS}) e^{j2\pi f_m t} \right\} = \mathfrak{Re}\left\{ b_n(t) e^{j2\pi f_0 t} \right\} \tag{3.1.1}$$

$$b_n(t) = K_s \sum_{i=-\infty}^{\infty} A_n^i g_x(t_i - T_{OS}) e^{j2\pi \Delta f t} \tag{3.1.2}$$

where K_S is a constant and $g_x(t)$ is the generic finite-energy waveform used for each symbol. Looking to this scheme, the implementation is not spectral efficient, since the Δf must be wide enough to ensure an acceptable interference between the sub-channels (i.e. inter-carrier-interference), sacrificing the spectral efficiency. Alternatively, each sub-carrier should be band-pass filtered to limit the inter-carrier-interference, which increases the modulator complexity.
The previous scheme can be simplified under the assumptions that $g_x(t) = rect(\frac{t}{T_{OS}})$

and $\Delta f = \frac{1}{T_{OS}}$, hence the signals $s_n(t)$ are orthogonal as such:

$$\int_{iT_{OS}}^{(i+1)T_{OS}} b_n(t) \cdot b_m(t)dt = 0, \forall n \neq m, \forall i \tag{3.1.3}$$

in this condition, the sub-carriers are orthogonal, therefore filtering and wide Δf are not required to avoid inter-carrier-interference, and hence the spectral efficiency is increased. Under these assumptions, the signal $s(t)$ becomes:

$$s(t) = \sum_{n=0}^{N-1} s_n(t) = \mathfrak{Re}\left\{ K_s \sum_{n=0}^{N-1} \sum_{i=-\infty}^{\infty} A_n^i g(t - iT_{OS}) e^{j2\pi(f_0 + n\frac{1}{T_{OS}})t} \right\} \tag{3.1.4}$$

and re-written as

$$s(t) = \mathfrak{Re}\left\{ b(t) \cdot e^{j2\pi f_0 t} \right\} = \mathfrak{Re} \sum_{i=-\infty}^{\infty} \left\{ b_S^{(i)}(t) g(t - iT_{OS}) e^{j2\pi f_0 t} \right\} \tag{3.1.5}$$

$$b_S^{(i)}(t) = K_s \sum_{n=0}^{N-1} A_n^i e^{j2\pi \Delta f t n} \tag{3.1.6}$$

next, $s(t)$ is sampled with sampling frequency $\dfrac{1}{T_{OC}}$, where $T_{OC} = \dfrac{T_{OS}}{N}$, then the samples of the complex envelope u_k^i are given by:

$$b_S(t) = b^{(i)}(t), t \in [iT_{OS}, (i+1)T_{OS}[\tag{3.1.7}$$

$$u_k^i = b^{(i)}(iT_{OS} + kT_{OC}) = K_S \sum_{n=0}^{N-1} A_n^i e^{j2\pi n \frac{1}{T_{OS}} iT_{OS}} e^{j2\pi n \frac{1}{T_{OS}} kT_{OC}} \tag{3.1.8}$$

$$= K_S \sum_{n=0}^{N-1} A_n^i e^{j2\pi \frac{nk}{N}} \tag{3.1.9}$$

$$= K_S N \{\mathcal{F}_d^{-1}[\overrightarrow{A^i}]\}_k, 0 \leq k \leq N-1 \tag{3.1.10}$$

where $\mathcal{F}_d^{-1}[\overrightarrow{A^i}]\}_k$ is the inverse discrete Fourier transform (IDFT) of the vector of dimension N and the signal spectrum is shown in Figure 3.2.

One of the main advantages of the IDFT is that it can be calculated by using

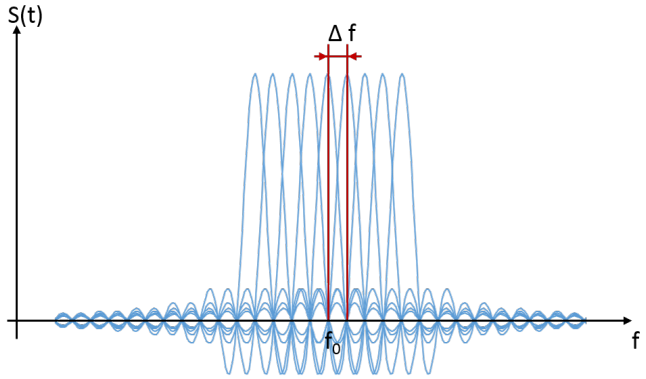

Figure 3.2. Plot of an OFDM spectrum with 9 sub-carriers.

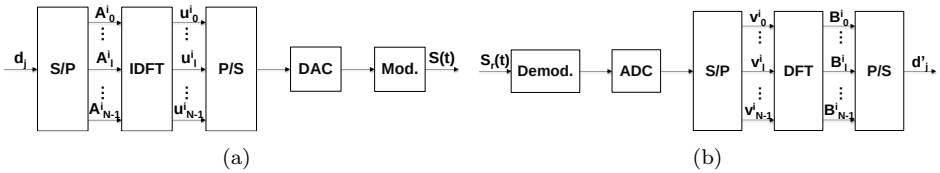

Figure 3.3. OFDM transmitter (a) and receiver (b) schemes.

inverse fast Fourier transform (IFFT), which is proved to have lower computational requirement [62]. Then, the digital samples u_k^i are digital to analog converted and modulated on the RF carrier at frequency f_0, as shown in Figure 3.3a, and transmitted. At the receiver, the same operation are repeated in the reverse order as shown in Figure 3.3b to retrieve the received information d'_j.

The popularity of the OFDM coding is related with the low complexity and the reliability against ISI by multi-path propagation. Looking to the latter, this is possible through the introduction a cyclic prefix, which simplifies the ISI cancellation at the receiver [63]. In particular, a cyclic prefix of duration T_g is the repetition of the last part of the signal $s(t)$ of duration T_g at its beginning, as

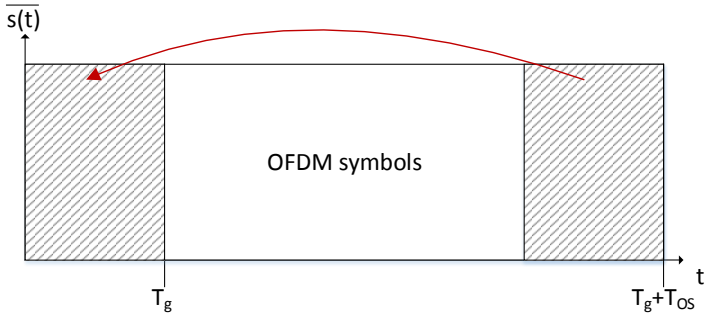

Figure 3.4. Cyclic prefix allocation scheme.

shown in Figure 3.4. Hence, the cyclic prefix is defined as follows:

$$\overline{s}(t) = \begin{cases} s(t + T_{OS}) & \text{, if } 0 \leq t \leq T_g \\ s(t) & \text{, if } T_g \leq t \leq (T_{OS} + T_g) \end{cases} \tag{3.1.11}$$

the cyclic prefix does not increase the transmitted quantity of information since it is a repetition of the last part of the signal, instead it increases the time needed to transmit the same amount of bit from T_{OS} to $T_{OS} + T_g$. Nevertheless, the advantage of adding the cyclic prefix is the easier symbol recovery at the receiver side in presence of ISI due to a multi-path wireless channel. In particular, in case the longest multi-path delay is smaller than T_g, the OFDM receiver can retrieve the symbol with a phase shift and amplitude change due to the timing offset and the frequency response at each sub-channel, respectively [62]. Meanwhile, in a single-carrier signal, the detection of the symbols when ISI happens is more difficult.

Furthermore, from the OFDM coding derives the multiple-access scheme defined orthogonal frequency-division multiple access (OFDMA). Here, a single or a subset of sub-carriers is allocated to different users and the OFDM signal can serve multiple users.

3.1.2 LTE-A signal

LTE and LTE-A are mobile network standards developed by 3GPP with the standard releases 8 and 10 and appeared in 2004 and 2011, respectively.

Table 3.1. Main parameters of LTE Release 8 downlink radio signal [4].

Parameter	Value
Access Scheme DL	OFDMA
Bandwidth (MHz)	1.4, 3, 5, 10, 15, and 20
Minimum transmission time interval (ms)	1
Sub-carrier spacing (kHz)	15
Cyclic prefix (μs)	4.7 (short), 16.7 (long)
Modulation	QPSK, 16-QAM, 64-QAM

LTE-A is the successor of LTE and it is deployed in order to match the new challenges given to the mobile networks. LTE-A satisfies all the requirements for international mobile telecommunications (IMT) Advanced-4G system as defined by the ITU-T, then LTE-A and 4G are often used as synonymous. The LTE and LTE-A standards defines the requirements for the backhaul, fronthaul, and radio access networks.
Here, the most important downlink radio signal parameters of the LTE and LTE-A are discussed. Various modification were made in the LTE-A physical layer in comparison to LTE to support the updated features (e.g. larger bandwidths, coordinated base stations, scheduling, multiple-input and multiple-output (MIMO), interference management). Nevertheless, these changes marginally affect the radio signal structure, therefore the following discussion is valid for both the LTE and LTE-A signals.
The down- and up-link transmissions are supported by both time division duplex (TDD) and frequency division duplex (FDD). The LTE-A uses adaptive modulation and coding and variable transmission bandwidth in order to adapt to the link condition, MIMO transmission, and multi-user scheduling in frequency and time domains. The LTE-A downlink radio signal is based on OFDM modulation and is used to obtain a robustness against multipath interference and high affinity to MIMO.

In the time domain, the LTE-A signal is organized in *frames*. Each *frame* has a duration of 10 ms and it is divided in 10 *sub-frame*. Each *sub-frame* is based on 2 *slots* of 500 μs and each slot has 7(6) symbols for normal (extended) cyclic prefix.

Table 3.2. Performance of the LTE and LTE-A standards [4].

Parameter	Value	
	LTE	LTE-A
Peak data rate downlink (Mb/s)	300	1000
Peak data rate uplink (Mb/s)	75	500
Mobility	Optimized for low speeds ($< 15km/h$)	
Coverage	Full performance up to 5 km	
Scalable bandwidths (MHz)	1.4, 3, 5, 10, 15, and 20	Up to 20-100

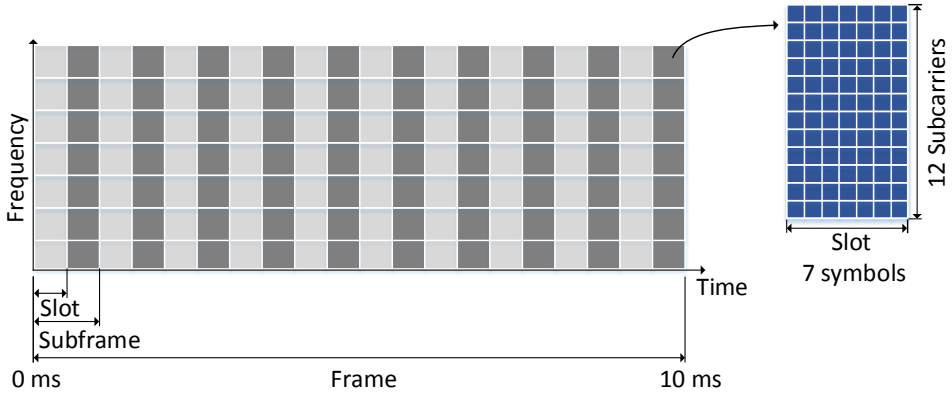

Figure 3.5. LTE FDD 1.4 MHz bandwidth with normal cyclic prefix frame diagram and the RB grid in blue.

In the frequency domain, the OFDM sub-carriers have 15 kHz spacing. The maximum transmission bandwidth varies with the carrier frequency as defined by the E-UTRA standard and listed in Table 3.3. Instead of indicating the couple *(number of slots, number of symbols)*, 3GPP defines the resource element (RE) as the smallest discrete part of a frame that contains a single complex value of data or signaling and it is formed by a sub-carrier and has 1 symbol duration.
The minimum unit of resources that can be allocated to a user is defined at resource block (RB) and has 180 kHz bandwidth and has 1 *slot* duration, as shown in Figure 3.5. The LTE-A RB can encapsulate the data, control, synchronization,

precoding, and multiple access signaling in order to correctly decode the signal at the receiver side. According with the LTE-A terminology the user's data are indicated as physical downlink shared channel (PDSCH).

LTE-A carrier aggregation

During the evolution of mobile networks one of the key requirements is the increase of throughput. As mentioned in section 2.1, the straightforward solution is to increase the transmission bandwidth. Hence, new wider bands should be licensed, which requires time and considerable investments by the operators. Instead, this can be done by using the already licensed bands for E-UTRA (i.e. carrier aggregation), as implemented in the current LTE-A releases. In this way, the operators are allowed to deploy extended bandwidth by using different narrower licensed bands. LTE-A[i] allows carrier aggregation up to 100 MHz (e.g. 5 bands at 20 MHz bandwidth each) of total bandwidth in downlink and increases the peak data rate up to 1 Gb/s by 3 types of carrier aggregation:

- Contiguous intra-band, for which multiple contiguous sub-carriers are put together in the same operating band as shown in Figure 3.6a.
- No-contiguous intra-band, same as the previous but the sub-carriers are spaced by a frequency gap as shown in Figure 3.6b.
- No-contiguous inter-band, the sub-carriers are located in different operating bands as shown in Figure 3.6c. In this case, the multiband transmission must be supported.

3.1.3 From LTE-A toward 5G

In this thesis the transmission of LTE-A instead of 5G signal over POF is studied for three reasons:

- LTE-A will play a key role in the initial 5G deployment. The deployed 4G radio access network (RAN) and core network are used for mobility support and coverage in the sub-6 GHz frequency range, meanwhile new 5G features are deployed (i.e. 5G non-standalone phase) [64, 65].

[i] LTE does not support carrier aggregation.

Table 3.3. LTE-A E-UTRA bands designated for FDD up to 2 GHz carrier frequency with f_{UL}, f_{DL}, and B_w, respectively the uplink band, downlink band, and maximum allowed bandwidth.

E-UTRA operating band	f_{UL}(MHz)		f_{DL}(MHz)		Maximum B_w (MHz)
31	452.5	457.5	462.5	467.5	5
71	663	698	617	652	20
12	699	716	729	746	10
17	704	716	734	746	10
13	777	787	746	756	10
68	698	728	753	783	15
14	788	798	758	768	10
28	703	748	758	803	20
20	832	862	791	821	20
27	807	824	852	869	10
26	814	849	859	894	15
18	815	830	860	875	15
5	824	849	869	894	10
19	830	845	875	890	15
8	880	915	925	960	10
11	1427.9	1447.9	1475.9	1495.9	10
21	1447.9	1462.9	1495.9	1510.9	15
24	1626.5	1660.5	1525	1559	10
3	1710	1785	1805	1880	20
2	1850	1910	1930	1990	20
25	1850	1915	1930	1995	20
70	1695	1710	1995	2020	15

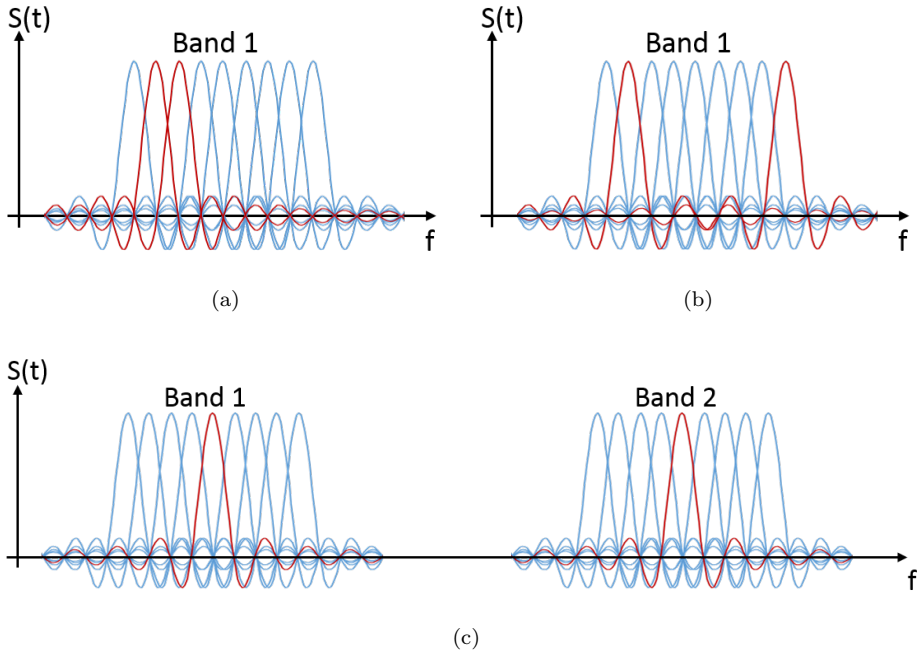

Figure 3.6. Illustrative LTE carrier aggregation spectra for the contiguous intra-band (a), no-contiguous intra-band (b), and no-contiguous inter-band (c).

- 5G envision of M-RAT approach brings close collaboration with the LTE-A.
- The 5G RAT specifications were not published at the time the FlexCom project started. The academia was not converging to any particular solution, hence LTE-A is also chosen as a reference signal, waiting for the 5G specification[ii].

Furthermore, the transmission of a standard-compliant LTE-A signal gives more stringent requirements than LTE-like signal. In order to comply with the standard,

[ii] 5G RAT specifications were published in December 2017.

in this thesis, the LTE and LTE-A signals are generated using the evolved test model (E-TM) 3.1. The E-UTRA E-TM is a set of waveforms defined by 3GPP to test specific performance of the base station, as well as, mobile devices (user equipment (UE) in 4G terminology). In all the experiments the 64-quadrature amplitude modulation (QAM) coding is used for the 4G signals and EVM is used as the reference parameter of the quality of the received signal. The designed E-TM for EVM measurement of 64-QAM is E-TM 3.1 [66]. The EVM is calculated in accordance with [67], which sets the EVM threshold for the 64-QAM at 8%.

3.2 Study and characterization of a VCSEL-based GI-POF link

The optical link is depicted in Figure 3.7 and it is composed by the Firecomms VCSEL optical transmitter, 20 m PMMA Optimedia OM-Giga S E 100 large core GI-POF, and the p-i-n optical receiver.
In order to set an optimal operating condition for VCSEL, the bias voltage is measured against the coupled optical power, as shown in Figure 3.8. A bias voltage equals 3.3 V is found to be in the middle of the linear regime of the VCSEL. At this point, the emitted power ($P_{emitted}$) is 0.8 dBm, which is measured by placing an optical power meter probe aligned to the VCSEL.
Knowing the coupling loss between VCSEL and fiber is important for system performance. As shown in Figure 3.9, the VCSEL is connected to 1 m GI-POF by OptoLock connector. The other fiber end is then plugged into the same visible light power meter, the measured power ($P_{coupled}$) is equal to 0.25 dBm. The VCSEL central wavelength is measured equal to 679 nm and the GI-POF loss at 680 nm (L_{680nm}) is equal to 0.32 dB/m. Hence, the coupling loss ($L_{coupling}$) is calculated as follows

$$L_{coupling}[dB] = P_{emitted}[dBm] - P_{coupled}[dBm] - 1[m] \cdot L_{680nm}[dB/m] \quad (3.2.1)$$

and it is equal to 0.23 dB.

In this experiment, the VCSEL is connected to 20 m of GI-POF, which is then coupled to the optical receiver and the received optical power is -6 dBm, including the coupling losses. The optical receiver consists of a Hamamatsu S5052 Si p-i-n photodiode followed by a TIA front-end designed and produced by POF Application Center (POF-AC). The optical link is a simple intensity modulated

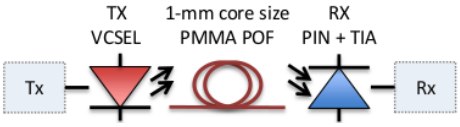

Figure 3.7. Experimental setup diagram of the optical link.

Table 3.4. LTE-A bands and main parameters.

Index (i)	1	2	3	4	5	6	7	8
E-UTRA operating band	31	12	13	14	20	18	19	8
Carrier frequency (MHz)	465	738	751	763	806	868	883	944
Bandwidth	5		10		20	15		10
Modulation Format	64-QAM							
Band amplification gain G_i (dB)	-3		0		3		4	2

direct detection (IM-DD) system. In the following section, the link frequency response and noise figure (NF) are characterized.

3.2.1 Link frequency response and gain

The frequency response and the gain of the optical link are measured by the S parameters. The electrical power at the VCSEL input is equal to -20 dBm and the S parameters are measured using the Keysight FieldFox network analyzer connected at the optical link output.
In Figure 3.10 the $S21$ values are depicted and the -3 dB bandwidth is measured equal to 340 MHz, which is smaller than the first LTE-A signal. The POF link gain or attenuation can be calculated separately for each LTE-A band with index i as the average $S21$ within the band and is denoted as $G_{POF,i}$. Considering the LTE-A bands in Table 3.3 with a downlink carrier frequency lower than 1 GHz, with maximum bandwidth, and not overlapping, then the E-UTRA bands 31, 12, 13, 14, 20, 18, 19, and 8 are used. Considering the $S21$ values in each of these

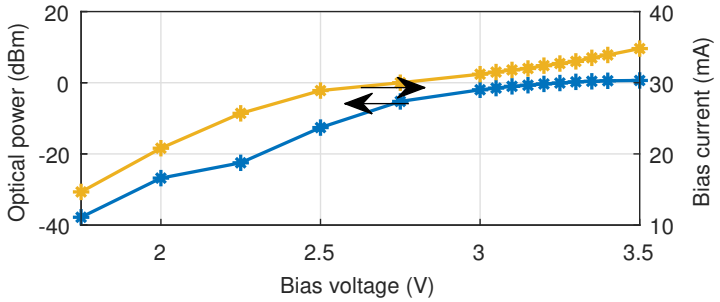

Figure 3.8. Bias voltage vs. coupled optical power of the VCSEL after 1 m GI-POF.

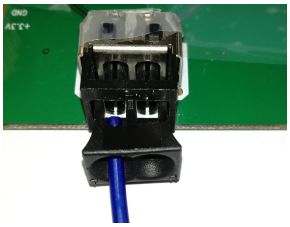

Figure 3.9. OptoLock connector mounted on the VCSEL and the POF in blue.

bands, the POF link attenuation in these bands is between 7 and 14.8 dB. For instance, band 8 has a loss of 7.8 dB compared with the first LTE-A band (band 31). The reason of this electrical attenuation is explained by the limited power budget of the optical link and the limited bandwidth of the optical receiver.

3.2.2 Noise figure

The NF of a linear system having SNR_{in} and SNR_{out} as the SNR at the input and output, respectively, is defined as follows [68]:

$$NF[dB] \triangleq SNR_{in}[dB] - SNR_{out}[dB] \tag{3.2.2}$$

for NF measurement, the method used is described in [69]. The noise power spectral density of the optical link in the $\mathrm{i_{th}}$ band ($N_{0,i}[dBm/Hz]$) is measured as

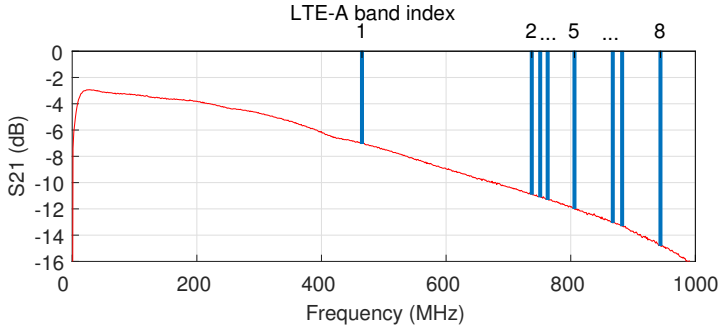

Figure 3.10. 20 m POF link $S21$, -3 dB bandwidth and attenuation experimental results.

the power spectral density at the optical link output when the input is terminated by a 50 Ω impedance. Given the gain $G_{POF,i}$[dB], the $NF_i[dB]$ is calculated by

$$NF_i[dB] = 10 \cdot log_{10}\left(\frac{N_{0,i}[W/Hz]}{G_{POF,i} \cdot T_0 \cdot k}\right) \tag{3.2.3}$$

$$= N_{0,i}[dBm/Hz] - 10 \cdot log_{10}\left(\frac{T_0 \cdot k}{1\,\mathrm{mW}}\right) - G_{POF,i}[dB] \tag{3.2.4}$$

where T_0 and k are the room temperature of 290°K and the Boltzmann constant in J/K, respectively, and $N_{0,i}[dBm/Hz]$ is between -130 and -133 dBm/Hz in all the cases. As shown in Figure 3.11, the noise figure is between 50 and 56 dB for all the LTE-A bands, in particular, the NF change is equal to the gain variation as described in (3.2.4). Furthermore, the POF link introduces an attenuation for all the LTE-A bands. The attenuation is equal to a negative gain $G_{POF,i}[dB]$ in (3.2.4), which therefore increases the NF and explains such high NF values.

3.3 Early multi-format transmission

The frequency response of the 20 m POF link in section 3.2.1 showed that even having a limited bandwidth, the blunt roll-off of the optical link allows transmitting narrow band LTE signals at frequencies higher than the 3 dB cut-off frequency. In the following experiment, the first simultaneous transmission of a digital baseband signal and a multiband LTE is demonstrated and discussed.

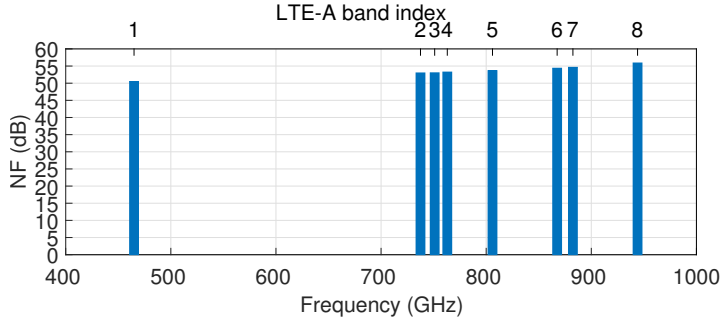

Figure 3.11. Noise figure of the 20 m POF link.

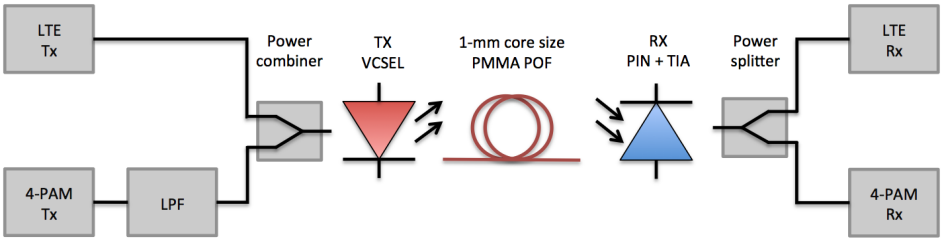

Figure 3.12. Block diagram of the transmission setup.

3.3.1 Experimental setup

The transmission testbed is shown in Figure 3.12. The baseband signal of 4-PAM symbols is created offline in Matlab using a pseudorandom binary sequence (PRBS) of 2^7-1 bit and repeated to create a bit sequence of 409 kb, then the bits are coded in the 4-PAM symbols by Gray coding. The electrical signal is generated by a Tektronix 7122B arbitrary waveform generator (AWG) and is low-pass filtered. No equalization or precoding is used.

The aim is to maximize the number of transmitted LTE bands, avoiding frequency up/down shifting, bands overlapping, and maximizing the baseband bit rate. Following these criteria, 3 downlink bands are available between 800 MHz and 1 GHz and generated by a Keysight MXG N5182B vector signal generator (VSG), as listed in Table 3.5. In order to maximize the bit rate, only the highest

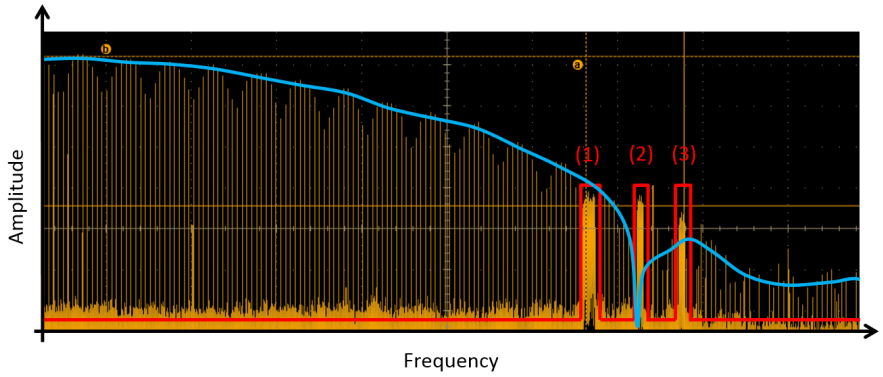

Figure 3.13. Signal at the TIA output after the optical back-to-back (oB2B) link formed by the 4-PAM filtered spectrum (blue line) and LTE signals (red line), band 20 (1), band 5 (2) and band 8 (3).

standardized LTE bandwidth and modulation order are considered.

The 4-PAM signal and the LTE-A bands are multiplexed in the frequency domain. Hence, the interference provided by the baseband signal is reduced by a low-pass filter (LPF) Mini-circuit SLP-750 and with nominal -3 dB cut-off frequency of 770 MHz, which is chosen to be lower than the first LTE band carrier frequency [70]. To ensure the multiband transmission is of paramount importance to limit the out-of-band interference between the signals. 4-PAM signal provides a considerable interference to the LTE bands, due to the poor attenuation of the electrical filter, which is equal to 5, 13, and 20 dB in the LTE-A bands 20, 5, and 8, respectively. Hence, the LTE-A bands are placed around the first notch frequency of the 4-PAM spectrum in order to further limit the PAM interference, as shown in Figure 3.13. In particular, the notch frequency of the main lobe of the 4-PAM spectrum is matched with the LTE-A band 5. Then, the 4-PAM and the RF signals are combined by an electrical power combiner and transmitted over short length GI-POF links similar to the one described in section 3.2.

At the POF link output, the electrical signal is divided by an electrical power splitter, the first output is connected to a Tektronix 72304DX digital phosphor oscilloscope (DPO) and acquired by Matlab. Here, the LTE signal is filtered by

Table 3.5. LTE bands used during the test and their main parameters.

LTE band number	20	5	8
Downlink channel (MHz)	791-821	869-894	925-960
Bandwidth (MHz)	20	10	10
Modulation format	64-QAM		

Table 3.6. Notch filter parameters used in the baseband receiver.

Parameter	Value		
Central frequency (MHz)	806	881.5	942.5
Band-stop bandwidth (MHz)	25	15	

four digital filters: a LPF with cut-off frequency equals the symbol-rate and three band-stop filters as described in Table 3.6. The second output of the power splitter is connected to the LTE receiver, consisting of a Keysight MXA N9020A vector signal analyzer.

3.3.2 Experimental results

The LTE signals are inserted around the first notch frequency of the 4-PAM spectrum, which limits the bit rate between 1.6 and 1.8 Gb/s. The optimum baseband bit rate in the electrical back-to-back (eB2B) link is equal to 1.8 Gb/s. The 4-PAM transmission is below the forward error correction (FEC) bit error rate (BER) threshold of 1×10^{-3} for the oB2B, 20 m and 35 m POF links.

The LTE signal is transmitted firstly over an oB2B link to evaluate the influence of the optical devices. Then, the distance is increased to 20 and 35 m, and the eB2B EVM value measured beforehand is equal to 0.9%. As illustrated in Figure 3.14, in the oB2B case, the EVM is slightly higher, up to 2%, which suggests a small penalty introduced by the optical link compared with the eB2B. After the transmission over 20 m POF, the EVM increases of 1.5% and for the 35 m case, the EVM significantly rises from 6.32% for the band 20 and up to 10.4% for band 5. This sharp increase in EVM values is largely attributed to the low received power, which is very close to the receiver's sensitivity. Therefore, the maximum achievable distance for these 3 LTE bands, even without 4-PAM signal is between

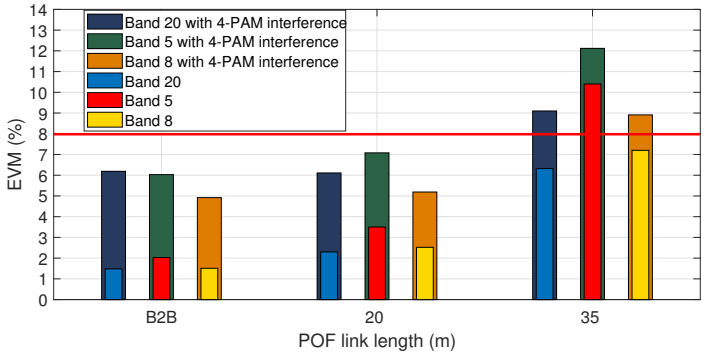

Figure 3.14. LTE EVM values for different link lengths.

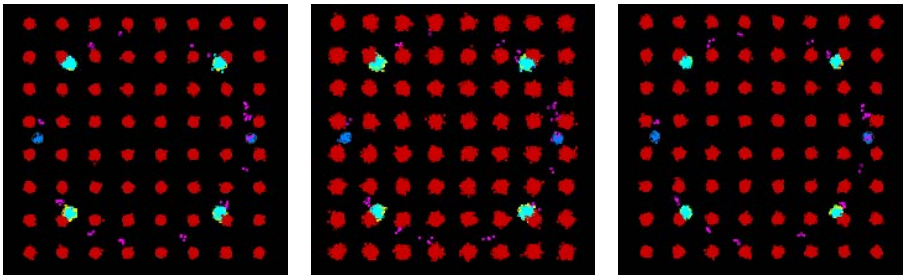

(a) (b) (c)

Figure 3.15. Constellation diagrams for 20 m POF of band 20 (a), 5 (b) and 8 (c) without 4-PAM interference. The user downlink channel with 64-QAM (red marks) and control channels (other colors) are shown.

20 and 35 m. As shown in Figure 3.15, among the different bands, the quality of the received signal varies. In all cases, band 20 and 8 have better performance than band 5, which is shown by the larger spread of symbols in the constellation plots of band 5 (see Figure 3.15b) with respect to band 20 and 8 (see Figure 3.15a and 3.15c, respectively). The reason for this unequal performance is the spectral response of the system.

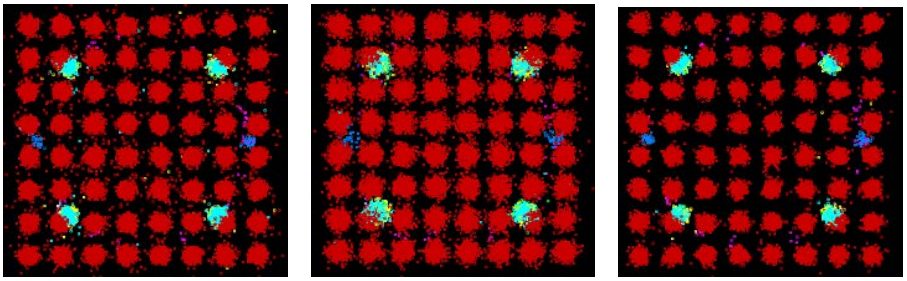

(a) (b) (c)

Figure 3.16. Constellation diagrams for 20 m POF of band 20 (a), 5 (b) and 8 (c) with 4-PAM interference. The user downlink channel with 64-QAM (red marks) and control channels (other colors) are shown.

In case of simultaneous transmission, the 4-PAM transmission achieves a BER lower than 1×10^{-3} up to 35 m. The LTE performance in the presence of 4-PAM interference is also considered, as depicted in Figure 3.14 (see the first three items in the legend), the EVM increases with the fiber length, more rapidly between 20 and 35 m. In this scenario, LTE band 5 is the most affected band by the presence of 4-PAM. At 20 m, all three LTE bands still comply with the EVM requirement for good transmission. However, at 35 m no single LTE band shows a good performance although bands 20 and 8 are 1% above the threshold. Figure 3.16 shows constellations of all three LTE bands at 20 m, the constellation points are more spread for band 5, confirming the higher EVM value compared with band 20 and 8. Since the received power after 35 m is very close to the receiver sensitivity, one aspect that may help in decreasing their EVM values is to improve the power budget, so that the received power no longer affects the performance evaluation.

3.4 Baseband signal filtering and LTE signal pre-equalization

The configuration presented in section 3.3 needs careful spectrum control in order to position the LTE bands around the 4-PAM frequency notch. The proposed electric filter could not avoid the 4-PAM interference on the LTE signals. The

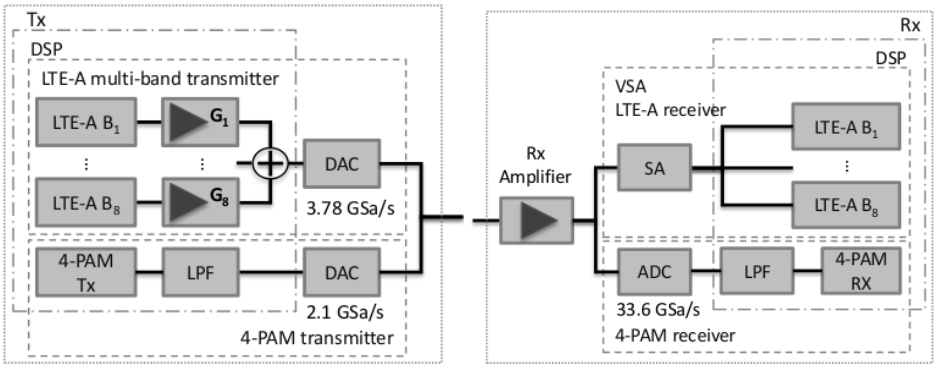

(a) (b)

Figure 3.17. Experimental setup diagram consisting of the transmitter (a) and the receiver (b).

introduction of finite impulse response (FIR) filtering achieves higher selectivity and decreases the 4-PAM interference over the LTE signal. Furthermore, allows using software-defined radio (SDR) to tune the filter parameters and ultimately to effectively transmit multiple LTE bands.

3.4.1 Experimental setup

This experiment aims to maximize the number of transmitted LTE-A bands, hence 8 LTE-A bands with the downlink channel carrier frequency between 460 MHz and 960 MHz are transmitted, as listed in Table 3.7. As shown in section 3.3, the LTE performance varies with the band carrier frequency and depends on the frequency response of the POF link. Given the wider range of carrier frequencies used in this experiment and the large variation of the POF link attenuation over the frequencies (as shown in Figure 3.10), a further degradation of the performance is expected. A straightforward solution is to pre-amplify the multiband signal. In this case, the band at highest frequency would still be the most penalized. Hence, equalization of individual channels by signal processing is required to flatten the power spectrum after the POF link. The equalization is carried out by digital signal processing through the tailored amplification of band B_i by gain G_i, which is chosen in order

Table 3.7. LTE-A bands and main parameters.

Band	31	12	13	14	20	18	19	8
Index i	1	2	3	4	5	6	7	8
Carrier frequency f_{DW} (MHz)	465	738	751	763	806	868	883	944
Bandwidth B_w (MHz)	5		10		20		15	10
Modulation format	64-QAM							
Band gain G_i (dB)	-3		0		3		4	2

to have the same received power spectrum. The equalization balances the low-pass frequency response of the link, which typically does not change over time once installed, hence the G_i tuning is performed only once. According to the LTE-A frequency allocation, the first 460 MHz band remains unused, allowing us to fill this by the baseband signal. Consequently, the LTE-A and 4-PAM signals are sent to two AWGs working as DACs and the outputs are combined. The obtained signal is directly modulated in the 20 m POF link, the same as described in section 3.2. The output signal of the optical receiver is amplified by 19 dB and acquired by either the baseband or the LTE-A receiver, as shown in Figure 3.17. The baseband receiver consists of a digital sampling scope functioning as an ADC at 36.6 GS/s, a digital LPF with the same bandwidth as in the transmitter, and the 4-PAM receiver. The LTE-A signals are received and processed by a vector signal analyzer (VSA).
The performances are measured over the eB2B, oB2B, and 20 m links, respectively, having the same received power in all the three cases.

DSP filters

A digital filter is implemented in the transmitter in order to reduce the interference of the 4-PAM signal on the LTE-A bands. As shown in Table 3.8, the stopband edge frequency is set in accordance with the lowest transmitted LTE-A carrier frequency. The passband frequency is maximized in order to give the broadest bandwidth to the 4-PAM signal, so, the transition bandwidth is equal to 25 MHz, as shown in Figure 3.18a. The attenuation of the stopband is set to 100 dB to minimize the 4-PAM out-of-band emission. Further tests show that the out-band

Table 3.8. Transmitter digital filter parameters.

Filter type	Low-pass
Passband edge frequency	700 MHz
Stopband edge frequency	725 MHz
Stopband attenuation	100 dB
Passband ripple	0.5 dB
Sampling rate	2.55 GS/s
FIR type	Direct form
Stable	yes
Linear phase	yes
Number of multipliers	655
Window type	Kaiser

emission is also related with the noise introduced by the DAC, which cannot be reduced by DSP filtering. Therefore, a second electrical LPF with -3 dB cutoff frequency of 800 MHz is used to reduce the DAC noise. The DSP filter sampling rate depends on the 4-PAM bit rate as follows:

$$SR_{tx}[S/s] = OF_{tx} \cdot \frac{Br}{log_2 M} \tag{3.4.1}$$

here OF_{tx} is the oversampling factor used in the transmitter, Br is the bit rate of the 4-PAM signal, and M is the number of PAM levels (i.e. $M = 4$). The choice of the OF_{tx} and the narrow transition bandwidth leads Matlab to generate a FIR filter with 655 multiplications, which can be decreased by using a multistage FIR type instead of direct form.

On the receiver side, a second digital FIR filter is implemented in the 4-PAM receiver, which removes the LTE-A signals from the 4-PAM signal before decoding it. As shown in Table 3.9, the stopband frequency, passband ripple, and frequency are the same at the transmitter filter, meanwhile the stopband attenuation is reduced to 50 dB as shown in Figure 3.18b, in order to decrease the filter complexity. The sampling rate SR_{rx} is the same used by the DPO for the acquisition, given the

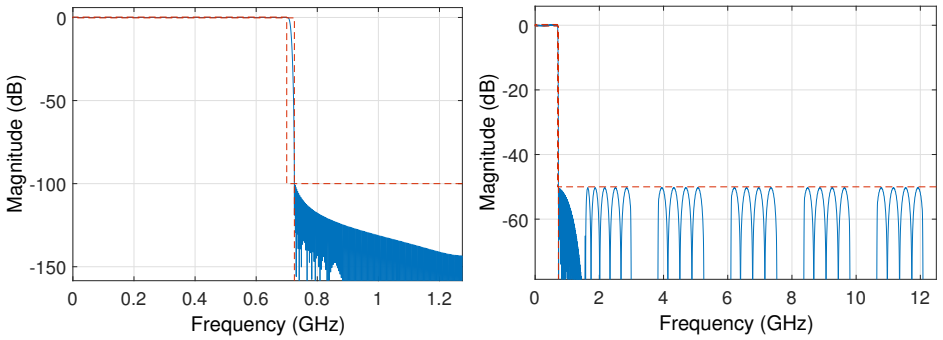

Figure 3.18. Magnitude and phase response of the transmitter (a) and receiver (b) filters.

limited set of sampling rate available in the DPO, SR_{rx} is calculated as follows:

$$SR_{rx}[S/s] \geq SR_{tx} \cdot OF_{rx} \tag{3.4.2}$$

where OF_{rx} is the receiver oversampling factor equals to 8. As defined in Table 3.8, the SR_{tx} is equal to 2.55 GS/s, then SR_{rx} is equal to 20.4 GS/s, which is rounded to 25 GS/s, the closest sampling rate available in the DPO. The high sampling rate is required in order to perform the cross-correlation needed to recover the received bits and calculate the BER. Nevertheless, the sampling rate can be decreased by avoiding the cross-correlation and instead using a low sample rate symbol timing recovery algorithm, such as Gardner's algorithm for 4-PAM [71]. The FIR cannot be designed with direct form since the number of multiplications would be equal to 2930, which requires a long computation time in order to process the signal. Instead, a multistage filter with a cascade of 2 stages filter is implemented and the number of multiplications is reduced to 262.

3.4.2 Experimental results

The LTE-A multiband signal is transmitted over the eB2B, oB2B, and over the 20 m GI-POF link, as depicted in Figure 3.19, the eB2B EVM is always lower than

Table 3.9. Receiver digital filter most significant parameters.

Filter type	Low-pass
Passband edge frequency	700 MHz
Stopband edge frequency	725 MHz
Stopband attenuation	50 dB
Passband ripple	0.5 dB
Sampling rate	25 GS/s
FIR type	Cascade - 2 stages
Stable	yes
Linear phase	yes
Number of multipliers	262

3.3%. Generally, all the transmitted LTE-A bands have similar EVM values, due to the equalization technique implemented, except bands 31 and 8, which have better performance.
Next, the oB2B link is considered, the maximum EVM value is 4.7% (band 18). Moving to the 20 m link, that value increases up to 6.5% (band 18). In all the cases, band 18 has a slightly higher EVM than the remaining bands, most probably due to the proximity to band 19.

The 4-PAM performance is evaluated over the oB2B and 20 m links, and the pre-FEC BER threshold is equal to 1×10^{-3} is considered. As depicted in Table 3.10, the oB2B and 20 m transmission achieve a bit rate of 1.56 Gb/s and 1.52 Gb/s, respectively.

Finally, the 4-PAM baseband and the 8 LTE-A signals are transmitted simultaneous, hence, crosstalk between them could arise which may influence the system performance. The main system parameters of the 4-PAM and LTE-A signals are kept the same. In the presence of LTE-A, the baseband bit rate decrease to 1.4 Gb/s, as depicted in Table 3.10 and this value still corresponds to error-free operation with FEC. This result suggests that a minor impairment on the PAM signal is caused by the LTE-A signals.
Next, the LTE-A performance in the presence of the 4-PAM signal is consid-

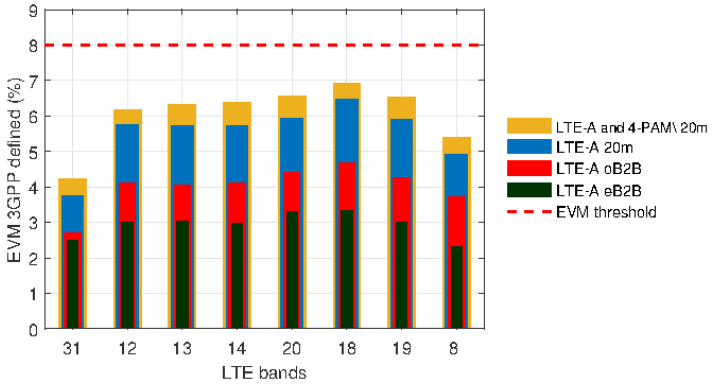

Figure 3.19. LTE-A EVM results for the eB2B, oB2B, and 20 m GI-POF link, the bands are according to Table 3.7.

Table 3.10. 4-PAM transmission experimental results.

Link	Bitrate (Gb/s)	BER ($\times 10^{-4}$)
oB2B	1.56	5.9
4-PAM over 20 m	1.52	6.6
4-PAM+LTE-A over 20 m	1.4	7.7

ered. As depicted in Figure 3.19, the EVM of all the bands increases up to 6.9% (band 18), slightly higher than without the 4-PAM case. However, the overall EVM values remain below the 8% threshold. In particular, the nearest-neighbor LTE-A band to the 4-PAM spectrum (i.e. band 31) has a negligible EVM increase. This suggests a good out-of-band interference suppression between the LTE-A and PAM spectra, as is also confirmed by the constellation diagrams in Figure 3.20a and 3.20b. In addition to the nearest neighbor, Figure 3.20c and 3.20d show the signal constellations of one of the farthest neighbors of the 4-PAM signal, i.e. band 18, which look very similar with and without the PAM signal.

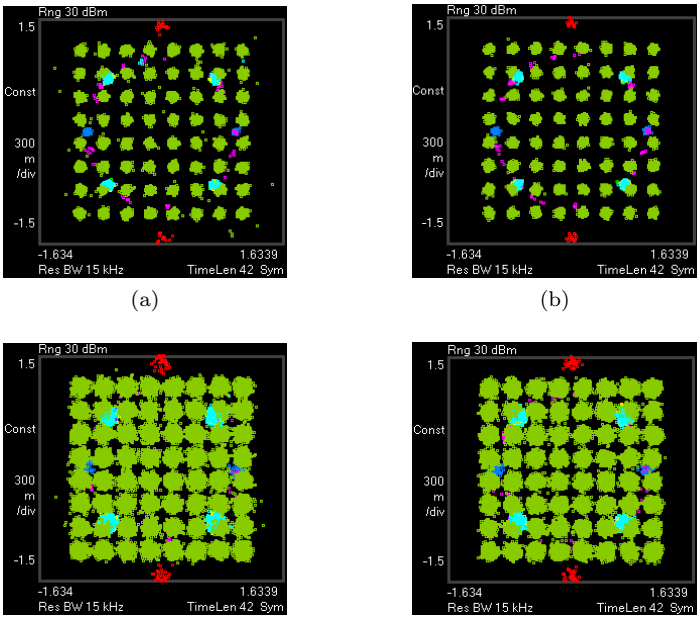

Figure 3.20. Received constellations of LTE-A for (a) with and (b) without 4-PAM for band 31. The constellation of band 18 is depicted in (c) with and (d) without 4-PAM. The user downlink channel with 64-QAM (green marks) and control channels (other colors) are shown.

3.5 Optical link budget and bandwidth improvement

In section 3.2 the transmitted optical power and the optical link bandwidth are measured and section 3.3 shows that the optical transmitter launched power and the receiver bandwidth are the two major limitations to improve the optical link length and the number of radio signals transmitted. The VCSEL transmitted power is constraining the link length to 20 m, while the p-i-n bandwidth is the bottleneck of the POF link. In this section, the optical transmitter and receiver are changed in order to ensure a higher power budget and broader bandwidth. Fur-

thermore, both SI and GI POFs are used, the first ensures lower losses and higher power budget, the latter higher bandwidth distance product and bandwidth.

3.5.1 Experimental setup

The general setup is shown in Figure 3.21, here a low-cost FP EE-LD with emitted optical power of 5.7 dBm at a wavelength of 650 nm is used. The coupling loss is measured equal to 1 dB. The laser driver was designed and provided by POF-AC with limited datasheet in which no characterization is provided. According to the available information, the embedded EE-LD is a Union Optronics Corp. U-LD-650571A[iii] [72]. The laser driver integrates a 10 dB monolithic microwave integrated circuit (MMIC) amplifier, and a ball lens is mounted on the LD case to improve the optical coupling.
The optical link is an IM-DD system, the POFs used are 35 m long with 1 mm core diameter PMMA Optimedia GI-POF and ESKA GH-4001 standard SI-POF. The experiment uses a new optical receiver, which is a Graviton SPD-2 with a FC connector, consisting of a p-i-n photodiode followed by a TIA. The bare fiber is plugged into the Graviton FC connector without any connector. According with the specifications, the -3 dB bandwidth is equal to 1.1 GHz and the maximum allowed input power is -4 dBm [73], hence a back-off of 2 dB is used to have the maximum level of -6 dBm.

The frequency response of the two links is measured according with the procedure in section 3.2.1 and the results are shown in Figure 3.22. The GI and SI POF -3 dB bandwidth is equal to 1.1 GHz and 365 MHz, respectively. Hence, 12 LTE-A bands are transmitted over the GI-POF link, as listed in Table 3.11. Regarding the SI-POF link, the subset of 7 LTE-A bands (band 1, ..., band 7) is chosen. The equalization technique already implemented in section 3.4 is here further exploited, the gain or attenuation of the POF link in the transmitted LTE-A bands is used as starting value for the equalizer taps tuning. The two links, even having different frequency response, provide similar relative gain or attenuation between the LTE-A bands, hence the same set of equalizer tap can be used.
The LTE-A bands are generated offline, equalized, combined in the digital domain, and then sent to an AWG.

According to the LTE-A bands allocation, the frequency range up to band 1 (i.e. 733 MHz) is unused. In this interval, a PRBS 2^7-1 data sequence is offline

[iii] Former model code SLD-650-P5.

Table 3.11. LTE bands used in the experiments and their most significant parameters.

Parameter	Value											
Band index i	1	2	3	4	5	6	7	8	9	10	11	12
Carrier frequency (MHz)	738	751	763	806	868	883	944	1474	1542	1843	1862	1963
E-UTRA operating band	12	13	14	20	18	19	8	32	24	3	9	25
Bandwidth (MHz)	10			20		15		10	20	10	20	
Gain of the digital transmitter amplifier G_i (dB) GI link	0			3		4	2	6	5		8	
G_i (dB) SI link	0		3		4		2	-	-	-	-	-
Modulation format	64-QAM											

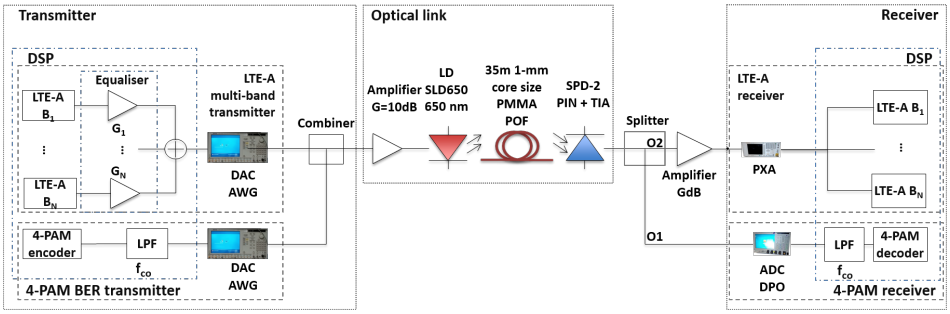

Figure 3.21. Block diagram of the transmission setup with 7 (N=7) and 12 (N=12) LTE-A bands for the SI-POF and the GI-POF link, respectively.

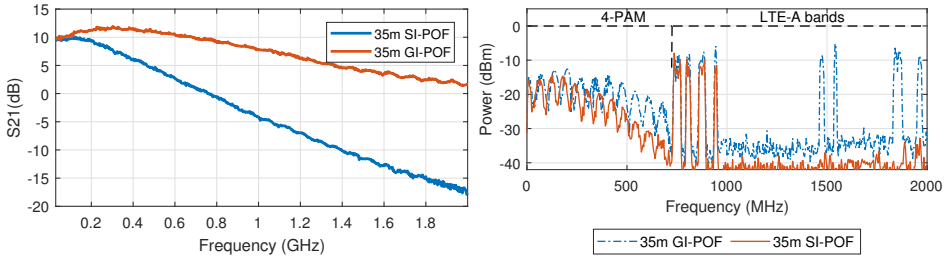

(a) (b)

Figure 3.22. GI and SI POF frequency responses (a), simultaneous transmission spectra (b) at the LTE-A receiver input after the GI-POF (dashed blue line) and SI-POF (solid orange line).

encoded by 4-PAM modulation and further processed. The symbol sequence is filtered by a digital LPF with a cut-off frequency (f_{co}) of 700 MHz as described in Subsection 3.4.1. Subsequently, the baseband signal is generated by a second AWG.

As shown in Figure 3.21, the electrical output of the optical receiver is fed into an amplifier with a gain G. G is optimized on both links and is equal to 29 dB and 26 dB for the SI and GI POF links, respectively. The signal is then acquired by

either the baseband 4-PAM or the LTE-A receiver as explained in Subsection 3.4.1.

3.5.2 Experimental results

As a reference, the individual transmission of the 4-PAM and LTE-A signals is evaluated for both the links. The received spectrum is analyzed as shown in Figure 3.22b. Over the GI -POF, the 4-PAM signal is limited by the transmitter LPF, while over the SI-POF it is distorted due to the lower SI-POF bandwidth. Looking to the LTE-A, in both the cases all the bands have similar power, on account of the equalization, which balances the higher losses for the higher frequencies.

Let us consider the GI-POF link first. The 4-PAM maximum bit rate is 1.9 Gb/s and 2 Gb/s with and without LTE-A co-transmission, respectively. Therefore, the difference is minimal, which suggests the LTE-A crosstalk is negligibly affecting the 4-PAM throughput. Next, the solitary LTE-A transmission is considered, as shown in Figure 3.23a. Over the eB2B link the EVM is lower than 3%, and the higher frequency bands have a better performance because the equalization is enabled. Moving to the 35 m link, the maximum EVM is 5% (band 12). Moreover, the bands from band 8 to band 12 have slightly higher EVM increment, up to 2% (band 12), than the first 7 bands. This increase is related with the low-pass behavior of the link, which is not fully balanced by the equalization. When the 4-PAM signal is co-transmitted, the EVM increases up to 6.5% (band 12). Furthermore, the EVM performance slightly depends on the band, the first 9 LTE-A signals have a smaller EVM increase than the last three. Nevertheless, the EVM growth related with the 4-PAM transmission is relatively small. In summary, all the 12 LTE-A bands have the EVM value smaller than the threshold.

Next, the SI-POF link is analyzed, the 4-PAM bit rate is equal to 1.7 Gb/s with and without the LTE-A co-transmission. Also in this case, the baseband throughput is bandwidth-limited, thus the bit rate does not increase by boosting the transmitted power. However, the SI-POF link limits the bandwidth and introduces the distortion, while in the GI-POF link the bandwidth is limited on purpose by the LPF in the transmitter. Considering the LTE-A transmission, as shown in Figure 3.23b, the EVM over the eB2B is lower than 3%, as the previous eB2B test, the EVM is lower for the highest bands due to the equalization, which is done for the complete system. Moving to the 35 m link, the maximum EVM is 4.6% (band 6), and here the increase is mainly caused by two factors. Firstly,

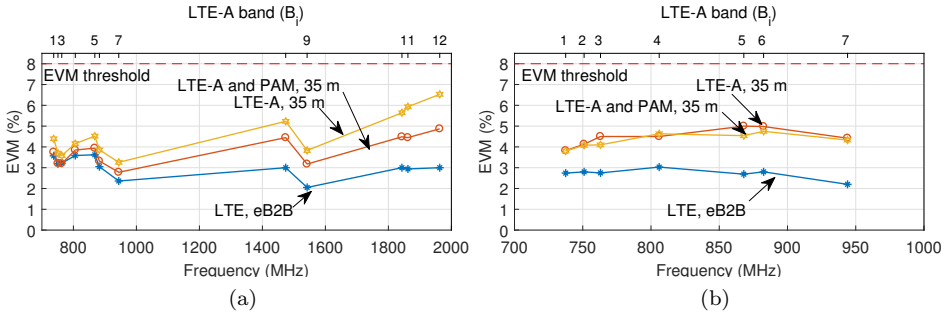

Figure 3.23. LTE-A EVM results for the GI -POF (a) and SI-POF (b) link for the eB2B and 35 m, with and without 4-PAM transmission, the bands B_i are according to Table 3.11.

for the lower frequency bands, the noise added by the optical link degrades the performance. Secondly, for the high frequency signals, together with the added noise, the equalization only partially balances the low-pass behavior of the link in comparison to the GI -POF. When the 4-PAM signal is co-transmitted, the LTE-A EVM remains almost the same (less than 1% increase) for all the bands as compared to the solitary transmission. In summary, all the 7 LTE-A bands have an EVM lower than the threshold of 8%.

3.6 Optical and wireless transmission

The previous section showed how the improved GI-POF link provides the required A-RoF multiband transmission capability up to 35 m length. Here, the radio signals are further wirelessly transmitted in order to test the end-to-end link from the femtocell base station to the mobile device.

3.6.1 Experimental Setup

The multiple standard-compliant LTE-A bands are generated with the parameters listed in Table 3.12. As shown in Figure 3.24, the LTE-A signals are created, equalized by tailoring the amplifier gains (G_i), as explained in Subsection 3.4, combined,

Table 3.12. LTE-A transmitted bands and their most significant parameters.

Index i	12	13	14	20	18	19	8	32	24
Carrier frequency (MHz)	738	751	763	806	868	883	944	1470	1540
Bandwidth (MHz)		10		20	15		10	20	10
Gain of the digital transmitter amplifier G_i (dB)		0		3		4	2	6	4.5
Modulation format	64-QAM								

and sent to the DAC. The baseband signal and LTE-A signals are electrically combined and sent over the optical link described in section 3.5. The optical signal is then transmitted over 35 m of GI-POF and the received optical power is limited to -5.2 dBm for the oB2B and 35 m links. After the optical link the signal is split. The first splitter output (O1) is connected to the baseband receiver, which consists of the ADC, a FIR LPF with cut-off frequency f_{co}, and the 4-PAM receiver. The second splitter output (O2) is connected to the antenna amplifiers. A cascade of two amplifiers is chosen to boost the LTE-A signal power up to 10 dBm, as shown in Figure 3.24. Before the wireless transmission the baseband signal must be removed, hence a high-pass filter (HPF) with cutoff frequency f_{co} is implemented. The amplified and filtered signals are then transmitted through the antenna.
The selected off-the-shelf antennas shown in Figure 3.25a have broadband capability in order to transmit all the radio signals received from the optical link. Their $S11$ is measured and shown in Figure 3.25b, the antenna is considered to have a matched impedance when the $S11$ is small enough (i.e. lower than -15 dB), which occurs in the frequency range 700-1520 MHz and 2270-2700 MHz. According with the specification the gain is 3 dBi between 700 MHz and 2.7 GHz [74]. An estimation of the wireless link loss is made with the free-space Friis equation, aiming at a minimum received power at (Pt. A in Figure 3.24) of -20 dBm, from the equation a 3.5 m link length seemed to be feasible. The wireless transmission is performed indoor on a line-of-sight (LOS) and a non-line-of-sight (NLOS) link. The obstacle used in the NLOS link is a person of middle size placed in the innermost Fresnel zone [75]. The receiver antenna is connected to the front-end and then to the LTE-A receiver.

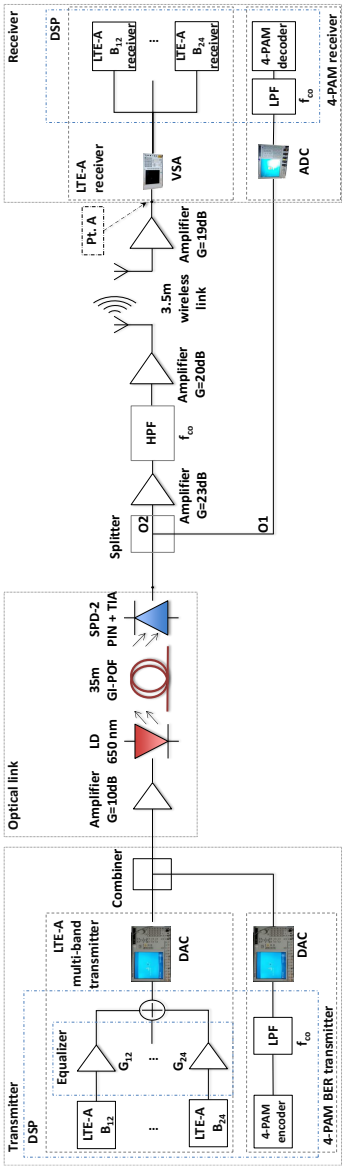

Figure 3.24. Experimental setup block diagram.

(a)

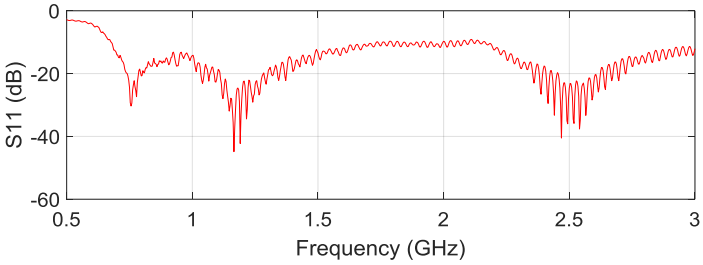

(b)

Figure 3.25. The antenna used for the wireless test (a) and its $S11$ (b).

3.6.2 Experimental results

As a reference, the individual transmission of the 4-PAM signal and LTE-A signal for the oB2B link are evaluated. The oB2B performance of the 4-PAM transmission achieves 2 Gb/s. Moving to 35 m link, the bit rate does not decrease and no further reduction is provided when the LTE-A bands are co-transmitted. Next, the LTE-A signals are considered. Since wireless transmission is involved, the presence of interference in the received signal must be studied. As shown in Figure 3.26, the LTE-A bands 13, 20, and 8 suffer from interference. According to the European frequency allocation plan, the interferences are provided by TV broadcasting in the two bands 746-762 MHz and 781-820 MHz and cellular transmission on band E-GSM in the range 918-963 MHz.
Next, the received signals after the 3.5 m LOS and NLOS propagation are analyzed. All the bands have a sufficient signal-to-interference-plus-noise ratio (SINR), except for band 8, which is influenced by the interference.
The EVM performance is now considered. As listed in Table 3.13, the solitary LTE-A multiband transmission over the oB2B or 35 m followed by the 3.5 m LOS link shows no major EVM difference. 8 bands out of the 9 transmitted have good performance ($EVM < 8\%$), thanks to the equalization technique implemented. Band 13, 20, and 8 have the highest EVM, most probably due to the interference, while, bands 32 and 24 have the best performance in all the cases. When the 4-PAM signal at 2 Gb/s is co-transmitted, the LTE-A EVM slightly rise and 7 bands out of 9 have good performance. Finally, on the NLOS link 6 LTE-A bands

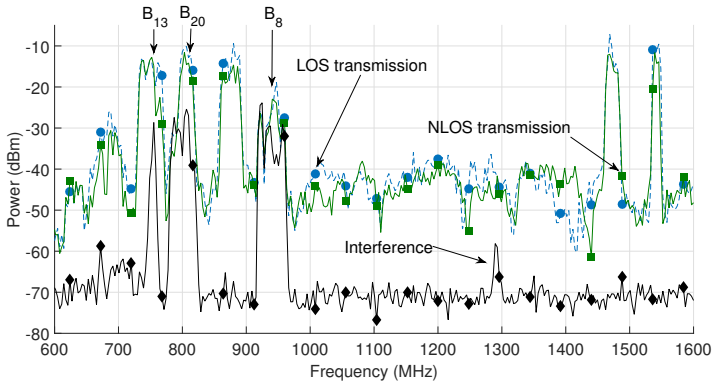

Figure 3.26. LTE-A received spectra at Pt. A of the link together with the received interference.

have EVM lower than the threshold and the EVM increases at maximum of 2.5% (band 18) with no increase for band 32 and 13, which suggests a minor impairment caused by the obstacle.

3.7 Study and characterization of the 50 m GI-POF link

In the previous sections the length is increased from 20 to 35 m, which is satisfactory for the deployment is small houses. The extension of the POF link length to 50 m allows to match the requirement of the current Gigabit Ethernet over POF standard and furthermore to install the fiber also in larger buildings. The optical link is shown in Figure 3.21 and is the same as described in section 3.5, with the received optical power at the SPD-2 photodiode equals -8.5 dBm, including the coupling losses. In the following subsections, the frequency response of the link is measured up to 2.4 GHz, in order to test the feasibility of the POF link to transmit the WLAN signals in the 2.4 GHz ISM band. Hence, the frequency response is used to calculate the link budget and the NF.

Table 3.13. LTE-A EVM results the bands EVMi are according to Tab. 1, the EVM higher than 8% are underlined.

Wireless link	Wired link	Transmitted signals	i	12	13	14	20	18	19	8	32	24
LOS	oB2B	LTE-A		4.3	7.4	5.5	7.6	5.9	5.0	$\underline{>10}$	5.0	4.0
LOS	35 m GI-POF	LTE-A		4.7	7.4	5.3	7.6	5.6	4.6	$\underline{>10}$	4.8	4.2
LOS	35 m GI-POF	LTE-A and 4-PAM		5.3	7.6	5.1	$\underline{8.3}$	6.5	5.0	$\underline{>10}$	5.0	4.2
NLOS	35 m GI-POF	LTE-A and 4-PAM		5.8	7.3	7.2	$\underline{9.4}$	$\underline{8.9}$	6.8	$\underline{>10}$	5.1	5.4

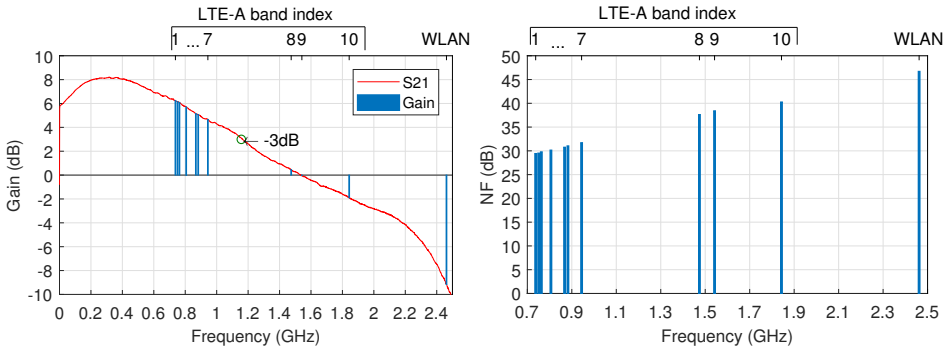

(a) (b)

Figure 3.27. 50 m POF link $S21$, -3 dB bandwidth and gain (a) and noise figure of the 50 m POF link (b) experimental results.

3.7.1 Link frequency response and gain

The frequency response and the gain are measured according with the procedure described in section 3.2.1. As shown in Figure 3.27a, the link frequency response resembles a LPF behavior, the -3 dB cut-off frequency is calculated as the frequency for which $S21$ is reduced of 3 dB compare to the $S21$ at direct current (DC).
The POF link gain is calculated separately for each LTE-A and WLAN band with carrier frequency 2.46 GHz and 40 MHz bandwidth and shown in Table 3.14. The average gain of the i_{th} band ($G_{POF,i}$) is computed as the average $S21$ within the band. As shown in Figure 3.27a, the gain of the first seven LTE-A bands is between 6 and 4 dB. The LTE-A bands 8 and 9 have a gain close to 0 dB, and the WLAN has an attenuation close to 9 dB. Hence, the power loss of the WLAN compared with the first LTE-A signals is close to 15 dB.

3.7.2 Noise figure

The NF of the link is calculated according with section 3.2.2, in which T_0 is still equal to 290°K and $N_{0,i}$[dBm/Hz] is equal to $-137\,\mathrm{dBm/Hz}$ in all the cases. As shown in Figure 3.27b, the NF is close to 30 dB for the first seven LTE-A bands,

around 40 dB for band 8 and 9, and 45 dB for the WLAN band. This NF variation is related with the link gain, the WLAN band has a lower gain compared with the first seven LTE-A bands, hence, given (3.2.4), the noise figure is higher.

3.8 Improved pre-equalization tuning based on the received SINR

The pre-equalization method proposed in section 3.4 has a main practical limitation. The pre-equalizer taps are tuned based on the LTE-A EVM results measured at the POF receiver, which is integrated in the RRU, as shown in Figure 2.10. The EVM measurement involves the decoding of all the LTE-A bands at the RRU in order to feed the EVM value back to the transmitter and tuning the tap. Such approach involves the integration of a multiband LTE-A signal receiver in the RRU, increasing its complexity.
Here the pre-equalizer taps are trained on the received SINR instead of the EVM, in this way at the RRU only the SINR is measured, involving much less complexity. Furthermore, the effect on the pre-equalization and optical link of transmitting a new radio signal is analyzed.

3.8.1 Experimental setup

10 LTE-A bands are generated in accordance with the parameters in Table 3.14, the LTE-A signals are created, equalized, combined, and then digital-to-analog converted, as shown in Figure 3.28. According to the LTE-A bands allocation, the spectrum up to 738 MHz is unused, in this frequency range the filtered 4-PAM is transmitted.

The baseband and LTE-A signals are combined and the signal peak-to-peak amplitude is kept under 160 mV_{pp}. The optical link is the one characterized in section 3.7 and the received optical power is -8.8 dBm. After the optical link, the signal is split, the output O1 in Figure 3.28 is connected to the baseband receiver, which consists of the DPO and the 4-PAM decoder as described in section 3.4.
The splitter output O2 in Figure 3.28 is connected to the RF front-end and the baseband signal is removed by a HPF with cutoff frequency f_{co}. A cascade of two amplifiers is chosen to boost the LTE-A signal power unequally between 7.6 dBm (band 3) and 12.4 dBm (band 10). The wireless transmission is performed over a 3.5 m indoor (i.e. unshielded mid-size room, with multi-path propagation) LOS

Table 3.14. LTE-A bands and main parameters.

Parameter	Value									
Index (i)	1	2	3	4	5	6	7	8	9	10
Carrier Frequency (MHz)	738	751	763	806	868	883	944	1474	1542	1843
E-UTRA operating band	12	13	14	20	18	19	8	32	24	3
Channel Bandwidth (MHz)	10			20	15		10	20	10	20
Gain of the digital transmitter amplifier G_i (dB)	0.4	0.2	0	3.5	4	4	1.3	0 to 15	5	10

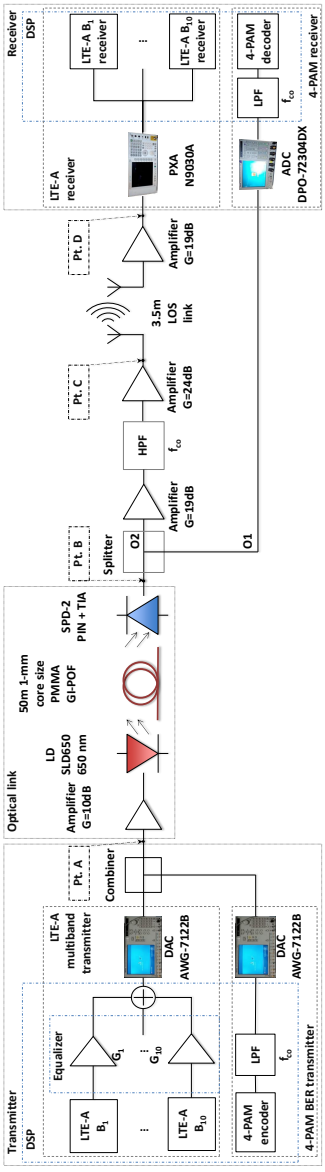

Figure 3.28. Experimental setup diagram and optical link frequency response.

link. The receiver antenna is finally connected to the front-end amplifier and then to the LTE-A receiver.

Equalization: As shown in Figure 3.28, the equalization is carried out by digital signal processing through the tailored amplification of each band i by gain G_i.

In the previous tests, the equalization optimization is based on the EVM parameter, a good balance of received EVM among the LTE-A bands is difficult to be reached and, secondly, assessment of the multiband LTE-A EVM requires the signal to be decoded. Here, the received SINR is used as reference parameter, which has the advantage to be immediately calculated from the radio LTE-A spectrum without the need to decode the signal and it gives directly the correction needed for the G_i.
The SINR of the $\mathrm{i_{th}}$ band is defined as follows:

$$SINR_{i,dB} = P_{Si,dBm} - 10 \cdot log_{10}\Big(\frac{N_{i,mW} + I_{PAMi,mW} + I_{WLi,mW}}{1 \cdot 10^{-3}}\Big) \quad (3.8.1)$$

where P_{Si} is the in-band power measured for the $\mathrm{i_{th}}$ band when all the LTE-A bands, the 4-PAM, and eventually the wireless channel interference signals are received. $N_i + I_{PAMi} + I_{WLi}$ is measured as the in-band power in the $\mathrm{i_{th}}$ band when the noise (N_i), the 4-PAM interference (I_{PAMi}), and the wireless channel interference (I_{WLi}) signals are received. I_{WLi} is null when the $\mathrm{SNIR_i}$ is measured before the transmitter antenna.

3.8.2 Experimental results

Firstly, the 4-PAM performance is considered, the solitary 4-PAM transmission achieves 1.9 Gb/s over oB2B and 50 m links with pre-FEC BER lower than 1×10^{-3}. When also the multiband LTE-A signal is co-transmitted, the bit rate has an insignificant decrease to 1.8 Gb/s over the 50 m link.

Secondly, the received SINR balancing between the LTE-A bands by the equalization is shown. Given several LTE-A bands transmitted over the POF link, when a new LTE-A band i is co-transmitted, its gain G_i has to be found. Here, band 8 is supposed to be a new band to be transmitted and the gain G_8 optimized.
As shown in Figure 3.29a, increasing G_8, the transmitted $\mathrm{SINR_8}$ improves but

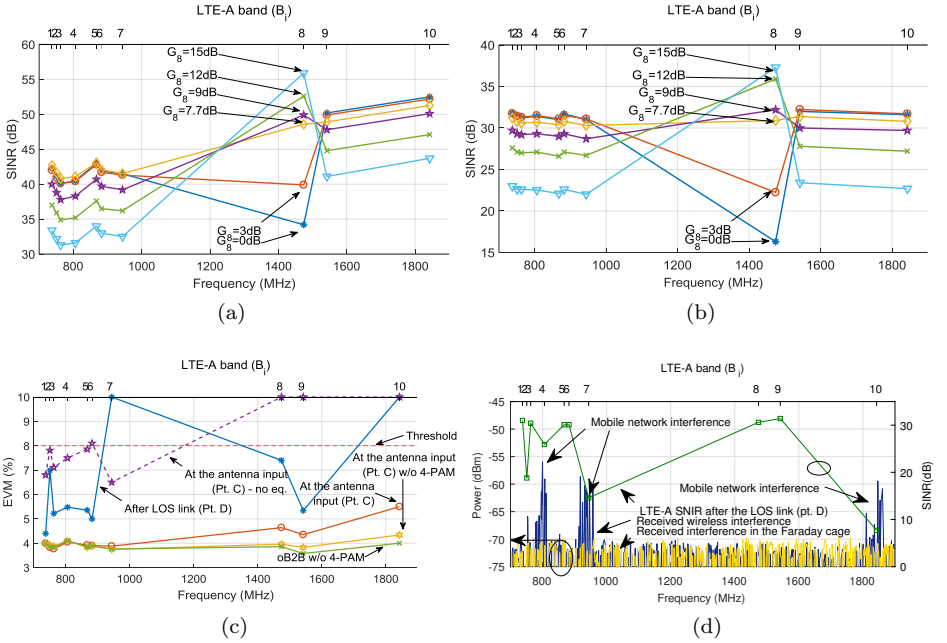

Figure 3.29. $SINR_i$ (for i=1,..., 10) measured at Pt. A (a) and Pt. C (b) of the link in Figure 3.28 for 0 $dB \leq G_8 \leq 15$ dB with the 4-PAM co-transmission. Measured EVM vs. frequency and band index (c). Measured SINR and power spectrum of the received interference at the antenna output and after the wireless link (d).

comes with the drop of the remaining transmitted $SINR_i$. As shown in Figure 3.29b, after the optical link, band 9 and 10, at 1.5 GHz and 1.8 GHz carrier frequency, have SINR similar to the lower frequency LTE-A bands between 700 MHz and 1 GHz, on account of the equalization. As depicted in Figure 3.29b, the optimum G_8 is equal to 7.7 dB.

Thirdly, the POF link LTE-A EVM is considered for the oB2B and 50 m. As shown in Figure 3.29c, when the LTE-A multiband signal is transmitted, the EVM is lower than 4.5% for the oB2B and 50 m link. When also the 4-PAM is co-

transmitted, the EVM is increased to 5.5% (band 10). The 4-PAM co-transmission affects mainly the bands 8, 9, and 10, which is not accounted by the SINR. The cause may be related with nonlinearity of the link, which cannot be measured by the defined SINR.

Fourthly, the impact of the equalization is shown by transmitting the LTE-A bands without equalization by setting G_i=0 dB for i=1,..., 10. The bands 8, 9, and 10 have EVM higher than 8% due to the low-pass behavior of the link. The remaining bands have an EVM increase between 2.5% (band 7) and 4% (band 6), reducing the margin for the wireless transmission.

Finally, the LTE-A EVM over the full-link, including the wireless channel is considered. As shown in Figure 3.29d, the bands 2, 4, 7, and 10 have a SINR penalty related with in-band interference given by the wireless link, which is not present when the measurement is repeated in the Faraday cage. According with the European table of frequency allocation, band 2 is used for "mobile/fixed communications", whereas bands 4, 7, and 10 are used by licensed mobile operators [76]. As consequence, as shown in Figure 3.29c, band 7 and 10 have EVM higher than 8% and 8 LTE-A bands are correctly received.

3.9 Summary

This chapter discusses in details the simultaneous transmission of a baseband 4-PAM signal and multiband LTE-A signal over a large core PMMA POF link by frequency division multiplexing scheme. The POF link feasibility to simultaneously transmit baseband and radio over fiber is studied and demonstrated. A-RoF technique is used to simplify the receiver architecture, but most of the LTE-A bands have carrier frequencies higher than the optical link bandwidth. Hence, a time-invariant pre-equalization method is demonstrated to stretch the frequency response of the POF link. The pre-equalization can be realized by a set of narrow band amplifiers with variable gain, one for each LTE-A band, having the gain optimized to pre-compensate the POF frequency response in each LTE band. The gain is calculated during the setup time and is not changed due to the time-invariant POF link frequency response. Hence, its implementation requires low-complexity components in line with the requirements of simplicity of POF in-home backbone. In section 3.1, a brief introduction on the OFDM coding scheme and its application in the RAT of LTE and LTE-A is given. Then in section 3.2, the first POF link based on VCSEL optical transmitter and p-i-n receiver is characterized. In

section 3.3, the simultaneous transmission of 3 LTE bands and 1.8 Gb/s 4-PAM baseband signal is demonstrated up to 20 m GI-POF link. The proposed method is based on careful frequency allocation of the LTE bands in the 4-PAM spectrum notches, which was difficult to scale to a large number of LTE bands and limit the 4-PAM throughput. The proposed electric filter did not avoid the 4-PAM interference on the LTE signals. The introduction of a DSP filter allows increasing the filter selectivity, reduces the 4-PAM interference, and furthermore allows tuning the filter parameters and ultimately to effectively transmit multiple LTE bands, as shown in section 3.4. Regarding the FIR filter complexity, a common reference parameter for the filter complexity is the number of multiplications, which determines then number of logical gates needed. The FIR filters implemented in section 3.4.1 requires up to 655 multiplications, which can be decreased by optimizing the FIR architecture [77]. Furthermore, the number of multiplications can be decreased by reducing the sampling rate through the implementation of low sample rate symbol timing recovery algorithm as discussed in section 3.4.1. The results showed that 8 LTE-A 64-QAM signals (with a total throughput of 479 Mb/s) and a 1.4 Gb/s 4-PAM signal can be transmitted simultaneously over 20 m of thick-core GI-POF using off-the-shelf POF transceiver.
For a bi-directional link, a two-fiber solution using separate fibers for the down and upstream is a realistic topology. Due to the short lengths in home networks, the cost of fibers will not be a major issue. Advanced optical components such as optical circulator, (de)muxers, and splitters/combiners which are common for silica fibers, are not available for POFs or they are available but too bulky and lossy [10].

The major disadvantage of the VCSEL based POF link is within the limited power budget, which bound the maximum link length to 20 m, far below the target distance of 50 m for a reliable in-home installation.
The optical link budget is increased by optimizing a second POF link based on high power EE-LD and more sensitive p-i-n photodiode. In section 3.5, the experimental demonstration of the co-transmission of a multiband LTE-A signal with a 4-PAM baseband signal over 35 m of GI-POF and SI-POF links is provided. The 12 LTE-A band signals (total throughput 910 Mb/s) and a 1.9 Gb/s 4-PAM signal are jointly transmitted over the GI-POF link and 7 LTE-A bands (total throughput 450 Mb/s) and 1.7 Gb/s are successfully transmitted over the SI-POF link.
The simultaneous transmission over the SI-POF showed lower interference of the 4-PAM signal over the LTE-A than over the GI-POF link, which can be related

with the lower 4-PAM bit rate. Improvement of the LTE-A performance over the GI-POF link can be achieved by a finer tuning of the equalization taps, in particular for the higher frequency bands.
Longer link length is possible for both GI and SI POF. In particular, the GI-POF link length extension is feasible by just increasing the link budget. Longer link length does not severely affect the link bandwidth, which is limited by the transceivers. For SI-POF, longer link lengths will be at the expenses of a lower 4-PAM bitrate and decreased number of LTE-A bands.

In section 3.6, the first successful transmission of 9 LTE-A compliant 64-QAM bands and a 4-PAM 2 Gb/s baseband signal over 35 m GI-POF and further re-emitted the LTE-A bands over 3.5 m wireless LOS and NLOS links is performed. 7 and 6 LTE-A bands are received over the LOS and NLOS links with total throughput of 380 and 450 Mb/s, respectively.
The optical and wireless transmission showed enough EVM margin to increase the POF length up to the desired 50 m length. The 50 m GI-POF link based on EE-LD and broadband p-i-n receiver frequency response and noise performance are characterized in section 3.7.
Finally in section 3.8, the successful transmission of 10 LTE-A compliant 64-QAM bands and a 4-PAM 1.8 Gb/s signal over 50 m GI-POF and further transmitted the LTE-A bands over a 3.5 m wireless link is shown. 8 LTE-A bands are correctly received after the wireless link, with total throughput of 550 Mb/s. Furthermore, the time-invariant pre-equalization achieves better balance of the EVM between the LTE-A bands without needs of the LTE-A full decoding at the RRU. Hence, the trade-off between the SINR budget and link throughput is shown. The link throughput can be increased by adding LTE-A bands at higher frequency. The further attenuation at higher frequency will be compensated by the equalization at the cost of decreasing the average SINR for the remaining LTE-A bands.

Chapter 4

Live 4G transmission over POF

In the previous chapter the transmission of an offline multiband LTE-A and a 4-PAM signals over up to 50 m GI-POF link is demonstrated. The transmission of an offline LTE-A signal gives fewer challenges than transmitting a live 4G signal. Firstly, the offline transmission is performed by E-TM test signal, which involves only the PHY layer of the LTE-A protocol stack and the evaluation of only few parameters is required (e.g. EVM, SNR, and constellation). Secondly, the offline LTE-A test is performed on a unidirectional link, which requires the optimization of only a single POF link. Thirdly, the signal is generated and decoded by high-end laboratory instruments (e.g. AWG and VSA). Instead, the transmission and reception of a live LTE-A signal involves many more challenges, all the LTE-A requirements from the entire protocol stack levels must be satisfied to keep the connection stable, and the communication involves off-the-shelf devices, on which there is no control.
In this chapter, the transmission over a 35 m GI-POF link of a live LTE signal is demonstrated. The experiment is realized in collaboration with Netherlands Organisation for Applied Scientific Research (TNO) institute and took place at TNO network laboratory in Den Haag.

4.1 Experimental setup

The experimental setup is composed by four parts: the LTE core network emulator, the E-UTRA network emulator, the bidirectional POF link, and the wireless

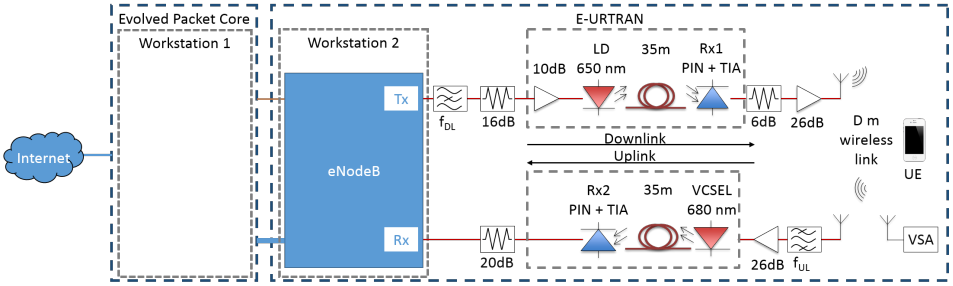

Figure 4.1. LTE-A live transmission setup block diagram.

channel. In section 4.1.1, the LTE core and E-UTRA network emulators provided by TNO are briefly described. Thus, in section 4.1.2, the optimization of the bidirectional POF link is shown.

4.1.1 The LTE network emulator

The 4G mobile network architecture is divided in the IP-based, packet-switched core network and the access network, denoted in 4G terminology evolved packet core (EPC) and E-UTRA, respectively. As shown in Figure 4.1, the EPC is the interface between the E-UTRA and the other networks. The EPC network gets the IP traffic from/to Internet and the other networks, and provides the data and control planes signaling to/from the E-UTRA for the downlink and uplink.

The E-UTRA main purpose is to transmit the information between the EPC and the mobile device (UE in 4G terminology).

The E-UTRA is formed by the LTE-A base station (eNodeB), the fronthaul link, the wireless channel, and the UE. TNO provides the infrastructure emulating the EPC and E-UTRA through 2 workstations: *Workstation 1* and *Workstation 2* specified in Table 4.1 and shown in Figure 4.2. As shown in Table 4.2, the EPC functionalities are emulated by *Fraunhofer Open5GCore Rel2* software through the operating system (OS) Ubuntu 14.04 LTS.

The second workstation, *Workstation 2*, is optimized for low-latency data processing, it emulates the eNodeB functionalities by the *Openairterface5g* software, and provides the LTE-A radio signal by the Express MIMO 2 PCIe output ports. In particular, the Openairterface5g software is able to support up to 5 MHz trans-

Table 4.1. Hardware parameters of the workstation 1 and 2.

	Workstation 1	Workstation 2
CPU	Intel i7-5820K	
Motherboard	ASROCK x99 extreme 3	
RAM	16 GB	
HDD	1 TB	250 GB SSD
Peripheral devices	Intel PCIe Network adapter	Express MIMO 2 PCIe card

Table 4.2. Software parameters of the workstation 1 and 2.

Parameters	Workstation 1	Workstation 2
OS	Ubuntu 14.04 LTS Kernel 3.19-generic	Ubuntu 14.04 LTS Kernel 3.19- low latency
Software installed	Wireshark *Fraunhofer Open5GCore Rel2*	*Openairterface5g software*

mission bandwidth on a single band. The Express MIMO 2 PCIe output signal is carried by the fronthaul link to the antenna. In this test, the fronthaul link is the POF duplex link. The band used is E-UTRA band 20 in Table 3.3, having 791-821 MHz downlink band and 832-862 MHz uplink band.

4.1.2 The POF duplex link

The scheme is shown in Figure 4.1 and the setup is shown in Figure 4.3. As shown in the Figure 4.1, the signals to and from the *Workstation 2* are here transmitted over the POF links with A-RoF technique. Two separated POF links are used for the downlink and uplink. The best POF link for both uplink and downlink is the one described in section 3.7 and based on FP EE-LD and SPD-2, but only a FP laser and SPD-2 were available at the time of the experiment. Therefore, two different optical links are optimized.
The optical downlink is based on the already described FP EE-LD, 35 m 1 mm core diameter PMMA GI-POF, and POF-AC optical receiver based on S8701 Si p-i-n photodiode having -5 dBm optical received power.

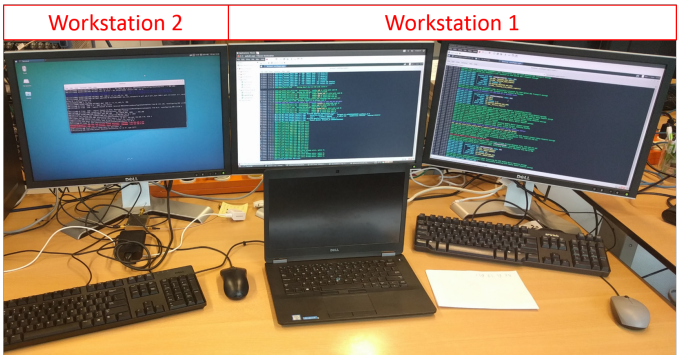

Figure 4.2. LTE-A workstations picture.

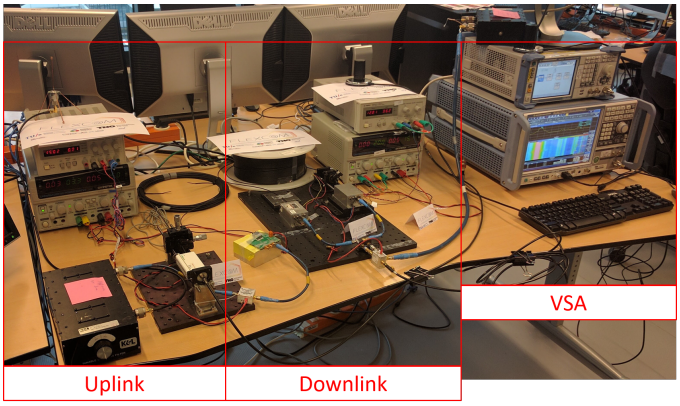

Figure 4.3. Optical link setup picture.

The optical uplink is based on the already described VCSEL optical transmitted, 35 m GI-POF, and SPD-2 optical receiver, having a received power equals -10 dBm. The combination of the devices is chosen in order to have the most balanced performances in the up and down links. The higher power EE-LD is chosen in combination with the narrower bandwidth photodiode in order to increase the received SNR of the LTE-A band. At the same time, the lower power

VCSEL transmitter is used in combination with the higher sensitivity and broader bandwidth receiver in order to improve the lower received optical power.

The signals are processed before being transmitted over the optical links. In the downlink, the LTE signal receiver from *Workstation 2* is filtered by a notch filter with central frequency equals 847 MHz (f_{UL}) in order to remove any interference generated by the eNodeB on the frequency used by the uplink signal. Then, the signal is attenuated by 16 dB to ensure that the maximum transmitter power of the eNodeB does not exceed the maximum input power of the optical transmitter. Finally, the radio signal is transmitted over the optical downlink, the signal is then amplified by 20 dB and wirelessly transmitted.

In the uplink, the signal transmitted by the UE (i.e. smartphone Samsung S5) is received by the uplink antenna, filtered by a bandpass filter with central frequency (f_{DL}) equals f_{UL}, in order to remove any out-of-band interference. Finally, the signal is amplified by 26 dB gain amplifier and is transmitted over the optical uplink to the *Workstation 2*.

4.2 Experimental results

During the live transmission, any signal parameter such as EVM cannot be measured at the UE, either to demodulate the signal by the VSA. Therefore, the two POF links compliance with the EVM requirement is tested using the E-TM 3.1 waveform.
Firstly, a 20 MHz bandwidth LTE waveform with 64-QAM modulation format and power varying between -45 dBm and -5 dBm is transmitted over the POF downlink and the EVM vs. transmitted power is measured and depicted in Figure 4.4a. The minimum EVM is equal to 2% at a transmitted power of -28 dBm, far below the 8% threshold. Furthermore, the EVM value is even lower than the 4.5% 256-QAM threshold[i] [66]. For comparison, the EVM at the POF link input is also measured, in this case the EVM is 0.7%, and therefore the optical link introduces 1.3% EVM penalty and 5 dB attenuation on the signal.

Next, the same test is repeated for the POF uplink. As shown in Figure 4.4b, the minimum EVM is 0.7% at the received electrical power equals -10 dBm. The lower transmitted power of the downlink is due to the presence of a 10 dB amplifier in the EE-LD driver, which is missing in the VCSEL driver. The EVM at the POF

[i]This modulation format is not supported by the VSG and VSA.

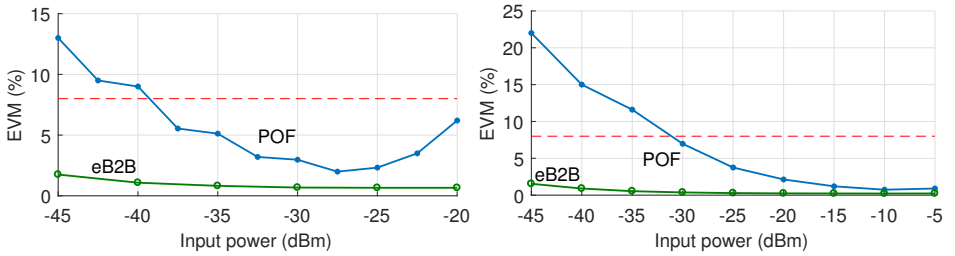

Figure 4.4. LTE-A EVM vs transmitted power measurement for the downlink (a), uplink (b) POF links by using E-TM 3.1 and the red dashed line of the 8% EVM threshold.

link input is equal to 0.2%, therefore a penalty of 0.5% is given by the optical uplink, while an attenuation of 20 dB is introduced. The uplink and downlink POFs have different performance, nevertheless both fully comply with the EVM requirements.

The live LTE transmission is performed, the link performance is measured by quality of different services: VoIP call, HD video streaming, remote desktop control and maximum bit rate, and ping time tests.
Firstly, the UE is positioned at 1.5 m far from the EnodeB antenna, the video streaming has negligible delay at HD quality, keeping good quality of the image. Secondly, at the same distance, a video Skype call is made simultaneously to HD video streaming, no call drops or delay are recorded either video lag or drop of quality, as shown in Figure 4.5. At the same time, a third antenna is placed close to the transmitting antenna in order to acquire the uplink and downlink spectra, the instantaneous spectrum as well the waterfall diagram of the spectrum changing in time is analyzed. As shown in Figure 4.6a, the downlink antenna is transmitting most of the power due to the bit rate downlink test, while the uplink is almost idle. When the bit rate is measured for the uplink, the situation is the opposite, as shown in Figure 4.6b, where the downlink is idle, while high peak power for long period is transmitted by the uplink. Furthermore, the spectral analysis allowed verifying if the spectra are widening due to the optical link and amplifiers non-linearity. As shown in Figure 4.6, the spectra remain confined in the given bands

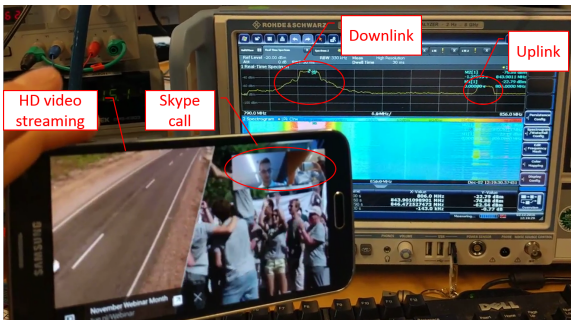

Figure 4.5. Live LTE transmission with simultaneous Skype call and HD YouTube video streaming. On the background is visible the bands usage, in particular the high power transmitted in downlink due to the video and call services.

with typical sharp edges of the OFDM signal after both the POF links.

Finally, the coverage of the femtocell is measured. The UE is used to measure the bit rate in upload and download and the ping by *Speedtest* application at different distances from the EnodeB. In Figure 4.7 is shown the site plan of the room in which the setup is located and the furniture position. Firstly, the upload and download bit rates are measured in different places of the room. Secondly, the uplink and downlink antennas are connected directly to the EnodeB, without POF, and bit rates are measured in the same positions as reference. The bit rate can be measured in all the places of the room up to 14.7 m distance without any connection drop or major bit rate decrease. Furthermore, the bit rate results with and without POF links show marginal differences. The ping time is between 19 and 22 ms for all the measurements points. The bit rate does not decrease with the distance because the *Speedtest* bit rate is performed at the application layer, which involves many layers, protocols and bit rate bottleneck, which might not be related with the fronthaul.

4.3 Summary

This chapter discusses in details the transmission of a live LTE-A signal over a large core PMMA GI-POF link. The Internet IP packets are transmitted through the EPC and E-UTRA emulators to the eNodeB, over the POF link, wirelessly to

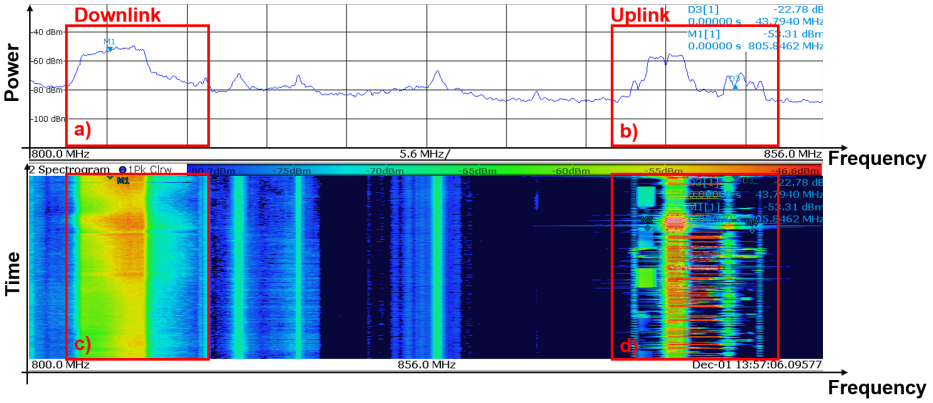

(a)

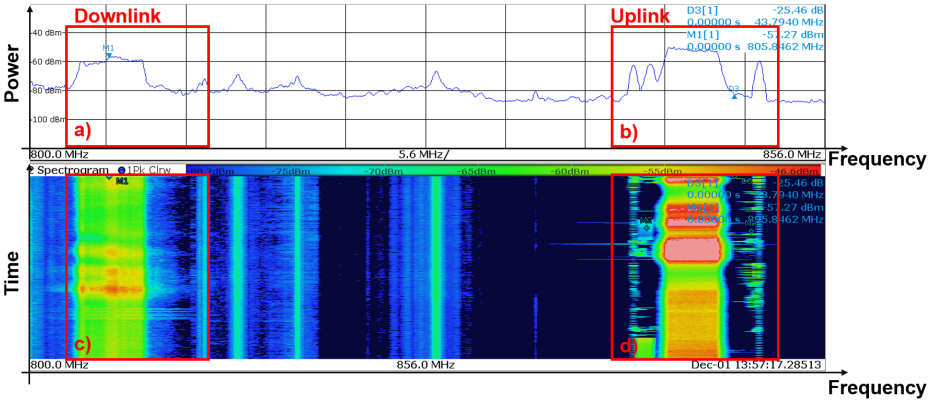

(b)

Figure 4.6. Acquired spectrum by the third antenna for heavy downlink traffic (a) and heavy uplink traffic (b). In a) and b) the instantaneous spectrum of the downlink and uplink, in c) and d) the power spectrum variation of the downlink and uplink in the time.

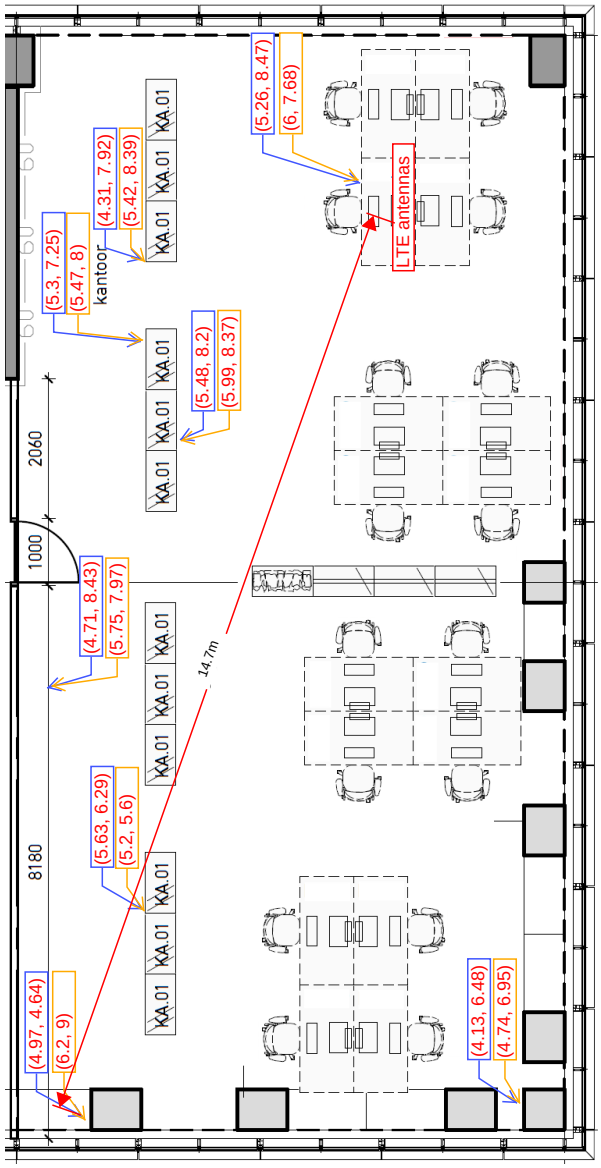

Figure 4.7. Received LTE-A bit rate for the downlink and uplink in different places of the laboratory. In the orange textbox there is the measured value when the POF link is not used, in the blue textbox when it is. In each textbox there is a couple of number representing respectively the downlink and uplink bit rate in Mb/s, no major differences are found.

the UE in the downlink and backward in the uplink. The maximum POF distance is 35 m due to the use of the low-power transmitter in the uplink. Preliminary tests demonstrated a limited EVM increase related with the transmission over the optical link. Then, the live LTE transmission in the licensed bands showed the support of multiple broadband services at the same time, such as high-definition video streaming and videophone calls without significant penalty incurred by the POF link. No disconnections or drops in the service quality are measured within the 15 m wireless distance.
50 m or longer POF length is feasible by using symmetric downlink and uplink POF links based on EE-LD. Multiband transmission is feasible given the proper upgrade of the network emulators and UE capability. Hence, the time-invariant pre-equalization can be applied to the live LTE multiband signal after being implemented online. Finally, the simultaneous transmission of a live multiband LTE-A signal and an offline digital baseband signal is possible but is not demonstrated due to the lack of AWG and DPO equipment at the location of the test.

Chapter 5

Network convergence of services over POF

In the present in-home networks many services are used in everyday life, each one with its dedicated link, which leads to high CapEx and OpEx, as discussed in chapter 1. A more cost-effective approach is achieved by the network convergence, providing the connectivity for all the services by a single wired network backbone. Such network backbone must primarily be able to support a better indoor wireless connectivity. As discussed in chapter 1, nowadays wireless devices such as smartphones and tablets are preferred and looking to the future the wireless traffic generated indoor is forecast to increase [3, 82]. The converged HAN provides a reliable low-cost connection between the residential gateway, where most of the signal processing is performed, and the RRU located in each room, from which the last meter wireless connectivity is provided. Such networks should also support the baseband digital transmission for the remaining in-home wired services.

POFs can meet those requirements, bringing the multi-format radio signals to each RRU, by providing an optical backbone for both wired and wireless based in-home services.

The capability of transmitting multiband LTE-A and gigabit/s 4-PAM baseband signal over 50 m GI-POF link and several meters wireless link is demonstrated in chapter 3. The LTE-A bands are transmitted with A-RoF technique up to 1.8 GHz carrier frequency thanks to the implemented time-invariant pre-

This chapter is based on the results published in [78–81]

equalization.
The transmission of additional radio signals over the POF link is demonstrated in this chapter. The extra signals are demonstrated to either decrease the average received SINR or increasing the transmitted power and intermodulation distortion (IMD). In order to carry the WLAN signal having a carrier frequency within the ISM band at 2.4 GHz and 5 GHz different approaches must be pursued.

The capability of a single POF to support the simultaneous transmission of WLAN and WSN signals at 2.4 GHz and 5 GHz carrier frequency, together with the baseband and LTE-A multiband signals, is shown in this chapter. In section 5.1, the Volterra's model for nonlinear systems is recalled and then in section 5.2 the GI-POF dynamic range and IMD are studied. In section 5.3, the WLAN IEEE 802.11ac signal is transmitted with IFoF technique, the WLAN IEEE 802.11n signal is transmitted without frequency shifting in section 5.4. Finally, the WSN is also added to the set of transmitted signals in section 5.5.

5.1 Link nonlinearity analysis

Given a linear system with impulse response $h(t)$, the relation between input $x(t)$ and output $y(t)$ signal is written as [83]:

$$y(t) = y(t_0) + \int_{t_0}^{t} h(t-\tau) \cdot x(\tau) d\tau \tag{5.1.1}$$

where the signal at the output of a linear system is the infinite sum (i.e. integral) of all contributions due to the input signal of all the past instants, multiplied by the impulse response. If the system is instantaneous (e.g. ideal resistor), the impulse response is a delta function $h(t) = k \cdot \delta(t)$ and (5.1.1) becomes $y(t) = k \cdot x(t)$.
The optical links are linear systems for small variation of amplitude around the bias point. When the input power increases above a certain range, the model in (5.1.1) is not suitable anymore and instead a nonlinear model must be used. Different models are developed and one of the mostly used is the Volterra's model, defined as follows:

$$y(t) = \int_{-\infty}^{t} h_1(t-\tau_1) \cdot x(\tau_1) d\tau_1 + \int_{-\infty}^{t} \int_{-\infty}^{t} h_2(t-\tau_1, t-\tau_2) \cdot x(\tau_1) \cdot x(\tau_2) d\tau_1 \cdot d\tau_2 + \dots \tag{5.1.2}$$

where $h_n(t-\tau_1,\ldots,t-\tau_n)$ is the Kernel of n_{th} order. In case of $n=1$, then (5.1.2) is equal to (5.1.1) and the system is linear. The Volterra's series can be used under the assumptions:

- The system is weakly nonlinear.
- Few orders are sufficient to describe the system. Hence, the kernel amplitude decreases as the time passes between the time instants of the input contributions and the current time instant becomes larger.

These two hypotheses are in general satisfied by optical link and the Volterra's series is widely used to model optical links [84]. Furthermore, the model does not require any knowledge on the internal parameters of the optical link and therefore can model the entire system as a black box once the kernels are estimated.
The analysis of the Volterra's model in the frequency domain is more meaningful to understand the IMD, which is one of the most relevant problem in multiband RoF systems. Hence, the same analysis is repeated in the frequency domain by denoting the Fourier transform of $x(t)$, $y(t)$, and $h(t)$ as $X(f)$, $Y(f)$, and $H(f)$, respectively. The linear system in (5.1.1) in the frequency domain becomes:

$$Y(f) = H(f) \cdot X(f) \tag{5.1.3}$$

in case of a nonlinear system described by (5.1.2), the Fourier transform of $h_n(t-\tau_1,\ldots,t-\tau_n)$ is defined as follows:

$$H_n(f_1,\ldots,f_n) = \int_{-\infty}^{\infty}\cdots\int_{-\infty}^{\infty} h_n(\tau_1,\ldots,\tau_n) \times e^{-j2\pi(f_1\tau_1+\cdots+f_n\tau_n)} d\tau_1 \ldots d\tau_n \tag{5.1.4}$$

then, the relationship between the Fourier transform of the input and output signal $X(f)$ and $Y(f)$ is given by [83]:

$$\begin{aligned} Y(f) = \cdots + & \\ & \int_{-\infty}^{\infty}\cdots\int_{-\infty}^{\infty} H_n(f_1,\ldots,f_n)\cdot X(f_1)\cdot\cdots\cdot X(f_n) \\ & \times \delta(f-f_1-\cdots-f_n)\cdot df_1\cdot\cdots\cdot df_n + \ldots \end{aligned} \tag{5.1.5}$$

in which the output of a nonlinear system is the sum of an infinite number of terms of given orders. Each term is the integral of all the spectral contributions of the

input signal multiplied by itself n times, and weighted by the frequency-domain kernel of n_{th} order, which represents the effect of the system.

The importance of the Volterra's series in the IMD of a system becomes clear when a single and double tone signal are transmitted over the nonlinear link. Given a single tone as input to the system in (5.1.5) and its Fourier series:

$$x(t) = A \cdot cos(2\pi f_0 t) \tag{5.1.6}$$

$$X(f) = \frac{A}{2}\delta(f - f_0) + \frac{A}{2}\delta(f + f_0) \tag{5.1.7}$$

the (5.1.5) approximated at the 3rd order becomes:

$$\begin{aligned}
Y(f) =& Y_1(f) + Y_2(f) + Y_3(f) \qquad (5.1.8)\\
Y_1(f) =& H_1(f_0)\frac{A}{2}\delta(f - f_0) + H_1(-f_0)\frac{A}{2}\delta(f + f_0)\\
Y_2(f) =& H_2(-f_0, -f_0)\frac{A^2}{4}\delta(f + 2f_0) + H_1(f_0, f_0)\frac{A^2}{4}\delta(f - 2f_0)\\
& H_2(-f_0, f_0)\frac{A^2}{4}\delta(f) + H_1(f_0, -f_0)\frac{A^2}{4}\delta(f)\\
Y_3(f) =& H_3(-f_0, -f_0, -f_0)\frac{A^3}{8}\delta(f + 3f_0) + H_3(f_0, f_0, f_0)\frac{A^3}{8}\delta(f - 3f_0)\\
& H_3(-f_0, -f_0, f_0)\frac{A^3}{8}\delta(f + f_0) + H_3(-f_0, f_0, -f_0)\frac{A^3}{8}\delta(f + f_0)\\
& H_3(f_0, -f_0, -f_0)\frac{A^3}{8}\delta(f + f_0) + H_3(-f_0, f_0, f_0)\frac{A^3}{8}\delta(f - f_0)\\
& H_3(f_0, -f_0, f_0)\frac{A^3}{8}\delta(f - f_0) + H_3(f_0, f_0, -f_0)\frac{A^3}{8}\delta(f - f_0)
\end{aligned}$$

firstly, the first-order term $Y_1(f)$ generates the linear output signal at the same frequency of the input. Secondly, the second-order term $Y_2(f)$ generates a zero-frequency signal (rectified signal) and a signal at twice the input frequency (second harmonic). Finally, the third-order term $Y_3(f)$ creates a signal at input frequency and at three times the input frequency (third harmonic) and so on. In case of a single tone input, the nonlinearity up to the 3rd order has effect on the fundamental harmonic only through the 3rd order term $Y_3(f)$. The remaining harmonics have a frequencies multiple of the fundamental and they can be filtered out. This is not the case for a two tones input signal.

Given a two tones signal as input to the system in (5.1.5) approximated at the 3rd order, the following two tones signal is given in input:

$$x(t) = A_1 \cdot cos(2\pi f_1 t) + A_2 \cdot cos(2\pi f_2 t) \tag{5.1.9}$$

the output signal is demonstrated in [85] having a rectified component, the first, second and third order harmonics at the frequencies: DC, f_1, f_2, $2f_1$, $2f_2$, $3f_1$, and $3f_2$. Furthermore, the two tones case gives also cross products at the frequencies: $f_1 + f_2$, $f_1 - f_2$, $2f_1 - f_2$, $2f_2 - f_1$, $2f_2 + f_1$, and $2f_1 + f_2$. The n_{th} order cross products and harmonics generated by 2 tones is defined as follows:

$$f = n_1 \cdot f_1 + n_2 \cdot f_2, \text{ for } \forall n_1, n_2 \in \mathbb{Z} \mid |n_1| + |n_2| = n \tag{5.1.10}$$

hence, the nonlinear system generates cross products within the input signal spectrum, which cannot be filtered out due to the overlapping spectra. In particular, the chance of having in-band-interference increases with the number of transmitted tones (i.e. bands) through a nonlinear system. Considering now the case of the transmission of multiple narrow-band signals, the 2nd and in particular 3rd order cross product might fall within the bandwidth of the fundamental creating a distortion, which is called IMD.
Decreasing the nonlinearity by reducing the transmitted power brings the optical link back to the linear region but decreases the SNR. Therefore, it is important that the best trade-off between SNR maximization and IMD mitigation must be found.

5.1.1 IMD

A main concern for multiband RoF transmission over POF comes from IMD, which occurs due to the link nonlinearity caused by POF transceivers. In particular, considering n tones simultaneously transmitted, through the system in (5.1.2) the i^{th} harmonic and IMD components of second order will have frequencies equal:

$$f_{2,i} = \sum_{j=1}^{n} a_{2,j} \cdot f_j, \forall a_{2,j} \in [0, \pm 1, \pm 2] | \sum_j |a_{2,j}| = 2 \tag{5.1.11}$$

similarly for the third order:

$$f_{3,k} = \sum_{j=1}^{n} a_{3,j} \cdot f_j, \forall a_{3,j} \in [0, \pm 1, \pm 2, \pm 3] | \sum_j |a_{2,j}| = 3 \tag{5.1.12}$$

where $a_{2,j}$ and $a_{3,j}$ are the coefficients that are used to calculate the IMD frequencies. As defined by (5.1.11), $a_{2,j}$ is a relative number belonging to the set $[0, \pm 1, \pm 2]$, for which the sum of all the coefficient $a_{2,j}$ for $j+1, \ldots, N$ is equal to 2. Similar definition is given for $a_{3,j}$ in (5.1.12).
The (5.1.11) and (5.1.12) are applied to calculate the 2nd and 3rd IMD and harmonic components generated by the LTE-A bands in Table 5.1 and the WLAN band at 2.462 GHz. Each radio signal is approximated with a tone centered at the signal carrier frequency, which is possible given the narrow band of the signals. Once the frequencies are calculated, the number of harmonics and IMD falling within the band of each radio signal is computed, which allows to have an estimation about how severe is the IMD by the optical link. Furthermore, the IMD introduced depends on the kernels describing the link as well. The kernels are not calculated, therefore further studies should be conducted. Nevertheless, it can be reasonably supposed that whenever more harmonic and cross product components fall within the fundamental bands the IMD is more severe. The 4-PAM signal is transmitted with lower power than the radio signals, hence its effect on the IMD is not considered in this thesis.

As shown in Figure 5.1, the simultaneous transmission of the LTE-A bands with and without the WLAN signal do not change the number of 2nd order interfering harmonic and IMD components and the first LTE-A band at 738 MHz remains the most affected.

Moving to the 3rd order analysis, as shown in Figure 5.2a, the simultaneous transmission of the only LTE-A bands, gives the maximum IMD to the LTE-A band 20 at 806 MHz, followed by band 18, 19, and 32. When the WLAN is co-transmitted, the most interfered signal is the WLAN band with 13 harmonic and IMD components, followed by the LTE-A band 20 with 10 spurious components.

5.2 GI-POF link dynamic range characterization

In section 3.7 the frequency response and noise performance of the POF link based on the 50 m of 1 mm core diameter PMMA GI-POF, the FP EE-LD, and the SPD-2 photodiode is performed. In this section, the same POF link is studied by measuring the nonlinearity performance in order to determine the linear region of the optical link. In all the cases, the received optical power is equal to -8.5 dBm, including the coupling losses. The 1 dB compression dynamic range (CDR_1) and 3rd order spurious free dynamic range ($SFDR_3$) are measured and calculated.

Table 5.1. LTE-A bands used in the experiments and their most significant parameters.

Parameter	Value									
LTE-A band index	1	2	3	4	5	6	7	8	9	
E-UTRA operating band	12	13	14	20	18	19	8	32	24	
Carrier frequency fc_i (MHz)	738	751	763	806	868	883	944	1474	1542	
Bandwidth (MHz)	10			20	15		10	20	10	
Gain of the digital transmitter amplifier G_i (dB)	0.4	0.2	0.1	3.45	4.1	4.1	1.25	7.5	5.2	
Modulation format	64-QAM									

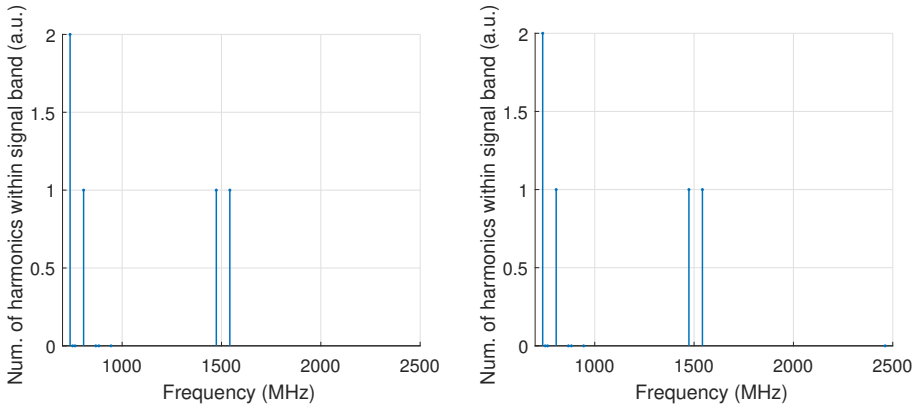

Figure 5.1. Simulated number of 2nd harmonic and IMD components falling within the radio signal bandwidths for LTE-A only transmission (a) and LTE-A and WLAN co-transmission (b).

5.2.1 Compression dynamic range characterization

The 1 dB compression point of a link is defined as the input power P_1 for which a variation of $\delta P[dB]$ in input is equal to a $\delta P - 1[dB]$ variation at the output ($P_{1,out}$). The CDR_1 is defined as the input power range between the noise floor and the P_1 and it is calculated as [86]:

$$CDR_1[dB \cdot Hz] \triangleq P_{1,out}[dBm] + 1 - N_0[dBm/Hz] \tag{5.2.1}$$

where CDR_1 is normalized with the respect of the bandwidth and N_0 is the noise spectral density at the output of the link.

The CDR_1 is measured by transmitting a continuous sine wave of frequency equals 100 MHz and variable amplitude through the POF link and the output power is recorded. Hence, the output power in the linear region is used to extrapolate the ideal linear behavior of the link. The comparison between the ideal curve and the measured output power defines P_1, as shown in Figure 5.3. Furthermore, the noise spectral density N_0 is also measured and is equal to -139 dBm/Hz. $P_{1,out}$ is equal to -6 dBm, therefore the CDR_1 is calculated by (5.2.1) and is equal to

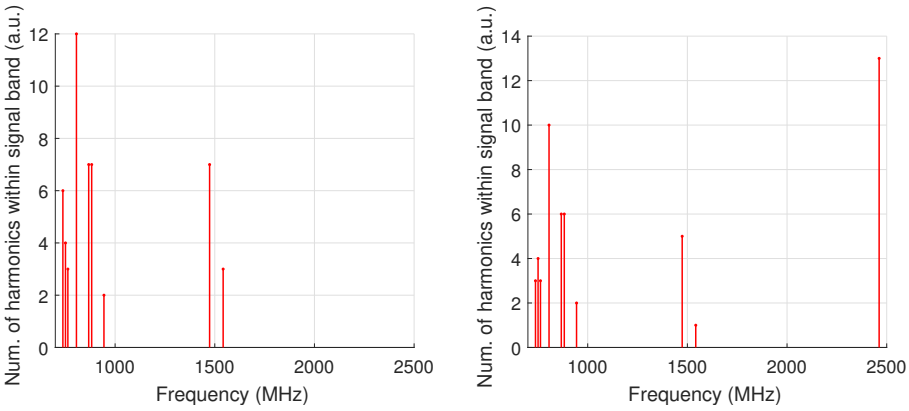

Figure 5.2. Simulated number of 3rd harmonic and IMD components falling within the radio signal bandwidths for LTE-A only transmission (a), LTE-A and WLAN co-transmission (b).

134 dB·Hz[i], so P_1 is equal to -12.5 dBm equivalent to a maximum input amplitude of 150 mV_{pp}.

5.2.2 IP3 and SFDR characterization

The 3rd order intermodulation by the optical link is studied by power combining 2 continuous waves at frequencies $f_1 = 100$ MHz and $f_2 = 105$ MHz, having same transmitted power, and sending them over the POF link. At the link output, the power of the 2 tones and the 3rd order components are measured. Only the 3rd intermodulation components at frequency $2f_1 - f_2$ and $-f_1 + 2f_2$ are considered. In Figure 5.4 the f_1 and $2f_1 - f_2$ fundamental and third intermodulation tones are shown, similar measurements are obtained for the remaining frequencies. From the measured values the third order intercept point (IP3) is defined by linear extrapolation of the fundamental and third order IMD curve. As shown in Figure 5.4,

[i]No other CDR_1 measurement for large core diameter POF link are available at the moment in literature in the best of author's knowledge.

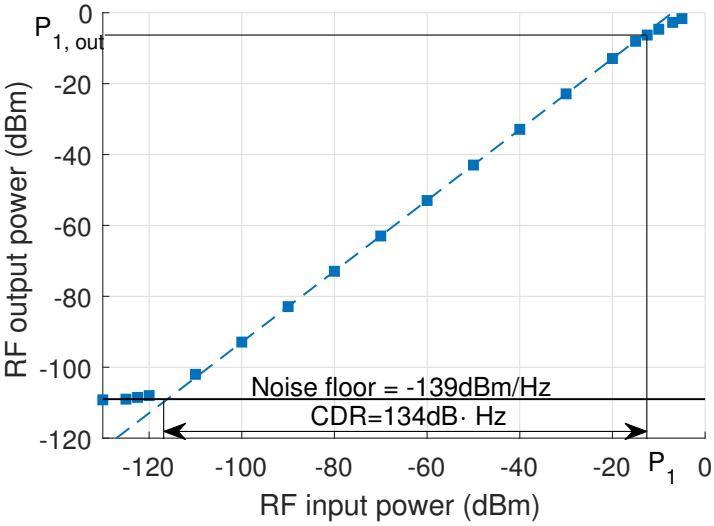

Figure 5.3. 50 m POF link compression dynamic range at 100 MHz tone.

the 3rd order input intercept point (IIP3) and 3rd order output intercept point (OIP3) are equal to 13 dBm and 15 dBm, respectively. In the best of author's knowledge only another IIP3 characterization is carried out on 50 m GI-POF link and the IIP3 is equal to 12 dBm, which is very similar to the one measured is this setup [87].
Thus, from the OIP3 value the SFDR_3 normalized to the bandwidth can be calculated as follows [86]:

$$SFDR_3[dB \cdot Hz^{2/3}] \triangleq \frac{2}{3} \cdot (OIP3[dBm] - N_0[dBm/Hz]) \tag{5.2.2}$$

from which the SFDR_3 is equal to 103 $dB \cdot Hz^{2/3}$.

5.3 WLAN IEEE 802.11ac simultaneous transmission

Nowadays one of the most popular WLAN standard is IEEE 802.11. Different versions are developed during the years and at the present the most deployed is

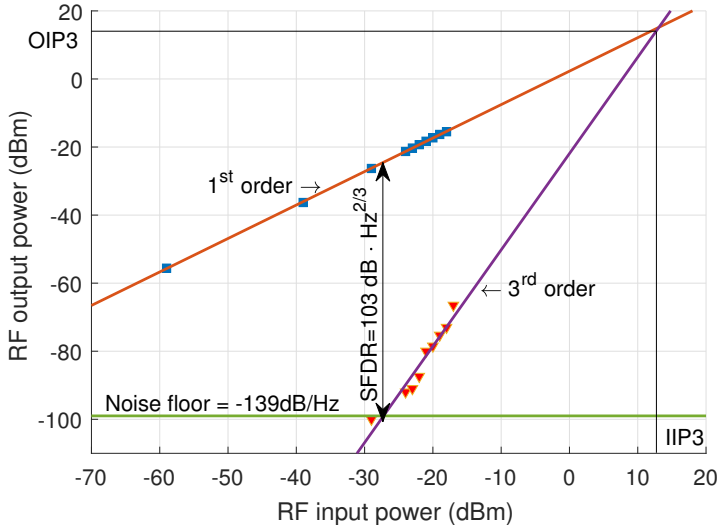

Figure 5.4. 50 m POF link fundamental harmonic and $2f_1 - f_2$ intermodulation product, $SFDR_3$ and 3rd order intercept point (IP3) at 100 MHz tone.

IEEE 802.11n. This version uses 40 MHz transmission bandwidth, OFDM modulation scheme, and supports both the ISM bands at 2.4 GHz and 5 GHz. To meet the new challenges, the IEEE 802.11 standard is moving to a wider bandwidth, higher carrier frequency (i.e. 5 GHz and beyond) and higher modulation order (i.e. 256-QAM). The latest standard released (IEEE 802.11ac) is already being supported by more than half of the devices nowadays and in 2020 virtually all the devices (96.6%) will support it.

In this section the transmission of an IEEE 802.11ac waveform over the POF link is demonstrated. The high carrier frequency employed by the standard (i.e. 5 GHz) cannot be supported by the POF link. Hence, the IFoF technique is implemented by frequency shifting of the WLAN to an intermediate low frequency, which is optimized to minimize the IMD.

Table 5.2. WLAN most significant parameters for the LTE-A and WLAN (Case I) and for LTE-A, WLAN, and 4-PAM (Case II).

	Value	
Parameter	Case I	Case II
Bandwidth (MHz)	80	
Modulation format	256-QAM	64-QAM
coding rate (CR) *CR*	5/6	
Guard interval *GI* (ns)	400	
Idle time (μs)	20	
Transmitted power at Pt. A (dBm)	-17	-27
IF frequency (MHz)	250	1200

Experimental setup

9 LTE-A bands are generated by the E-TM 3.1, as listed in Table 5.1, and transmitted with the A-RoF technique. Hence, the 4G signals are created, equalized, combined, and digital-to-analog converted, as shown in Figure 5.5. The time invariant equalization, described in section 3.8.1, compensates the low-pass behavior of the POF link.
The WLAN signal is generated in accordance with IEEE standard in [88], given the parameters in Table 5.2. The waveform is created by Matlab and generated by the VSG, as shown in Figure 5.5. A PRBS 2^7-1 sequence is encoded as user data and repeated to fit the payload of 1050 Byte of the WLAN waveform. Two transmission bandwidths are defined in [88], 80 MHz and 160 MHz but the VSG limits the WLAN bandwidth to the first choice. The signal is transmitted over POF with an intermediate frequency. Two different IFs are tested:

Case I The IF is equal to 250 MHz, in order to use the POF link spectrum with the highest gain, therefore the maximum modulation order of 256-QAM is used. Hence, the baseband signal cannot be transmitted because the frequency range is occupied, the power budget designed for the baseband signal is given to the WLAN signal and the transmitted power is equal to -17 dBm.

Case II The baseband 4-PAM signal is kept, therefore the IF frequency shifted to the next available spectrum, which is the range from 950 to 1470 MHz,

between the LTE-A band 7 and 8. Hence, 1.2 GHz is chosen as IF. In this case, the power budget must be shared also with the 4-PAM signal, therefore the WLAN transmitted power is decreased to -27 dBm and the modulation order to 64-QAM. A PRBS 2^7-1 sequence is 4-PAM offline encoded, filtered, by a digital LPF with -3 dB cutoff frequency (f_{co}) equals 700 MHz, and digital-to-analog converted.

In both the cases, the combined signal is then transmitted in the POF link characterized in section 5.2 and the received optical power is equal to -8.5 and -8.9 dBm in Case I and Case II, respectively.

At the POF link output, the signal is given to the VSA capable to decode both 4G and WLAN IEEE 802.11ac standards and the WLAN signal is decoded at IF. The WLAN EVM is root mean square averaged over 21 acquisitions. Meanwhile, the LTE-A EVM is calculated for each sub-carrier and averaged, the measurements are repeated 20 times and the maximum value is considered.

IF optimization-simulation results

The IF shifting of the WLAN signal gives one extra degree of freedom in the link design, the IF frequency can be chosen in order to minimize the IMD between the signals. Here, using the simulation method described in section 5.1.1, the number of 2nd and 3rd order spectral components falling with the other signals band is calculated. This can give a first estimation about the penalty introduced by the IMD.
Firstly, the IMD generated without WLAN transmission is considered as reference condition and shown in Figure 5.6a. Then, the IF is swept from 50 MHz to 650 MHz with steps of 100 MHz. As show in Figure 5.6d, an IF equals 250 MHz gives the same number of spurious components as in the reference case, with no further IMD.
The same procedure is repeated for the 3rd order IMD. As shown in Figure 5.7, this time there is no IF for which the IMD is null. The case for which f_{IF} is equal to 50 MHz should be avoided since it generated 40 interfering frequency components. In all the other cases, each IF frequency choice introduces the same number of interfering tones on the WLAN signal, hence 250 MHz is chosen as f_{IF} for the WLAN.

Similar simulation is executed for the Case II sweeping the IF between 1 GHz and 1.4 GHz, and 1.2 GHz as IF frequency is selected as the best choice for Case II.

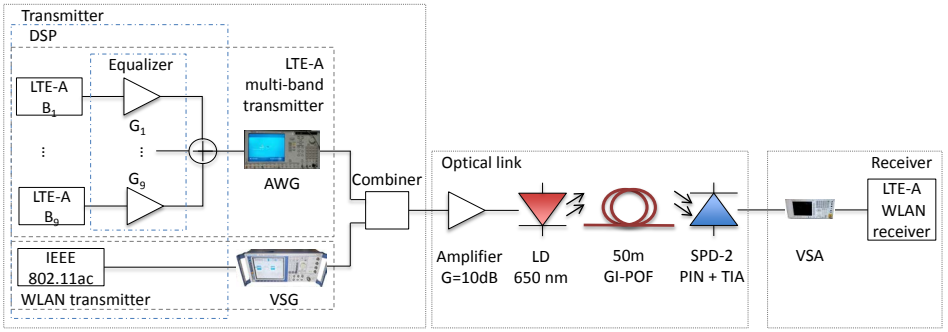

(a)

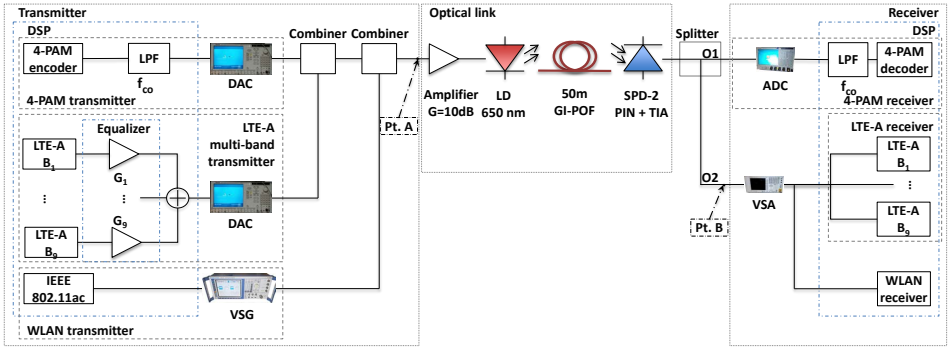

(b)

Figure 5.5. Experimental setup diagram for the LTE-A and WLAN transmission of case I (a) and for the LTE-A, WLAN, and 4-PAM of case II (b).

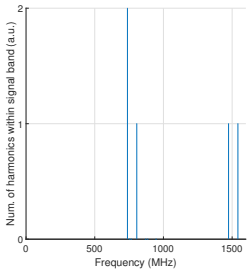

(a) LTE-A solitary transmission

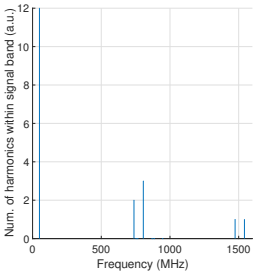

(b) $f_{IF} = 50$ MHz

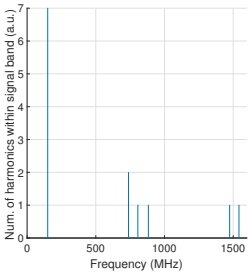

(c) $f_{IF} = 150$ MHz

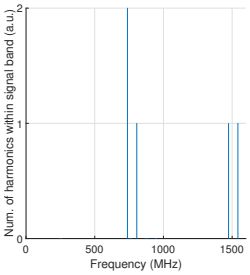

(d) $f_{IF} = 250$ MHz

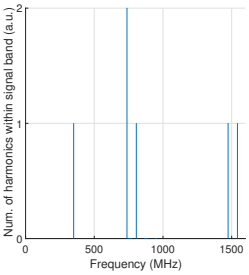

(e) $f_{IF} = 350$ MHz

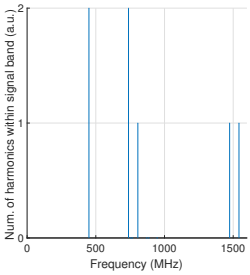

(f) $f_{IF} = 450$ MHz

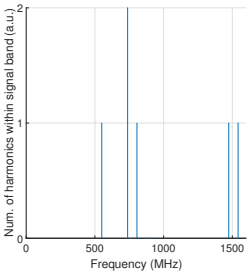

(g) $f_{IF} = 550$ MHz

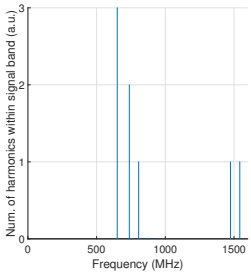

(h) $f_{IF} = 650$ MHz

Figure 5.6. Simulation results of 2nd order harmonic and cross product components interfering with the LTE-A and WLAN bands. In (a) the results for LTE-A solitary transmission, in (b), (c), (d), (e), (f), (h) the results of the LTE-A and WLAN co-transmission at f_{IF} equals 50, 150, 250, 350, 450, 550, and 650 MHz.

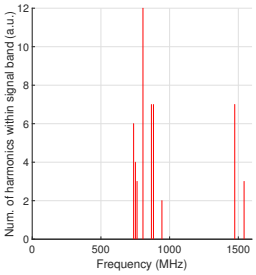

(a) LTE-A solitary transmission

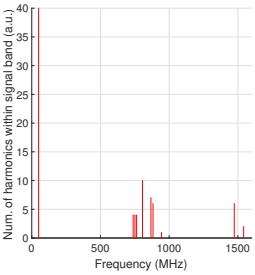

(b) $f_{IF} = 50$ MHz

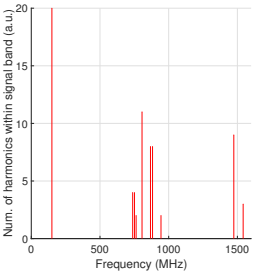

(c) $f_{IF} = 150$ MHz

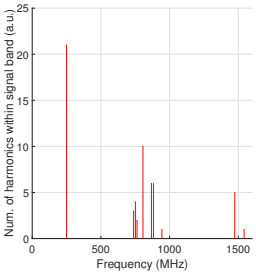

(d) $f_{IF} = 250$ MHz

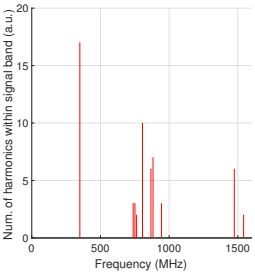

(e) $f_{IF} = 350$ MHz

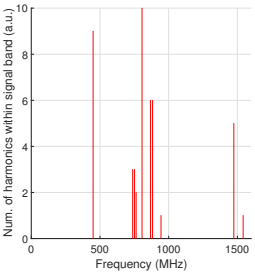

(f) $f_{IF} = 450$ MHz

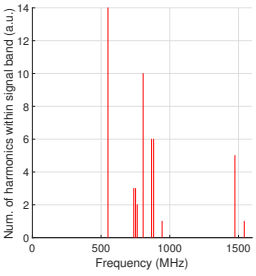

(g) $f_{IF} = 550$ MHz

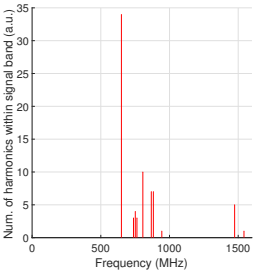

(h) $f_{IF} = 650$ MHz

Figure 5.7. Simulation results of 3rd order harmonic and intermodulation components interfering with the LTE-A and WLAN bands. In (a) the results for LTE-A solitary transmission, in (b), (c), (d), (e), (f), (h) the results for LTE-A and WLAN co-transmission at f_{IF} equals 50, 150, 250, 350, 450, 550, and 650 MHz.

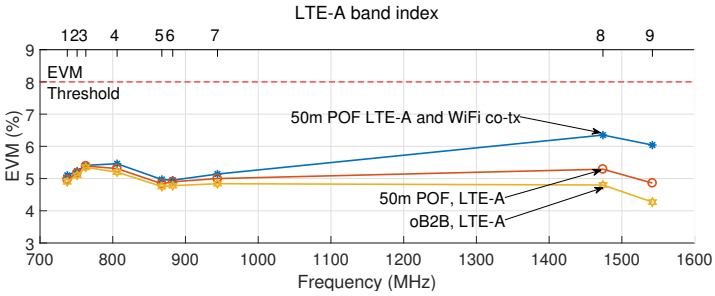

(a)

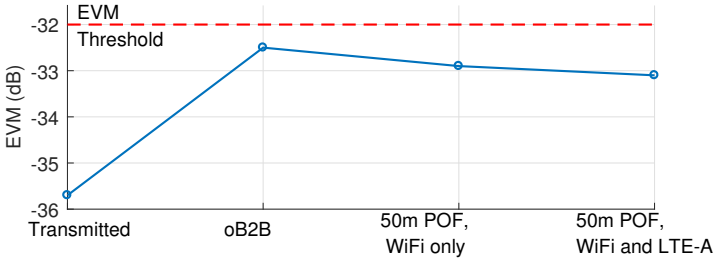

(b)

Figure 5.8. LTE-A (a) and WLAN (b) EVM experimental results.

Experimental results

Case I: The LTE-A experimental results are shown in Figure 5.8a, the oB2B and 50 m POF LTE-A solitary transmissions are also depicted for comparison. The EVM is around 5%, notably the band 8 and 9 have the same EVM as the lower frequency bands, on account of the equalization. The LTE-A bands 8 and 9 have slightly lower EVM in the oB2B than the 50 m link, related with the different frequency response of the links in that spectrum range. When the WLAN signal is co-transmitted, 2 behaviors can be seen for the LTE-A signals: the bands 1 to 7, do not show any EVM degradation while band 8 and 9 have a small EVM penalty of 1%. The reason for the higher EVM of band 8 and 9 can be related with the IMD between the LTE-A bands, which is triggered by the higher input power of the simultaneous transmission of LTE-A, WLAN, and 4-PAM signals. Still in the

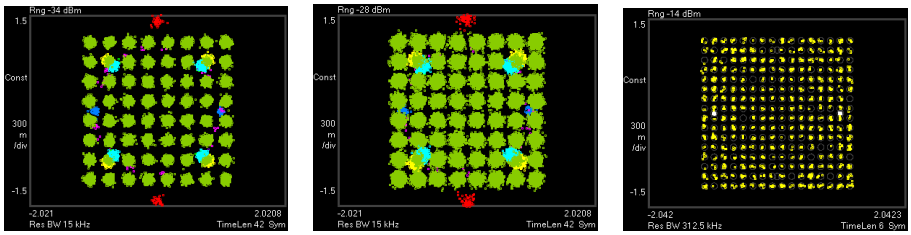

(a) (b) (c)

Figure 5.9. 4 LTE-A band 1 (a), band 8 (b), and WLAN (c) constellation diagrams. The user downlink channel with 64-QAM (green marks) and control channels (other colors) are shown for the LTE-A signals in (a) and (b).

same case, the LTE-A EVM is around 5.5% up to 6.4% for band 8. All the 9 LTE-A bands have EVM lower than 8%.
Moving to the WLAN transmission, the IEEE 802.11ac standard defines the EVM performance in logarithmic scale for comparison with the LTE-A measurements the values are also converted in percentage by the following formula and put between brackets:

$$EVM_{\%} = 100 \cdot 10^{EVM_{dB}/20} \tag{5.3.1}$$

the standard defined an EVM threshold equals $-32\ dB$ (2.5%) to use 256-QAM, CR 5/6 modulation scheme.
As depicted in Figure 5.8b, the WLAN solitary transmission has an EVM at the transmitter port close to -36 dB (1.6%), whereas after the oB2B the EVM is slightly higher, up to -33 dB (2.2%). Moving to the 50 m POF link, in all the cases the WLAN signal has EVM close to -33 dB (2.2%). No EVM penalty is shown for the 50 m POF transmission compared with the oB2B, while the penalty between the transmitted and received EVM is around 3 dB. After the POF link, a 1 dB margin is available for further amplification.
The constellation diagram of the LTE-A and WLAN signals are also considered. As shown in Figure 5.9, no phase noise or amplification compression are observed. The broader point spreading of constellation points for the LTE-A in Figure 5.9a and Figure 5.9b compared with the WLAN in Figure 5.9c, is related with the higher EVM.

Case II: The results of the LTE-A multiband transmission are depicted in Figure 5.10a. During the oB2B and 50 m POF links LTE-A solitary transmission, the EVM is lower than 5% (band 8), with a marginal increase of 0.5% for band 8 and 9 due to the different frequency response of the 2 links at those frequencies. Secondly, the LTE-A signals are co-transmitted with the WLAN waveform. All the LTE-A bands have an EVM lower than 6%: bands 1 to 7 have negligible increase of 0.5%, while for band 8 and 9 it is of 1%. The reason for the higher EVM of band 8 and 9 is the same as in Case I. Finally, when the 4G signal is co-transmitted with the baseband and WLAN, the LTE-A EVM has minor increment for band 9, as also confirmed by the constellation diagrams in Figure 5.11a and 5.11b. In all the cases, the 9 LTE-A bands have EVM lower than the threshold, up to 6% (band 8).

The 4-PAM signal is required to have a pre-FEC BER below $1 \cdot 10^{-3}$. The baseband solitary transmission reached a bit rate of 2 Gb/s on the oB2B and 50 m POF links, and the signal amplitude at the optical input (Pt. A in Figure 5.5b) is 26 mVpp. When all the signals are co-transmitted, the 4-PAM amplitude is reduced to 15 mVpp to diminish any out-of-the-band interference over the radio signals, hence the bit rate decreases to 1.7 Gb/s.

The WLAN signal is required to have an EVM lower than -27 dB (4.5%) and -30 dB (3.2%) for 64-QAM CR 5/6 and 256-QAM CR 3/4, respectively [88]. The transmitted WLAN signal (Pt. A in Figure 5.5b) has an EVM lower than -35 dB (1.8%), after the oB2B link this grown to -29 dB (3.6%), due to the link attenuation at the carrier frequency, as shown in Figure 5.10b. Moving to the 50 m POF link, the EVM is equal to -28 dB (4%). When the 9 LTE-A bands are co-transmitted the EVM of the WLAN signal has a negligible increase, when also the baseband signal is co-transmitted the WLAN EVM does not significantly change. The EVM performance of the WLAN signal with the transmission of all the 3 waveforms present is lower than the -27 dB (4.5%) threshold, as also depicted by the constellation diagram in Figure 5.11c. For both the LTE-A and WiFi transmission, the EVM of the received signal is lower than the respective threshold, which is promising for a further wireless transmission. The WLAN signal has a marginal increase of the EVM related with the LTE-A co-transmission, which suggests that the chosen IF minimizes the IMD and harmonic distortion and the method can be applied in the future to choose other IF. Looking to the WiFi signal, the bitrate can be further increased by exploring the 80+80 MHz multiband or 160 MHz transmission supported by the standard. The 4-PAM bitrate has a

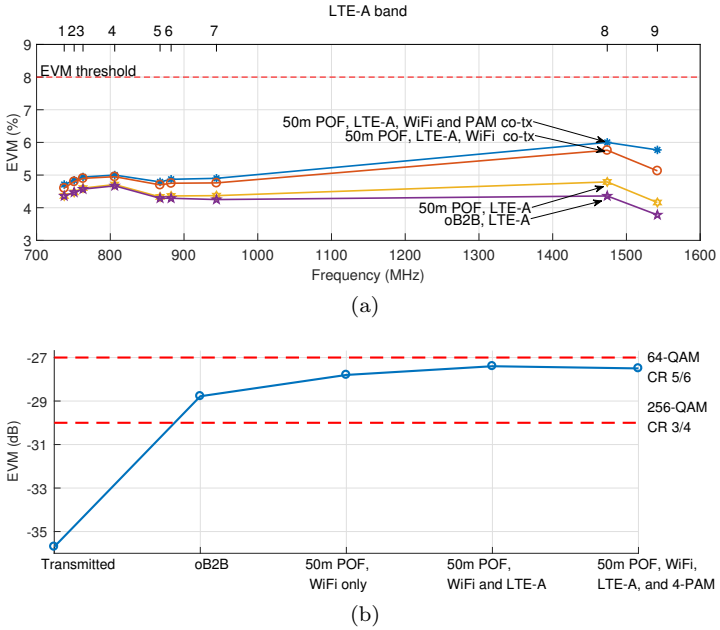

Figure 5.10. EVM results of the LTE-A bands (a) and WLAN transmission for different cases (b). The WLAN EVM threshold for the 64-QAM and 256-QAM modulation orders and coding rates are shown.

marginal decrease compared with the previous setups, which is related with the variation on the transmission power, which is adjusted in every setup in order to avoid to exceed the CDR_1 of the link.

5.4 WLAN IEEE 802.11n simultaneous transmission

Section 5.3 focuses on the latest and fast growing IEEE WLAN standard, which is expected to be supported by virtually all the network devices in few years. Meanwhile, the most popular IEEE 802.11 standard is the 2009 version (IEEE 802.11n), which operates in the 2.4 GHz band and is the most subject to interference.
The experimental results in section 3.8 showed the GI-POF capability to transmit

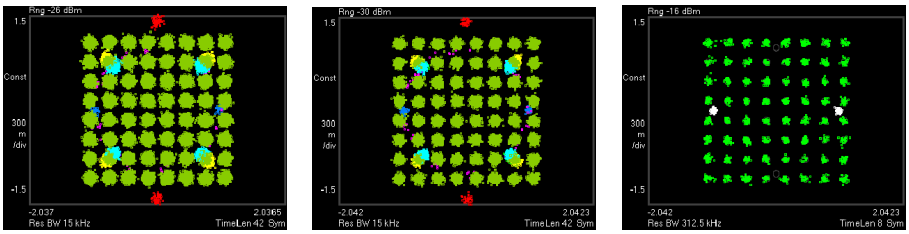

(a) (b) (c)

Figure 5.11. Constellation diagrams of the LTE A band 8 (a), LTE A band 9 (b), and WLAN (c) with simultaneous transmission of all the signals. The user downlink channel with 64-QAM (green marks) and control channels (other colors) are shown.

radio signals up to 1.8 GHz carrier frequency with acceptable EVM penalty. Furthermore, $S21$ of the link in Figure 3.27a depicts a challenging but still feasible attenuation of the GI-POF link in the 2.4 GHz spectrum. Hence, in this section the simultaneous transmission of an IEEE 802.11n waveform with A-RoF technique, together with the multiband LTE-A waveform, and 4-PAM signal is carried out. IFoF is not applied but the link power budget must be carefully balanced between the WLAN and LTE-A signals. This is challenged by the high peak power of the OFDM signals, which requires power back-off in order to avoid IMD. Here, firstly, the mathematical model of the peak power of an OFDM waveform is recalled, secondly the state-of-the-art techniques to reduce the peak power are reviewed. Thirdly, the signal clipping technique is applied on both the LTE-A and WLAN signals and the results discussed. Fourthly, the multiband LTE-A, WLAN, and 4-PAM transmission is performed over 50 m GI-POF and further wirelessly transmitted. The LTE-A and WLAN received signals are acquired for different wireless distances, and their quality unexpectedly does not change with the wireless link distance. The reason is in the optical link noise, hence the NF is measured, a model of the link noise is calculated, and the results are discussed.

5.4.1 OFDM signal PAPR

A major disadvantage of OFDM-based signals is the large peak power, which can-

not fully exploit the dynamic range of the link on which is transmitted. Hence, the signal with higher peak power requires a broader back-off in order to fit the link dynamic range.
The high peak power in the OFDM signals is given by the superposition of a large number of, most often, statistically independent sub-carriers that can constructively sum up to high peaks. In order to evaluate the modulation performance regarding the amplitude peak, different parameters are defined in literature (e.g. crest-factor and peak-to-average power ratio (PAPR)). The PAPR is among the most used parameters and is defined as the ratio between the signal peak power and its expectation. Given the samples of the OFDM envelope u_k^i at the symbol time i, with N sub-carriers in (3.1.1) the PAPR is defined as follow [89]:

$$u_k = u_k^i \tag{5.4.1}$$

$$PAPR(u_k) = \frac{\max\limits_{1\leq k\leq N-1} |u_k|^2}{E[|u_k|^2]} \tag{5.4.2}$$

$$PAPR_{dB}(u_k) = 10 \cdot log_{10}(PAPR(u_k)) \tag{5.4.3}$$

the $PAPR_{dB}(u_k)$ can be found in the worst case scenario for which all the N symbols have maximum amplitude at the same time, assuming the peak amplitude of the symbols are equal to one, $max(A_n^i) = 1$, it follows [90]:

$$\max_{1\leq k\leq N-1} |u_k|^2 = N^2 \tag{5.4.4}$$

$$E[|u_k|^2] = N \tag{5.4.5}$$

$$PAPR_{dB}(u_k) = 10 \cdot log_{10}(N) \tag{5.4.6}$$

for instance, a 20 MHz LTE-A signal with 2048 sub-carriers has the maximum $PAPR_{dB}(u_k)$ equals to 33.1 dB [91]. Fortunately, the probability that this case can happen is low.

The PAPR value depends on the combination of the input symbols, which is random. So, the PAPR is characterized by probability that the PAPR is larger than a certain value δ, this can be found by the complementary cumulative distribution function (CCDF) defined as follows:

$$CCDF(PAPR(u_k)) = Probability(PAPR(u_k) \geq \delta) \tag{5.4.7}$$

if N is large enough and the symbols statistically independent, then the central-limit theorem can be applied. Hence, the OFDM signal $s(t)$ defined in (3.1.1) has

Gaussian distribution and its envelope and power distributions have Rayleigh and exponential distribution [89], therefore (5.4.7) becomes:

$$CCDF(PAPR(u_k)) = 1 - (1 - e^{-\delta})^N \tag{5.4.8}$$

a last recommendation, the samples of the envelope u_k^i, according with the OFDM modulator, are analog-to-digital converted and modulated on the carrier frequency. Once transformed to the analog domain, the OFDM signal can reveal higher peaks, which are not shown by the envelope due to the sampling. In order to avoid it the envelope of the signal can be oversampled, but the hypothesis of independent samples does not hold anymore and approximated models are proposed [92].

PAPR reduction methods

The reduction of the PAPR of a waveform is highly desirable to avoid the back-off of the system, which deceases the average SNR. Alternatively, when the average power cannot be decreased, the amplifier or optical link dynamic range must be improved, which leads to more complex and expensive systems. Therefore, the reduction of the OFDM PAPR is topic of research for many years. Different techniques are proposed and they can be divided in two groups:

- Distortion-based techniques reduce the PAPR by clipping the power peaks. The main advantages are the possibility to apply such technique directly to the OFDM envelope or RF signal. So, the signal processing can be done at the transmitter side and the computational cost is limited. The main disadvantages are the introduction of the distortion, which deteriorate the signal EVM, and provide out- and in-band distortion.

- Distortion-less techniques avoid the peaks by discarding those symbols combinations for which the peaks are generated. Those sequences for which the PAPR limit is exceeded are memorized in a look-up table. The sequences to be transmitted are compared with the ones in the table and if they match a different sequence is transmitted. The table size can become prohibitive for long sequence lengths, also the changes of sequence performed in the transmitter must be acknowledged to the receiver [62, 89]. Hence, the PAPR can be reduced only at the cost of a higher computational complexity for the modulator and demodulator. Furthermore, the distortion-less techniques requires the knowledge of the signal, because applied before the IFFT block.

Hence, the method is not signal agnostic, the waveform must be decoded, the algorithm applied and modulated again, which increases the system complexity.

Since the distortion-less techniques involves higher complexity they are avoided in favor of the distortion-based algorithms.
The distortion-based techniques can be described by a nonlinear characteristic $f(x)$ applied to the OFDM signal:

$$f(x) = \begin{cases} x & \text{, if } x < x_{max} \\ x_{max} & \text{, if } x \geq x_{max} \end{cases} \tag{5.4.9}$$

where x_{max} denotes the clipping magnitude. The function $f(x)$, also called clipper, does not introduce any distortion if $x < x_{max}$ (i.e. the signal peaks do not exceed the peak power limit). The clipper is introduced after the conventional OFDM modulator, before or after the frequency up-conversion, and it is usually followed by a linear filter in order to remove the out-of-band components. Eventually, the linear filter can lead to a regrowth of some signal peaks.

5.4.2 Experimental setup

The setup is shown in Figure 5.12, firstly, a PRBS 2^7-1 sequence is encoded offline in a 4-PAM signal and is filtered by a digital FIR LPF described in section 3.4.1 with the cut-off frequency (f_{co}) equals 700 MHz and sent to the AWG (AWG1).
Secondly, the multiband LTE-A signal is generated according to the parameters in Table 5.1. 9 LTE-A signals are generated and the time-invariant-equalization described in section 3.8.1 is performed on each band i by gain $G_{tx,i}$, as shown in Figure 5.12.
The LTE-A signal peak power is further enhanced by the multiband transmission. To make sure that those peaks stay within the P_1 range of 150 mV_{pp} measured in section 5.2.1 and to ensure the linear behavior of the optical link the average power must be reduced, therefore affecting the signal quality. Alternatively, the amplitude peaks can be removed by signal clipping and the average power and signal quality are improved. The LTE-A bands are then combined, clipped and sent to the second AWG (AWG2).

Thirdly, the WLAN waveform is generated by Matlab in accordance with the IEEE 802.11n standard and the parameters in Table 5.3. The payload is a PRBS

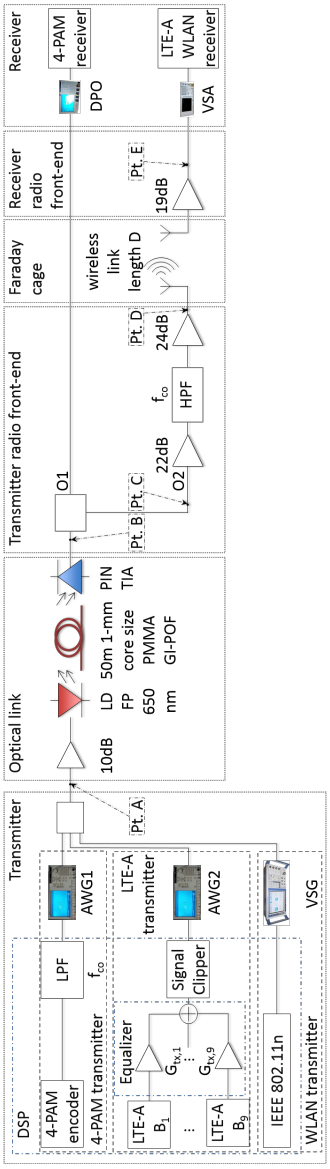

Figure 5.12. Experimental setup diagram.

Table 5.3. Main parameters of IEEE 802.11n WLAN signal.

Parameter	Value
ISM channel	11
Index (i)	10
Carrier frequency (MHz)	2462
Channel bandwidth (MHz)	40
Modulation format	16-QAM
Coding rate	1/2
Guard interval (ns)	400
Idle time (µs)	20
Transmitted power (at VSG) (dBm)	-18.5
PSDU payload (Byte)	1024

of 2^7-1 bit sequence encoded as user data and repeated to fit its size. The waveform is then uploaded to the VSG.

Both the WLAN and LTE-A waveform are transmitted at their original frequency bands. As shown in Figure 5.12, the 4-PAM, the LTE-A, and the WLAN signals are combined through power combiners and sent over the optical link described in section 3.7 and at the SPD-2 p-i-n photodiode the received optical power is equal to -8.5 dBm.

After the optical link the signal is split by a 1×2 electrical power splitter, the second output (O2) is connected to the transmitter RF front-end, which consists of two amplifiers and a HPF with cutoff frequency f_{co} to remove the 4-PAM signal. The transmitter radio front-end gain and NF are measured with the procedure described in section 3.2.1 and 3.2.2 and are equal to 47 dB and 5 dB, respectively. The radio signal power is boosted to 11 dBm for the WLAN waveform and between 6 dBm (band 2) and 11 dBm (band 4 and 8) for the LTE-A signals and then transmitted through the wireless link. Two identical off-the-shelf broadband antennas described in section 3.6.1 are used to perform the wireless transmission. As shown in Figure 5.13, the wireless link is LOS, taking care to avoid any obstacle within the first Fresnel ellipse and it is placed within a Faraday cage to avoid any interference on the licensed services [93]. The radio signals are received by the radio front-end, consisting of a single amplifier having gain and NF that are measured equal to 21 dB and 4.3 dB.

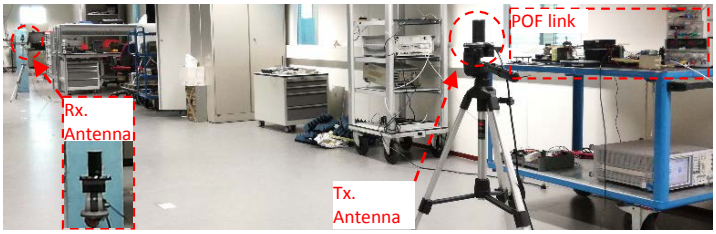

Figure 5.13. Wireless link and POF setup picture in the Faraday cage room, D=12 m.

In order to consider the out-of-band interference between the signals, SINR for the i_{th} band is defined as follows:

$$SINR_{i,dB} = PS_i[dBm] - 10 \cdot log_{10}\Big(\frac{N_i[mW] + I_{PAMi}[mW] + I_{RFi}[mW] + IWL_i[mW]}{1 \cdot 10^{-3}}\Big) \tag{5.4.10}$$

where PS_i is the in-band power measured of the i_{th} band when all the LTE-A bands, the 4-PAM, the WLAN, and eventually the wireless channel interference signals are received. The remaining terms are the in-band power in the i_{th} band when the noise (N_i), the 4-PAM interference (I_{PAMi}), the other radio frequency interferences (I_{RFi}), and the wireless channel interference (IWL_i) signals are received.

Clipping optimization

The PAPR reduction allows to increase the average transmitted power P_{AVG} and the SNR, hence to decrease the EVM [94]. Nevertheless, the PAPR reduction is accompanied by distortion introduced by the clipping, which would affect the EVM performance. Hence, the optimum clipping level for which the SNR is maximized without introducing further distortion must be found.

Given the LTE-A multiband signal $x(t)$ and its PAPR $PAPR_0$, after clipping the signal becomes $x'(t)$ and its new PAPR $PAPR'$. The clipping ratio is defined

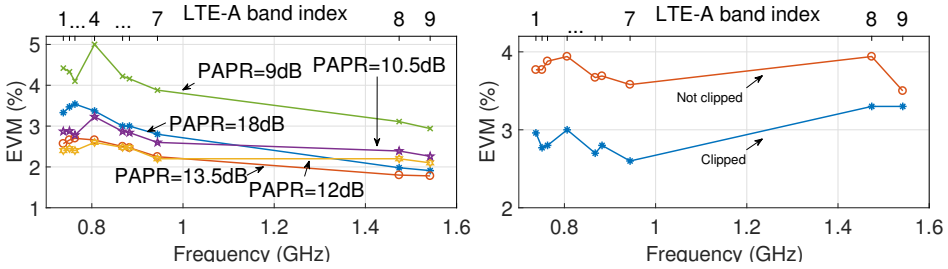

Figure 5.14. LTE-A EVM experimental results for different PAPR value at Pt. A (a) and not clipped and optimum clipping level at Pt. C (b) of the link in Figure 5.12.

as

$$ClR[dB] \triangleq PAPR_0[dB] - PAPR'[dB] \tag{5.4.11}$$

$$x'(t) = A \cdot \frac{x(t)}{|x(t)|}, \forall |x(t)| > A \tag{5.4.12}$$

where the maximum amplitude A after clipping is calculated and then performed.

The optimum clipping ratio is found by clipping the signal and measuring the EVM at the optical link input (Pt. A in Figure 5.12). Due to the instruments available the PAPR values of the multiband signal cannot be measured. Instead, the PAPR is calculated on the signal in Matlab, before being sent to AWG2. For all the measurements the signal peak-to-peak amplitude is kept equal to 120 $\mathrm{mV_{pp}}$.

As shown in Figure 5.14a, the multiband LTE-A PAPR before clipping is equal to 18 dB and the EVM is between 3.5% and 2%. The LTE-A bands 8 and 9 have lower EVM because the equalization is kept, even if the frequency response of the link if flat before the optical link. The PAPR is decreased to 12 dB and the LTE-A EVM has its minimum between 2.5% and 2%. The bands 8 and 9 have almost the same EVM as the remaining bands, which could affect the equalization over the optical link. Further PAPR reduction increases the EVM. Hence, the optimal clipping ratio is found to be 6 dB, reducing the PAPR of the multiband LTE-A signal from 18 dB to 12 dB.

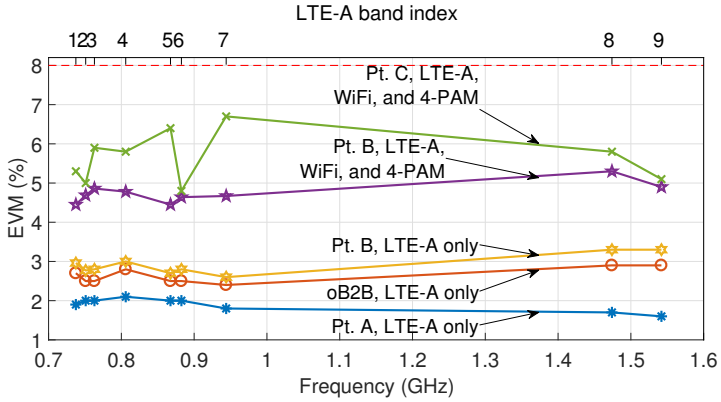

Figure 5.15. LTE-A EVM experimental results for solitary and simultaneous transmission over the 50 m POF link and the 8% threshold (dashed line).

The optimum clipping level is tested in the optical link, as shown in Figure 5.14b, when the LTE-A is clipped with ClR of 6 dB, the EVM decreases from 4% to 3%, with no effect on the equalization.

5.4.3 Experimental result

POF link transmission

The experimental results of the transmission over the POF link are obtained. Firstly, the 4-PAM bit rate is equal to 2 Gb/s over the oB2B and 50 m POF link. When the radio signals are co-transmitted, the 4-PAM amplitude is reduced, hence the 4-PAM bit rate is decreased to 1.7 Gb/s for a pre-FEC BER lower than $1\times\ 10^{-3}$.

Secondly, the LTE-A signal is considered, as depicted in Figure 5.15, the LTE-A EVM at the transmitter side and over the oB2B link show similar results, with a difference of around 1%. Moving to the 50 m link, the EVM is around 3%, almost identical to the oB2B link.

Next, the LTE-A signal is co-transmitted with the WLAN and 4-PAM signals. In the previous case, most of the available power budget is used for the LTE-A radio signal, in this case it must be shared also with the WLAN signal. Having

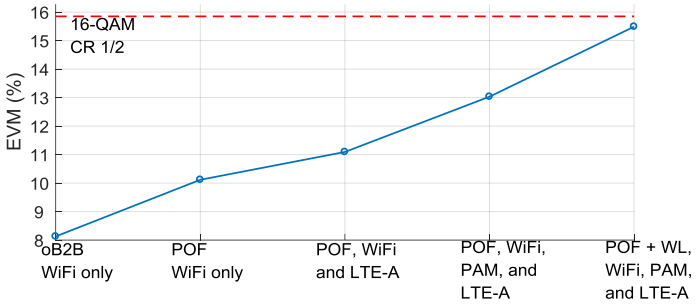

Figure 5.16. WLAN EVM results for the solitary and co-transmission at Pt. C and Pt. D of the link in Figure 5.12.

still a margin of 5% on the LTE-A EVM, the LTE-A transmitted power is halved, which results in a slight EVM increase to 5% (band 8), as depicted in Figure 5.15. Finally, the WLAN signal is considered, the IEEE 802.11n standard sets the maximum EVM to -16 dB (15.8%) [95]. As in section 5.3, the EVM threshold is set in logarithmic scale but the results are also calculated through (5.3.1) in percentage. As shown in Figure 5.16, the WLAN is solitary transmitted over oB2B and 50 m POF (Pt. C in Figure 5.12). The EVM is -21.9 dB (8%) and -20 dB (10%), respectively, which depends on the different frequency response of the two links at that frequency. When the LTE-A and 4-PAM are co-transmitted the WLAN EVM slightly increase to -17.7 dB (13%). Such increase is related with the IMD between the signals due to the nonlinearity as simulated in section 5.1.1.

Wireless transmission

Having correctly received the LTE-A and WLAN signal at the POF receiver, these are re-transmitted over the wireless link. The link distance D is increased from 1 m to 14 m by moving the receiving antenna. As shown in Figure 5.17a, the LTE-A EVM does not change considerably with the distance. At 14 m, the LTE-A bands 1, 4, and 5 have an EVM increase due to the different frequency response of the wireless link, which is caused by the fading given by the proximity of the furniture. As shown also in Figure 5.18a, the WLAN EVM change less than 1 % with the distance. The EVM would be expected to rise with the increase of D. The SINR

in (5.4.10) is measured at Pt. E of the link for the LTE-A and WLAN signals and the results are shown in Figure 5.17b and 5.18b, respectively. As depicted, in both the cases the SINR does not change considerably with D. As shown in Figure 5.17c, the received power decrease with the distance instead, the received power varies between 15 and 20 dB after 1 m compared to the transmitted power. Further increasing the distance up to 14 m the power decrease becomes 25 to 45 dB depending on the LTE-A band.

Looking to the WLAN, as shown in Figure 5.18b, similar observation can be made. In particular, the received power decreases by 30 dB (for $D = 1\ m$ case) and further by 40 dB (for $D = 14\ m$ case). For a constant SINR, the noise and interference received power will depend on the transmitter-receiver distance.

Having all the 3 signals transmitted over the POF, all the LTE-A bands are received with $EVM < 8\%$ up to 12 m, the WLAN signal up to 14 m. Longer wireless link lengths are in principle measurable, but they are limited by the other setups in the same Faraday cage.

5.4.4 Further evaluation of the link noise performance

The EVM and SINR results are related to the noise figure of the optical link measured in section 3.7.2. Recalling the NF defined by (3.2.2), it can be written in terms of noise temperature (T_e) of the system as follows [96]

$$NF[dB] = 10 \cdot log_{10}\Big(\frac{SNR_{in}}{SNR_{out}}\Big) = 10 \cdot log_{10}\Big(1 + \frac{T_e}{T_0}\Big) \tag{5.4.13}$$

$$T_e \triangleq \frac{N_0[mW/Hz]}{k} \tag{5.4.14}$$

where $N_0[W/Hz]$ is the noise power spectral density and k is the already defined Boltzmann constant. Given N linear systems connected in series, each with its noise temperature $T_{e,i}$ and gain G_i, the noise temperature at the output of the series $T_{e,tot}$ is given by [86]

$$T_{e,tot} = T_{e,1} + \frac{T_{e,2}}{G_1} + \frac{T_{e,3}}{G_1 G_2} + \cdots = T_{e,1} + \sum_{i=2}^{N} \frac{T_{e,i}}{\prod_{j=1}^{i-1} G_j} \tag{5.4.15}$$

in which the first term is the most relevant for the entire link.

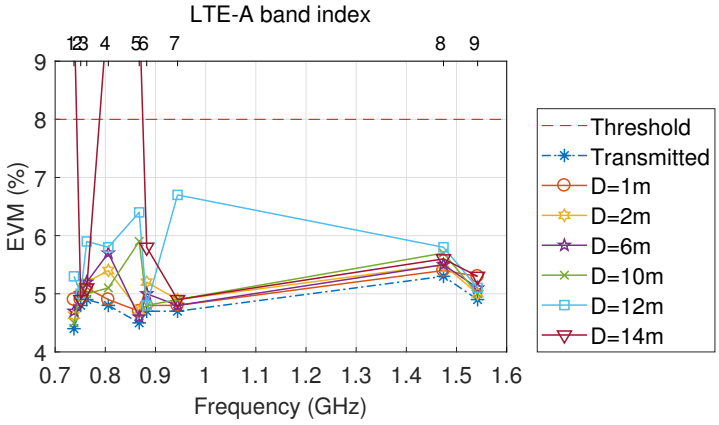

(a)

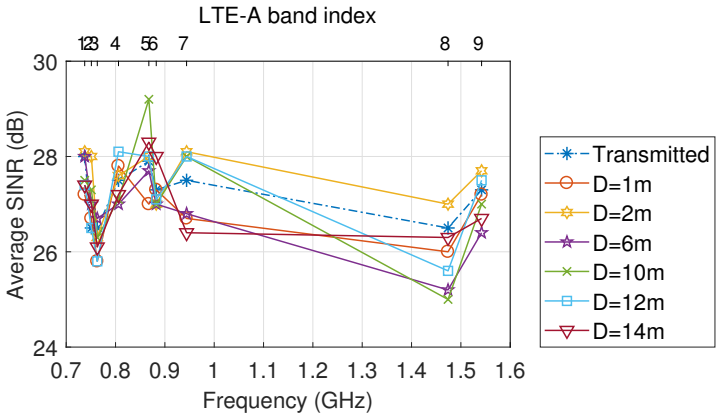

(b)

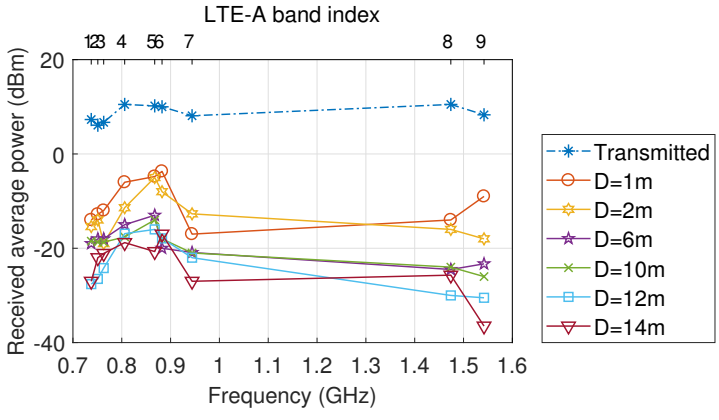

(c)

Figure 5.17. LTE-A EVM (a), SINR (b), and received power (c) results at Pt. C and Pt. D of the link in at Figure 5.12 for distance from 1 to 14 m.

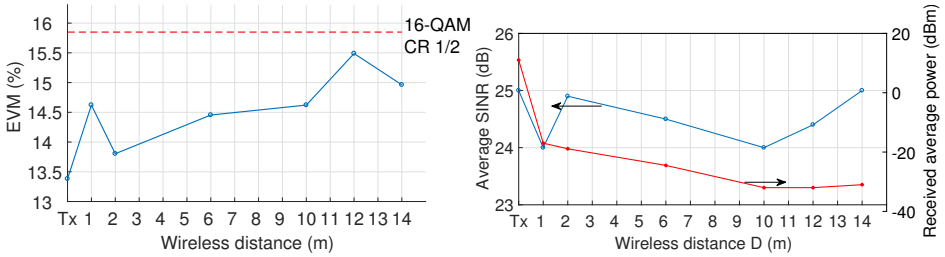

(a) (b)

Figure 5.18. WLAN EVM (a), SINR and received power (b) results at Pt. C and Pt. D of the link in at Figure 5.12 for distance from 1 to 14 m.

In the system under study, the POF link, the transmitter radio front-end, and the receiver radio front-end noise temperatures $T_{e,POF}$, $T_{e,TxFE}$, and $T_{e,RxFE}$ are respectively defined by (5.4.13), having each their own NF. Instead, the antenna equivalent noise temperature $T_{e,ant}$ is calculated through (5.4.14) by measuring its output noise power spectral density. This turns out to be comparable with the noise floor of the spectrum analyzer (i.e. much smaller than the other components). Therefore, $T_{e,ant}$ is smaller than the other temperatures.
Considering the noise temperature at Pt. E ($T_{e,E}$) of the link, (5.4.15) then becomes:

$$T_{e,E} = T_{e,POF} + \frac{T_{e,TxFE}}{G_{POF}} + \frac{T_{e,ant}}{G_{POF} \cdot G_{TxFE}} + \frac{T_{e,RxFE} \cdot A_{WL}(D)}{G_{POF} \cdot G_{TxFE}} \qquad (5.4.16)$$

where the contribution of the wireless impact on the third term is by $T_{e,ant}$ and on fourth term by the wireless link attenuation $A_{WL}(D)$. Firstly, in the third term the antenna noise temperature, already small, is further decreased by the high gain of the transmitter front-end and then is considered negligible. Secondly, in the fourth term the noise temperature of the receiver front-end is multiplied by the LOS attenuation and divided by the gain of the previous blocks (i.e. $\frac{A_{WL}(D)}{G_{POF} \cdot G_{TxFE}}$). For the distances considered (i.e. $D < 14\ m$) the wireless attenuation is smaller than the gain product, hence the fourth term is also considered negligible. Accordingly, the noise temperature contribution from the POF link and the transmitter front-

end are the most important, hence:

$$T_{e,POF} + \frac{T_{e,TxFE}}{G_{POF}} >> \frac{T_{e,ant}}{G_{POF}} + \frac{T_{e,RxFE} \cdot A_{WL(D)}}{G_{POF} \cdot G_{TxFE}} \tag{5.4.17}$$

and (5.4.16) can be written as follows:

$$T_{e,E} \approx T_{e,POF} + \frac{T_{e,TxFE}}{G_{POF}} = T_{e,D} \tag{5.4.18}$$

which is similar to the noise temperature at Pt. D, i.e. at the transmitter antenna port. Therefore, from $T_{e,D}$ and $T_{e,E}$ the SNR values can be calculated by (5.4.13) and they are alike. This confirms the results in section 5.4.3, the EVM and SINR at Pt. D and Pt. E of the link are similar and not decreasing with the distance D. This is because the noise is mainly generated at the transmitter, and all parameters constituting EVM and SINR are affected in the same way as they are propagating to the receiver.

5.5 Multiband WSN transmission over the POF link

In section 2.1, it is described how WSNs are becoming popular for home automation, smart home applications, and IoT. Furthermore, one of the main user cases for 5G will be massive M2M WSN communications. The requirements of such application are very different from the mobile and WLAN broadband network previously analyzed. WSNs are based on wireless sensors, are usually low-cost, low-energy, and small size data payload devices. Energy-consuming operations should be located on the infrastructure side, and operations on the device side should be kept as brief as possible to minimize the device on-time. Hence, a truly converged in-home network backbone should support the transmission of the WSN protocols.

Currently many standards for WSNs are available and they are differentiated depending on the target application, range and maximum coupling losses, and (un) licensed spectrum transmission [97]. IEEE 802.15.4 is among the most popular standards operating in the unlicensed bands. It defines the PHY and MAC layers of the protocol stack and it is the basis for many specifications (e.g. ZigBee, ISA100.11a, WirelessHART, MiWi, SNPA, Thread). IEEE 802.15.4 operates in 3 ISM bands 868 MHz (Europe), 915 MHz (North America), and 2442 MHz (Worldwide). Here the IEEE 802.15.4 signal is transmitted over the 2.4 GHz band

Table 5.4. Main parameters of the IEEE 802.11n signal.

Parameter	Value
ISM channel	11
Carrier frequency (MHz)	2462
Channel bandwidth (MHz)	40
Modulation format	QPSK
Coding rate	3/4
Transmitted power (dBm)	-17.55

because this band provides Worldwide operability. Furthermore, this band is used to test the optical link in the worst case scenario, due to the high optical link loss and the proximity to the IEEE 802.11n signal. Since the envisioned application is for supporting the massive M2M scenario, the IEEE 802.15.4 multiband transmission is performed, to support the simultaneous transmission over multiple bands by different sensors.

5.5.1 Experimental setup

Firstly, the baseband waveform is generated as described in section 5.3 and sent the AWG (AWG1). Secondly, the same 9 LTE-A bands listed in Table 5.1 are equalized by the time-invariant-equalization described in section 3.8.1.

As in section 5.4.2, the multiband LTE-A signal is digitally clipped and optimized to reduce the PAPR by 6 dB. The LTE-A, after being combined with the WSN signal, is generated by AWG2.
Next, the WLAN waveform is created by a VSG in accordance with the IEEE 802.11n standard and the parameters in Table 5.4. As shown in Figure 5.19, the signals are electrically combined, amplified, and sent over the optical link, which is the same as the system described in section 3.7.
Before the test the optical link showed 1 dB increment of the emitted optical power and consequently the received optical power after 50 m POF length is equal to -7.4 dBm. Further investigation on the $S21$ of the optical link showed a decrease for all the frequencies between 4 and 3 dB of the $S21$. This may be caused by an unexpected change in the bias voltage of the LD driver. The optical link -3 dB electrical bandwidth is re-measured and it is equal to 1.16 GHz.

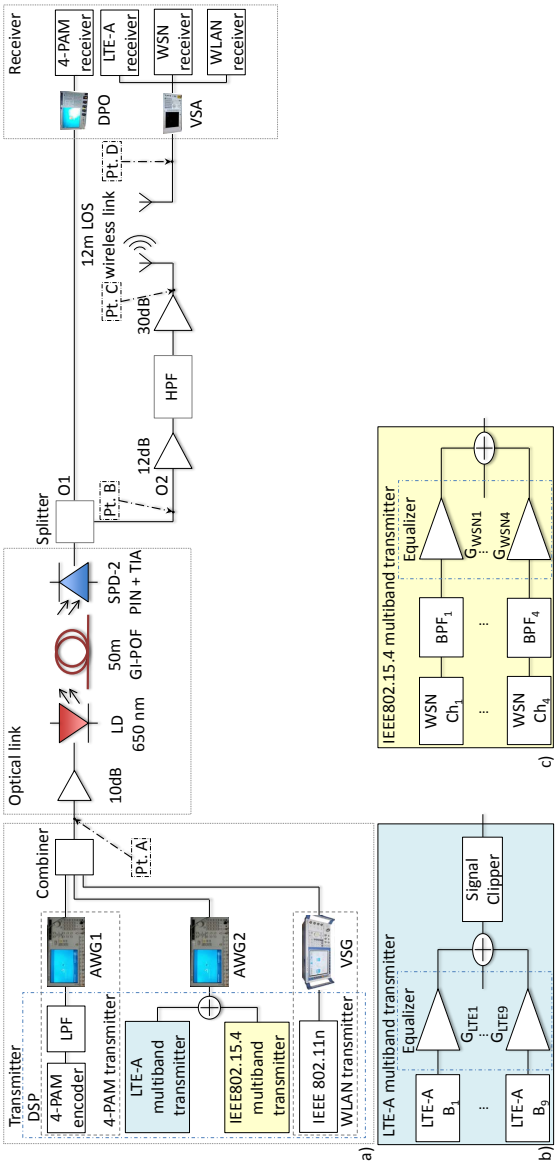

Figure 5.19. Experimental setup diagram: a) WLAN and 4-PAM transmitter with the optical and wireless link, b) LTE-A transmitter, and c)WSN transmitter.

After the transmission over the optical link and the optoelectrical conversion the electrical signal is split by a 1×2 power splitter. The first output (O1) is connected to the baseband receiver, the second output (O2) is connected to the RF front-end. The 4-PAM signal is removed by a HPF with cutoff frequency f_{co}. The transmitted power at the antenna port is between 2.2 and 6.6 dBm for the LTE-A bands, 6 dBm and -6.3 dBm for the WLAN and WSN signals, respectively. The signals are then re-transmitted through the antennas described in section 3.6.1 on the wireless link. A 12 m distance LOS wireless link is feasible and longer distances are limited by the Faraday cage size in which the experiment is performed. The received radio signals are decoded by the VSA.

WSN signal generation, pre-equalization, and filtering

The 4 IEEE 802.15.4 compliant WSN signals are generated in accordance with the parameters in Table 5.5. The standard does not support adaptive modulation and bandwidth, therefore only offset quadrature phase-shift keying (OQPSK) and 5 MHz bandwidth are used. Furthermore, the IEEE 802.15.4 is based on direct sequence spread spectrum (DSSS) coding, characterized by low PAPR, hence signal clipping is not applied. As shown in Figure 5.19, each WSN channel is digitally band-pass filtered and pre-equalized. The band-pass filters (BPFs) have a bandwidth of 5 MHz, the pre-equalization is similar to the one used to the LTE-A bands and it is carried out through the tailored amplification of each channel Ch_i by gain G_{WSNi}. Both the filtering and pre-equalization gain G_{WSNi} are optimized: to balance the adjacent channel interference between the WSN and the WLAN, to compensate the extra loss of the POF link at 2.4 GHz, and to tune the WSN signal power before being combined with the LTE-A signal.

5.5.2 Experimental results

The 4-PAM pre-FEC BER threshold is set to 1×10^{-3} and the maximum achievable bit rates are 1.7 and 1.66 Gb/s for the solitary and simultaneous 4-PAM transmission over 50 m POF, respectively. The decrease of the bit rate is related with the decrease of the POF link gain described in section 5.5.1.
As shown in Figure 5.20a, for the oB2B and 50 m the LTE-A solitary transmission achieves an EVM around 5%. When also the WLAN and WSN signals are co-transmitted, no LTE-A EVM performance degradation is measured, when all the waveforms are sent the LTE-A EVM at Pt. C augment to 6.5%. In total 9

Table 5.5. Main parameters of the IEEE 802.15.4 WSN signals in accordance with [98].

Parameter	Value			
Index (Ch_i)	1	2	3	4
Carrier frequency (MHz)	2410	2420	2430	2440
Band amplification gain G_{WSNi} (dB)	-9.9	-9.4	-9.4	-9.4
Channel bandwidth (MHz)	5			
Modulation format	OQPSK			

LTE-A bands are received with EVM lower than 8%, when the LTE-A waveform is transmitted over the wireless link and the maximum EVM in this case is equal to 7.5%.
The IEEE 802.11n WLAN standard defines an EVM threshold equals -16 dB (15.8%) and -13 dB (22.4%) for the 16-QAM and quadrature phase-shift keying (QPSK), respectively, through (5.3.1). As shown in Figure 5.20c, when only the WLAN signal is sent over 50 m POF link the EVM is around -19.2 dB (11%). When also the LTE-A and WSN are co-transmitted, the WLAN EVM increases by only 1%, therefore no major EVM penalty is incurred due to the adjacent WSN channels and 16-QAM modulation is used. When the 4-PAM waveform is co-transmitted, the WLAN EVM raises to 19%, which is related with the IMD between the signals, so the modulation format is switched to QPSK. Finally, the WLAN is then re-emitted over the wireless link, reaching an EVM of -13.4 dB (21.5%).
The IEEE 802.15.4 defines the EVM threshold at 35%, as shown in Figure 5.20b, the solitary WSN transmission over 50 m POF achieved 5% EVM for all the channels, on account of the pre-equalization. When the WSN, WLAN, and the LTE-A signals are co-transmitted, the WSN has a higher EVM up to 12%, due to the IMD of the LTE-A bands and the extra noise provided by the VSG. When also the 4-PAM is simultaneously sent, the WSN EVM increases between 15% and 20%. Similar to what happened for the WLAN, this increase is related to IMD. After 50 m POF link and the simultaneous transmission with the LTE-A, WLAN, and 4-PAM, the WSN has an EVM lower than 35% threshold. Furthermore, the WSN signal is sent over the wireless link with marginal extra penalty.

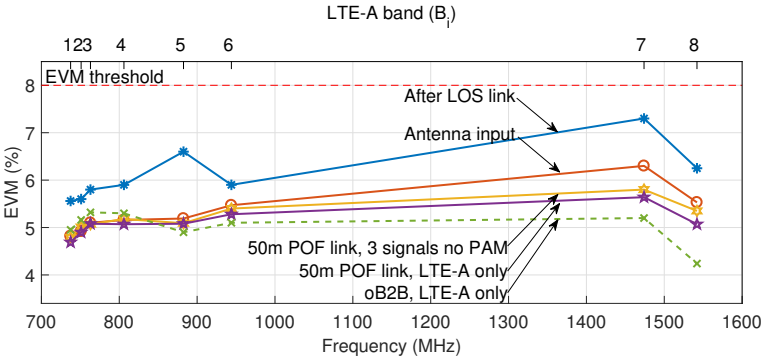

(a)

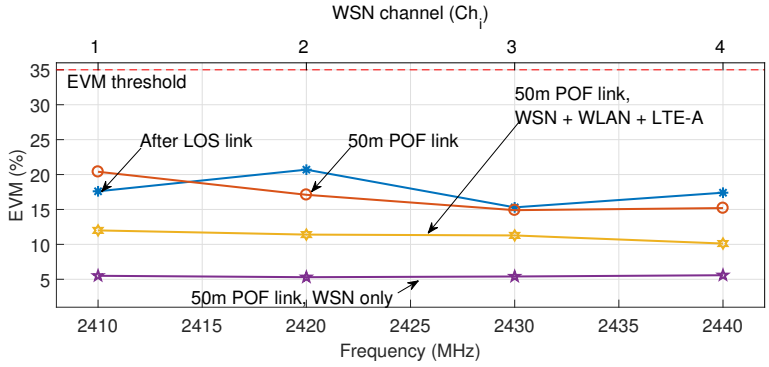

(b)

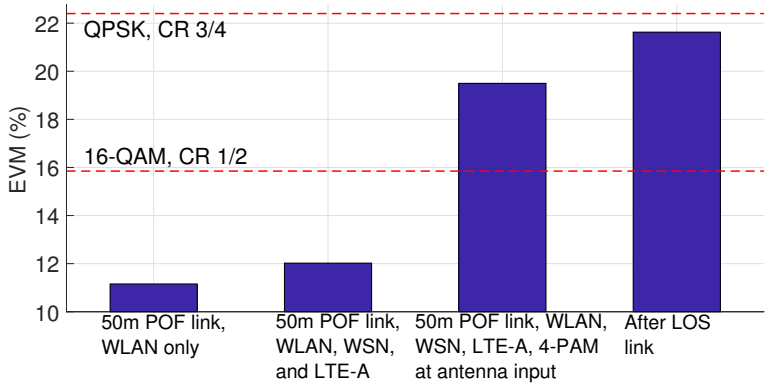

(c)

Figure 5.20. Measured EVM of the LTE-A (a), WSN (b), and WLAN (c) for the solitary and simultaneous transmission before and after the wireless link. *50 m POF link*, *Antenna input*, and *After LOS link* refer to Pt. B, C and D respectively in Figure 5.19.

5.6 Summary

In this chapter, a single large core POF link able to deliver 4 different standards and 3 type of services for in-home networks is presented. The single GI-POF is demonstrated to be able to simultaneously transmit a 4-PAM baseband signal, a multiband LTE-A signal, a WLAN signals, and a multiband IEEE 802.15.4 WSN signal, which proves the capability of POF as single wired backbone to support the network convergence for in-home networks.
In section 5.1 the mathematical model of a nonlinear system is recalled by using the Volterra's series, hence the higher order harmonics generation for a single and double tone signals is analyzed and the IMD is defined.
In section 5.2, the 50 m GI-POF link nonlinearity are measured by single and double tone measurements, which enable the calculation of the CDR_1 and $SFDR_3$.
In section 5.3, the successful transmission of 9 LTE-A bands and an IEEE 802.11ac WLAN signal is achieved. The multiband LTE-A signals are transmitted with A-RoF technique. The WLAN signal is transmitted with the IFoF, which is necessary given the high carrier frequency used by the IEEE 802.11ac. The IF is optimized in order to decrease the IMD between the radio signals, and two different cases are tested: IF close to DC and at 1.2 GHz.
In the first case, the WLAN reaches the best performance thanks to the higher power budget at cost of sacrificing the 4-PAM signal. The total throughput of the LTE-A and WLAN are equal to 605 Mb/s and 434 Mb/s, respectively. In the second case the IF allows the 4-PAM transmission but the WLAN power budget decreased slightly and consequently the modulation order is reduced. The total throughput is equal to 1.7 Gb/s, 605 Mb/s, and 325 Mb/s for the 4-PAM, LTE-A, and WLAN, respectively.
In section 5.4, the successful transmission of a baseband 4-PAM, 9 LTE-A bands, and an IEEE 802.11n WLAN signals over 50 m of GI-POF is demonstrated. The LTE-A and WLAN signals after the POF link are further retransmitted up to 12 m of wireless LOS link. The baseband signal throughput is equal to 1.7 Gb/s, the LTE-A and the WLAN throughput are 600 and 60 Mb/s, respectively. In this case, the WLAN is not shifted in frequency, being the 2.4 GHz ISM in reach of the POF link. In this case the IMD cannot be avoided by selecting the transmitting frequencies, therefore is necessary to avoid exceeding the optical link dynamic range and minimize the excitation of the nonlinearity. The WLAN can be transmitted at 2.4 GHz if the extra attenuation introduced by the POF link at that

frequency can be compensated by an increase of the transmitted power, such increased power must fit in the available POF link dynamic range in order to avoid the IMD generation. The peak power of the LTE-A is reduced by signal clipping. Hence, the multiband LTE-A PAPR is reduced by 6 dB. From the complexity perspective, different signal processing techniques are proposed in order to reduce the PAPR of the OFDM-based signals [99]. Here, the signal clipping technique is employed, which is one of the simplest method minimizing the signal processing complexity.

In section 5.4, a detailed evaluation of the noise performance of the link is presented. The overall noise figure measurements of the system including POF link and other blocks are presented for LTE-A and WLAN signals.
The POF link NF is desirable to be reduced. To do so, different techniques are suggested, among them increasing the transmitted SNR by increasing the transmitted optical power and the photodiode efficiency [100].
A final remark, the noise contribution from the optical link is predominant when an interference-free wireless link is used. This may not be the case for residential areas. In such scenario the interference from the neighboring WLAN APs and femtocells are among the most important causes of SINR degradation [101].

In section 5.5, the broadband wired and wireless services delivery over POF is enriched by the support to WSN for M2M communications. The WSN signals are closely located to the WLAN signal and limited interference between the bands is shown. At the transmitter, the LTE-A and WSN signal processing and combining is done in the digital domain and easier reconfiguration when different WSN standards are involved. The WSN channels closely located to the WLAN band showed minimal mutual interference thanks to the simple, yet effective, digital pre-equalization and filtering techniques applied. The successful transmission of 1.66 Gb/s 4-PAM modulated data, 600 Mb/s on 9 LTE-A bands, 45 Mb/s IEEE802.11n WLAN signal, and 4 IEEE802.15.4 WSN channels is achieved. The radio signals are then retransmitted over a 12 m wireless link.

In this chapter, the wireless distance is increased up to 12 m range, meaning a femtocell diameter of 24 m, able to cover most of the in-home room sizes and demonstrated the feasibility of low-cost 1 mm core diameter GI-POF links as in-home and in-building communication backbone.

Chapter 6

Conclusions and outlook

6.1 Conclusions

Indoor networks generate large amounts of Internet traffic through a wide range of applications by smart (portable) devices and home servers. Meanwhile, our houses become smarter by appliances that are able to communicate between each other through an increasing number of small and battery-powered devices. As described in chapter 1, the 5G mobile network is envisioning two major use cases:

- Broadband services with very high peak throughput, high average data-rate, and improved coverage.
- Massive machine-to-machine (M2M) connectivity.

Hence, the plethora of media and networks in the home increases the installation costs but also requires a more complex and more expensive management of the networks and services and limits the envisioned service convergence. The in-home network convergence over a single network backbone can ensure the coexistence of all the wired and wireless services. Furthermore, the single network can support the 5G envisioned user cases and can reduce the installation and management costs as explained in chapter 2.
Plastic optical fiber (POF) is a good candidate to become the wired backbone supporting the wired and wireless in-home services thanks its broadband capability, electromagnetic interference (EMI) immunity, and do-it-yourself technology.

In this thesis, a single POF link is demonstrated to provide the support for the baseband digital connectivity, as well as, for the broadband and M2M wireless communications.

In chapter 2, the results of the survey conducted within the FlexCom project on the end-user perspective of in-home networks, distributed antenna system (DAS), and POF networks were analyzed. The survey was conducted over 110 persons living in different European countries. The results showed the growing importance of mobile devices, in particular smartphones, and highlighted the predominance of Wi-Fi over the wired connection for the last meter. Hence, more than half of the participants were interested in deploying an in-home DAS in order to improve the Wi-Fi connectivity, showing the importance of an improved indoor wireless coverage. Nevertheless, the survey highlighted the need for further efforts in order to simplify the installation of the indoor wired network backbone, since the complexity of the installation of the network is the main concern. POF is resulted a convincing solution for the in-home network backbone and network convergence mainly thanks to the do-it-yourself technology. Further market penetration and wide-scale adoption will be achieved when the total cost of ownership becomes equal or lower than the other solutions.

In chapter 3, the convergence of wired and wireless mobile network services was discussed. Firstly, the main technical features of the mobile network signals were analyzed. Secondly, the first experiment over a 20 m 1 mm core diameter Poly(methyl methacrylate) (PMMA) GI-POF link showed the feasibility of the simultaneous transmission of the long-term evolution (LTE) and 4 level pulse amplitude modulation (4-PAM) offline signals by means of a frequency division multiplexing scheme. This solution achieved the simultaneous transmission of 3 long-term evolution - advanced (LTE-A) bands having carrier frequency between 790 and 960 MHz and 1.8 Gb/s 4-PAM signal. The main limitations were the tight frequency allocation of the services, unequal impairment among the LTE-A bands, limited optical power budget, and bandwidth of the optical transceivers. The tight frequency allocation requirement was eliminated through the filtering of the 4-PAM spectrum by a low-pass filter (LPF). In this way, the radio signals can be placed independently from the 4-PAM spectrum notches. Hence, a DSP-based time-invariant pre-equalization was introduced to balance the error vector magnitude (EVM) among all the radio signals transmitted. The equalizer is made by a set of amplifiers, one for each LTE-A band, the gain of the amplifier is tuned based on the received EVM, in order to ensure the same received EVM among

all the bands. This allowed achieving the simultaneous transmission of 8 LTE-A bands and 1.4 Gb/s 4-PAM baseband signal.
Thirdly, in order to support more services and longer link lengths, the optical link power budget and bandwidth were increased. A second link based on a Fabry-Pérot (FP) edge-emitting laser diode (EE-LD) optical source and broadband p-i-n photodiode allowed achieving 35 m link length and improved the bandwidth from 340 MHz to 1.16 GHz. At the same time the pre-equalization initially designed to balance the in-band LTE-A impairment was used to extend the POF link bandwidth and to transmit those LTE-A up to 1.8 GHz. In this way, 12 LTE-A bands were simultaneously transmitted together with 1.9 Gb/s 4-PAM signals. Therefore, in order to further increase the optical link distance a SI-POF was tested, which showed lower losses but distances longer than 35 m were not feasible due to the bandwidth-distance product (i.e 40 MHz·km) limitations of the SI-POF.
Finally, the optical link budget was further extended to 50 m length by using the GI-POF link based on the EE-LD transmitter and the wireless link transmission was demonstrated. Here the pre-equalization tuning method was based on the signal-to-interference-plus-noise ratio (SINR) feedback instead of the EVM, which further simplifies the radio resource unit (RRU) architecture. Furthermore, the effect of the transmission of a new LTE-A band and the limits of the pre-equalization method were showed. In total 8 LTE-A bands with carrier frequency between 730 and 1840 MHz and 1.8 Gb/s were transmitted over the 50 m POF link and the LTE-A multiband signal was further transmitted over 3.5 m wireless link.

In chapter 4, the transmission of a single band live LTE signal was performed over a 35 m POF link and over a 15 m wireless link toward a mobile device. The IP packets from Internet were transmitted over the LTE core and evolved universal terrestrial radio access (E-UTRA) network and from the base station, over the POF link, toward the mobile device over the downlink and vice versa on the uplink. The optical link distance was limited by the available optical devices at the moment of the experiment. The link length can be easily increased to the target distance of 50 m by using for both the uplink and downlink EE-LD optical transmitters and broadband p-i-n photodiodes. Preliminary tests demonstrated a limited EVM increase related with the transmission over the optical link. Then, the live LTE transmission in the licensed bands showed the support of multiple broadband services at the same time, such as high-definition video streaming and videophone calls without significant penalty incurred by the POF link.

In chapter 5, the network convergence over POF is demonstrated by support-

ing the simultaneous transmission of PAM, LTE-A, wireless local area network (WLAN), and wireless sensor network (WSN) signals over the same POF. Firstly, the WLAN IEEE 802.11ac signal at 5 GHz carrier frequency was transmitted by IF over fiber (IFoF) technique due to the too high carrier frequency for the POF link. The IFoF allowed to choose the intermediate frequency (IF) frequency in order to decrease the intermodulation distortion (IMD) and achieving a high modulation order (i.e. 64 and 256 quadrature amplitude modulation (QAM)) for the WLAN. Secondly, the WSN and the WLAN signals working at 2.4 GHz carrier frequency were transmitted over POF by analog radio over fiber (A-RoF) thanks to the LTE-A peak-to-average power ratio (PAPR) reduction. In section 3.8, the trade-off between pre-equalizing new radio bands at higher carrier frequency and the overall radio signal quality in terms of LTE-A EVM impairment was shown. In particular, the pre-equalization alone cannot balance the POF link electrical attenuation of the WLAN at 2.4 GHz carrier frequency. Furthermore, simulation of the IMD over the optical link showed a strong penalty on the WLAN related with the nonlinearity of the optical transceivers if the transmitted signals were able to overcome the dynamic range of the 50 m optical link. Hence, a clipping technique was implemented to decrease the LTE-A peak power and the WLAN transmitted signal-to-interference-plus-noise ratio (SINR) was increased without exceeding the dynamic range of the optical link. Then, the simultaneous transmission of 1.7 Gb/s 4-PAM signal, 9 LTE-A bands, and 1 IEEE 802.11n band was demonstrated over a 50 m GI-POF link and a 12 m wireless link.
Finally, the M2M WSN services were supported by simultaneously transmitting the 4-PAM signal, 9 LTE-A bands, 1 WLAN band and 4 IEEE 802.15.4 bands. The interference between the adjacent WSN and WLAN bands in the 2.4GHz industrial, scientific and medical (ISM) bands was limited by the low-pass finite impulse response (FIR) filters implemented on the transmitter side.

6.2 Outlook

In this thesis, the application of POF for the in-home network convergence of wired and wireless signals was demonstrated. Nevertheless, many challenges must be overcome in order to fully exploit the potential of POFs. The most important future directions of research are the following:

- As shown in chapter 5, the POF link non-linearity introduces IMD between

the radio signals. Hence, the link linearity should be improved in order to allow the transmission of more radio signals. Further studies should be pursued in the DSP compensation of the nonlinearity by Volterra filters [102]. The implementation of Volterra filters to compensate for the optical link nonlinearity is a known technique applied for long-haul optical networks. Volterra filters must be trained in order to define the filter taps. A more cost-effective implementation is possible under the assumption of a memoryless system. Therefore, the Volterra series can be approximated by Taylor polynomial and its DSP implementation requires less complexity.

- In the recent years, there has been a growing interest in multiple-input and multiple-output (MIMO) transmission. MIMO technology is already supported by many WLAN and mobile network standards. Furthermore, both IEEE and 3GPP are investigating the use of multi user (MU)-MIMO to deliver the promised broadband connectivity. Hence, a truly network convergence over POF will be achieved by supporting the transmission of the MIMO signal from the residential gateway to the RRU. Hence, a multiplexing scheme using a single POF link and supporting the MIMO transmission should be investigated. The transmission of MIMO signals over silica optical fiber link based on frequency shifting is demonstrated in [103] and the same multiplexing technique can be applied to the POF link. Nevertheless, the proposed scheme would also increase the number of radio signals simultaneously transmitted over the POF link. This increases the harmonic distortion and IMD if the dynamic range of the POF link is not improved.

- This thesis has demonstrated the capability of a POF network to support the in-home network convergence. The survey conducted within the project showed the necessity to decrease the POF link price, since it is a main concern for the end-user for its adoption. This can be achieved by avoiding expensive components and complex signal processing. The breakdown of POF network price shows that the cost of the E/O/E converters is predominant [104]. In this thesis VCSEL and EE-LD optical source are considered, further cost reduction can be achieved by exploring the use of resonant-cavity LED (RC-LED) optical sources. The digital signal processing complexity has been reduced by implementing 4-PAM coding instead of discrete multitone (DMT). Further decrease can be achieved by using low-sampling rate synchronization algorithm, thus reducing the finite impulse response (FIR)

filters sampling frequency. Moreover, the identification of a strategy that leads to mass production and leverages on the economy of scale to decrease the POF link costs at a comparable level with Cat 5 link cost should be pursued.

- The in-home network convergence over POF requires a broadband optical link able to accommodate all signals. In this thesis, both PMMA SI and GI POFs were investigated and the latter clearly showed broader bandwidth. Nevertheless, the Gigabit Ethernet over POF standard (i.e. IEEE 802.3bv) is based on the SI-POF. SI-POF is preferred thanks the standardized characteristics, the easier production, and due to the GI-POF limitations (i.e. high bending losses and higher losses per meter), which makes SI-POF a more reliable choice for POF market. Once these problems have been solved, GI-POF truly ensures the broadband connectivity needed by the network convergence. The proposed pre-equalization aim to balance the frequency response of the POF link from the optical source input to the optical receiver output. Such technique can be further exploited by increasing the POF transceivers bandwidth. In particular, the bandwidth of a 50 m GI-POF is 3 GHz, while, in this thesis, the maximum optical link bandwidth was limited to 1.1 GHz by the p-i-n optical receiver. Further study should be performed to improve the optical receiver frequency response. For instance, POF optical receivers based on metal-semiconductor-metal (MSM) photodiodes with active areas from 400 to 1000 μm and -3 dB bandwidth up to 11 GHz are demonstrated for digital baseband transmission over GI-POF [105]. Thus, their application for radio-over-POF link should be investigated together with the proposed pre-equalization scheme in order to stretch the POF link frequency response.

Bibliography

[1] A. M. J. Koonen and E. Tangdiongga, "Photonic home area network," *J. Light. Technol.*, vol. 32, no. 4, pp. 591–604, 2014.

[2] CISCO, "The Zettabyte Era: Trends and Analysis," *Cisco*, no. May, pp. 1–29, 2015.

[3] Ericsson Consumer lab, "The indoor influence: Regional report Europe," Tech. Rep. April, 2015.

[4] T. Ali-Yahiya, *Understanding LTE and its Performance*, Springer, Ed., New York, 2011.

[5] Nokia, "Going mobile with branded Wi-Fi," Espoo, Tech. Rep., 2017.

[6] ——, "Automated Wi-Fi Optimization differentiates your customers' experience," Espoo, Tech. Rep., 2017.

[7] S. V. Halde and S. T. Khot, "Efficient collection of big data in WSN," in *Proc. Int. Conf. Inven. Comput. Technol. ICICT 2016*, vol. 1, 2017, pp. 1–5.

[8] A. Seyedolhosseini, N. Masoumi, and M. Modarressi, "Performance Improvement of ZigBee Networks in Coexistence of Wi-Fi Signals," in *Proc. 7th Int. Conf. Inf. Commun. Manag.*, ACM, Ed., Moscow, Russian Federation, 2017, pp. 45–49.

[9] Y. Shi, E. Tangdiongga, A. M. J. Koonen, A. Bluschke, P. Rietzsch, J. Montalvo, M. M. De Laat, G. N. Van Den Hoven, and B. Huiszoon, "Plastic-optical-fiber-based in-home optical networks," *IEEE Commun. Mag.*, vol. 52, no. 6, pp. 186–193, 2014.

[10] A. Antonino, D. Zeolla, and R. Gaudino, "Experimental proof-of-concept of bidirectional gigabit transmission over single step-index plastic optical fiber," *IEEE Photonics Technol. Lett.*, vol. 22, no. 12, pp. 923–925, 2010.

[11] R. van der Linden, in *Adaptive Modulation Technique for Passive Optical Networks*, April 2018.

[12] Y. Shi, "Optical Broadband In-Home Networks for Converged Service Delivery," Ph.D. dissertation, Eindhoven University of Technology, 2013.

[13] I. F. Akyildiz, S. Nie, S. C. Lin, and M. Chandrasekaran, "5G roadmap: 10 key enabling technologies," *Comput. Networks*, vol. 106, pp. 17–48, 2016.

[14] Federal Communications Commission, "Millimeter Wave Propagation: Spectrum Management Implications," Tech. Rep. July, 1997.

[15] P. Mogensen, K. Pajukoski, E. Tiirola, J. Vihriala, E. Lahetkangas, G. Berardinelli, F. M. L. Tavares, N. H. Mahmood, M. Lauridsen, D. Catania, and A. F. Cattoni, "Centimeter-wave concept for 5g ultra-dense small cells," in *2014 IEEE 79th Vehicular Technology Conference (VTC Spring)*, May 2014, pp. 1–6.

[16] ETSI, "Universal Mobile Telecommunications System (UMTS); Wireless Local Area Network (WLAN) offload;," Tech. Rep., 2014.

[17] M. Deakin and H. A. Waer, "From intelligent to smart cities," *Intelligent Buildings International*, vol. 3, no. 3, pp. 140–152, 2011. [Online]. Available: https://doi.org/10.1080/17508975.2011.586671

[18] "Industry 4.0," https://www.bmbf.de/de/zukunftsprojekt-industrie-4-0-848.html, 2018, February.

[19] A. J. Cooper, "'fibre/radio' for the provision of cordless/mobile telephony services in the access network," *Electronics Letters*, vol. 26, no. 24, pp. 2054–2056, Nov 1990.

[20] "Allen telecom's radio-over-fiber technology powers mobile communications at olympics," https://www.wirelessnetworksonline.com/doc/allen-telecoms-radio-over-fiber-technology-po-0001, 2018, April.

[21] X. N. Fernando, *Radio over fiber for wireless communications from fundamentals to advanced topics*, wiley-ieee ed., Wiley, Ed., 2014.

[22] D. Wake, A. Nkansah, N. J. Gomes, and S. Member, "Radio Over Fiber Link Design for Next Generation Wireless Systems," *Lightwave*, vol. 28, no. 16, pp. 2456–2464, 2010.

[23] U. R. Bhatt, A. Chhabra, and R. Upadhyay, "Fiber-wireless (Fi-Wi) architectural technologies: A survey," *2016 Int. Conf. Electr. Electron. Optim. Tech.*, pp. 519–524, 2016.

[24] D. Novak and R. Waterhouse, "Advanced radio over fiber network technologies," *Opt. Express*, vol. 21, no. 19, p. 23001, 2013.

[25] J. A. M. Souza, M. M. Mosso, R. M. Ribeiro, A. P. L. Barbero, and O. S. Xavier, "Hybrid Wireless-Optoelectronic Transmitter for Low Frequency Radio over Polymer Optical Fibres (POFs)," in *20th Int. Conf. Plast. Opt. Fibres, POF 2011*, no. 1, 2011, pp. 443–448.

[26] B. G. Kim, K. Tanaka, T. Kobayashi, A. Bekkali, K. Nishimura, H. Kim, M. Suzuki, and Y. C. Chung, "Transmission Experiment of LTE Signals by IF-over-Fiber Using Commercial Base Station and Deployed Optical Fibers," in *42nd Eur. Conf. Exhib. Opt. Commun.*, no. 1, 2016, pp. 935–937.

[27] A. Nirmalathas, P. a. Gamage, C. Lim, D. Novak, and R. Waterhouse, "Digitized radio-over-fiber technologies for converged optical wireless access network," *J. Light. Technol.*, vol. 28, no. 16, pp. 2366–2375, 2010.

[28] M. El-Hajjar, D. Liu, L. Hanzo, and V. Thomas, "Experimental demonstration of plastic optical fibre-based digitised radio over fibre downlink," *Electron. Lett.*, vol. 51, no. 21, pp. 1679–1681, 2015.

[29] J. Heidarialamdarloo, A. Sousa, E. Silva, R. Oliveira, R. Ferreira, A. Shahpari, R. Nogueira, J. Costa, and A. Teixeira, "Digitized radio over plastic optical fiber for in-home network applications," *26th Int. Conf. Plast. Opt. Fibres, POF 2017 - Proc.*, pp. 10–15, 2017.

[30] "Optical fiber types," https://upload.wikimedia.org/wikipedia/commons/thumb/0/0e/Optical_fiber_types.svg/2000px-Optical_fiber_types.svg.png, 2018, February.

[31] O. Ziemann, J. Krauser, P. E. Zamzow, and W. Daum, "Optical Fibers," in *POF Handb. Opt. Short Range Transm. Syst.*, Berlin, 2008, ch. 2.

[32] "Plastic optical fibre," https://www.fia-online.co.uk/pdf/Whites/wp1007.pdf, 2018, February.

[33] "Specifications-optimedia 1 mm GI-POF," http://www.optimedia.co.kr/eng_optimedia_main_b_01.htm, 2018, February.

[34] R. Kruglov, J. Vinogradov, O. Ziemann, and W. Huber, "Application of 4-channel led module for wdm transmission over si-pof," 2017, pp. 33–35.

[35] "SI-POF and GI-POF loss vs optical spectrum," https://www.kdpof.com/wp-content/uploads/2012/07/shapeimage_8.png, 2018, February.

[36] O. Ziemann, J. Krauser, P. E. Zamzow, and W. Daum, "System Design," in *POF Handb. Opt. Short Range Transm. Syst.*, Berlin, 2008, ch. 6, pp. 451–452.

[37] ——, "System Design," in *POF Handb. Opt. Short Range Transm. Syst.*, 2008, pp. 451–452.

[38] C. Gimeno, C. Sánchez-azqueta, E. Guerrero, J. Aguirre, C. Aldea, and S. Celma, "Single-Chip Receiver for 1.25 Gb/s Over 50-m SI-POF," *Photonics Technol. Lett.*, vol. 27, no. 11, pp. 1220–1223, 2015.

[39] O. Ziemann, J. Vinogradov, E. Bluoss, and W. Eischer, "- 22 dBm receiver sensitivity for Gbps data communication on SI POF and glass fiber presented by :," Tech. Rep. 1, 2004.

[40] G. P. Agrawal, *Fiber-Optic Communications Systems, Third Edition.*, 3rd ed., Rochester, NY, 2002, vol. 1.

[41] J. B. Anderson, "Baseband pulse transmission," in *Digit. Transm. Eng.*, 2nd ed., IEEE, Ed. Wiley, 2006, ch. 2, pp. 13–78.

[42] C. Zerna, J. Sundermeyer, A. Fiederer, N. Verwaal, B. Offenbeck, and N. Weber, "Integrated PAM2 decision feedback equalizer for gigabit Ethernet over standard SI-POF using red LED," in *36th European Conference and Exhibition on Optical Communication*, Sept 2010, pp. 1–3.

[43] R. Kruglov, S. Loquai, C.-a. Bunge, M. Schueppert, J. Vinogradov, and O. Ziemann, "Comparison of PAM and CAP Modulation Schemes for Data Transmission Over SI-POF," *Photonics Technol. Lett.*, vol. 25, no. 23, pp. 2293–2296, 2013.

[44] R. Kruglov, S. Loquai, C.-A. Bunge, O. Ziemann, B. Schmauss, and J. Vinogradov, "10 Gbit/s Short-Reach Transmission over 35 m Large-Core Graded-Index Polymer Optical Fiber," in *Opt. Fiber Commun. Conf. Fiber Opt. Eng. Conf. 2011*, 2011, p. OThZ6.

[45] S. Loquai, R. Kruglov, B. Schmauss, C. Bunge, F. Winkler, O. Ziemann, E. Hartl, and T. Kupfer, "Comparison of Modulation Schemes for 10. 7 Gb/s Transmission Over Large-Core 1 mm PMMA Polymer Optical Fiber," *J. Light. Technol.*, vol. 31, no. 13, pp. 2170–2176, 2013.

[46] "IEEE standard for ethernet amendment 9: Physical layer specifications and management parameters for 1000 mb/s operation over plastic optical fiber," pp. 1–140, March 2017.

[47] L. C. Nadales, "Tomlinson Harashima Precoding for Multi-Gigabit short-haul Transrnission over Plastical Optical Fibers," Ph.D. dissertation, University of Stuttgart, 2010.

[48] Cisco System, "Cisco Visual Networking Index : Forecast and," Tech. Rep., 2017.

[49] G. Keiser, "Network implementation trade-offs in existing homes," *Int. Congr. Ultra Mod. Telecommun. Control Syst. Work.*, pp. 528–532, 2012.

[50] Nordx, "Commercial Building Telecommunications Standard 12 ANSI/TIA/EIA-568-B," Tech. Rep., 1999.

[51] "Deploying 10gbase-t with cisco switches: Choose the right cabling," https://web.archive.org/web/20160525052443/http://www.cisco.com/c/en/us/products/collateral/switches/catalyst-4900-series-switches/white_paper_c11-609513.html#close, 2018, February.

[52] R. T. Ltd, "Cat 7 600 MHz STP Horizontal Cable," Tech. Rep.

[53] "Specifications-utp CAT 6 cable," http://www.extron.nl/download/files/specs/UTP_CAT_6_cable_020402.pdf, 2018, February.

[54] "Distributed coverage and capacity solutions," http://openairinterface.eurecom.fr/expressmimo2, 2018, April.

[55] M. Beltrán, Y. Shi, C. Okonkwo, R. Llorente, E. Tangdiongga, and A.M.J. Koonen, "In-home networks integrating high-capacity DMT data and DVB-T over large-core GI-POF," *Opt. Express*, vol. 20, no. 28, pp. 29 769–29 775, 2012.

[56] A. J. Seeds and T. Ismail, "Broadband access using wireless over fibre systems," *J. Light. Technol.*, vol. 28, no. 16, pp. 2430–2435, 2010.

[57] F. Forni, H. P. A. V. D. Boom, Y. Shi, E. Tangdiongga, and A. Koonen, "Full-Service Home Area Networks Using Plastic Optical Fibers," in *24th Int. Conf. Plast. Opt. Fibers*, International Cooperative of Plastic Optical Fibers (ICPOF), Ed. Nuremberg, Germany: International Cooperative of Plastic Optical Fibers (ICPOF), 2015, pp. 223–226.

[58] F. Forni, Y. Shi, H. V. D. Boom, E. Tangdiongga, and T. Koonen, "Multiband LTE-A and 4-PAM Signals Over Large-Core Plastic Fibers for In-Home Networks," *IEEE PHOTONICS Technol. Lett.*, vol. 28, no. 20, pp. 2281–2284, 2016.

[59] F. Forni, Y. Shi, H. P. A. V. D. Boom, E. Tangdiongga, and A. M. J. Koonen, "Multiband 4G and Gigabit / s Baseband Transmission over Large-Core GI and SI POFs for In-Home Networks," in *25th Int. Conf. Plast. Opt. Fibres (POF 2016)*, Birmingham, 2016.

[60] F. Forni, Y. Shi, H. van den Boom, E. Tangdiongga, and A.M.J. Koonen, "LTE-A Multiband and Ethernet over Large-core Diameter Wired and Wireless Networks," in *ECOC 2016; 42nd Eur. Conf. Opt. Commun. Proc.* Düsseldorf (Germany): VDE, 2016.

[61] F. Forni, Y. Shi, H. P. A. V. D. Boom, E. Tangdiongga, and A. M. J. Koonen, "SINR-based Equalization for Multiband LTE-A and Gbps 4-PAM Transmission over 50m Thick-core POF and Wireless Link," in *OFC/NFOEC 2017*, Los Angeles, 2017.

[62] G. Li and G. L. Stüber, *Orthogonal frequency division multiplexing for wireless communications*. Springer US, 2006.

[63] J. G. Andrews, S. Buzzi, W. Choi, S. V. Hanly, a. Lozano, a. C. K. Soong, and J. C. Zhang, "What Will 5G Be?" *Sel. Areas Commun. IEEE J.*, vol. 32, no. 6, pp. 1065–1082, 2014.

[64] "3GPP agrees on plan to accelerate 5G NR the global 5G standard for 2019 deployments," https://www.qualcomm.com/news/onq/2017/03/09/3gpp-agrees-plan-accelerate-5g-nr-global-5g-standard-2019-deployments, 2018, April.

[65] "5G: What is Standalone (SA) vs Non-Standalone (NSA) Networks?" https://www.mediatek.com/blog/5g-what-is-standalone-sa-vs-non-standalone-nsa, 2018, April.

[66] ETSI, "TS 136 141 - V10.5.0 - LTE; Evolved Universal Terrestrial Radio Access (E-UTRA); Base Station (BS) conformance testing (3GPP TS 36.141 version 10.5.0 Release 10)," Tech. Rep., 2012.

[67] ——, "LTE; Evolved Universal Terrestrial Radio Access (E-UTRA); Base Station (BS) radio transmission and reception (3GPP TS 36.104 version 14.3.0 Release 14)," 3-GPP, Tech. Rep., 2017.

[68] B. Sklar, *Digital Communications*, 2nd ed., Prentie Hall, Ed., Tarzana (CA), 2001.

[69] "Three methods of noise figure measurement," https://www.maximintegrated.com/en/app-notes/index.mvp/id/2875, 2017, July.

[70] "Slp-750+ low pass fltr / sma / rohs," https://www.minicircuits.com/WebStore/dashboard.html?model=SLP-750%2B, 2018, April.

[71] W. Leng, Y. Zhang, and Z. Yang, "A modified Gardner detector for multilevel PAM/QAM system," *2008 Int. Conf. Commun. Circuits Syst. Proceedings, ICCCAS 2008*, no. 1, pp. 891–895, 2008.

[72] Z. Liu, private communication, 2016.

[73] "Spd-2 650nm & spd-2 850nm," http://www.graviton.co.jp/OE/Subpages/HP_OE_SPD-2_Eng.htmlf, 2018, February.

[74] "Bmlpvmb/lte," https://www.welotec.com/tradepro/shopen/artikel/allgemein/BMLPVMB-LTE-Datenblatt-DE.pdf, 2018, February.

[75] B. J. Henderson, "Radio Propagation and Radio Coverage Computer Simulation Program," Calgary, Tech. Rep., 2013.

[76] "The European Table of Frequency Allocations and Applications in the Frequency Range 8.3 KHz to 3000 GHz (ECA Table)."

[77] A. Chandra and S. Chattopadhyay, "Design of hardware efficient FIR filter: A review of the state-of-the-art approaches," *Eng. Sci. Technol. an Int. J.*, vol. 19, no. 1, pp. 212–226, 2016. [Online]. Available: http://dx.doi.org/10.1016/j.jestch.2015.06.006

[78] F. Forni, Y. Shi, H. P. Van Den Boom, E. Tangdiongga, and A. M. Koonen, "Multiband LTE-A, WiFi ac, and 4-PAM baseband simultaneous transmission over 50 m thick-core POF for in-home network," in *Int. Conf. Transparent Opt. Networks*, 2017, pp. 4–7.

[79] F. Forni, Y. Shi, H. P. A. V. D. Boom, E. Tangdiongga, and A. M. J. Koonen, "WLAN and Multiband LTE-A Simultaneous Transmission over 50m Thick-core GI-POF for In-home Distributed Antenna Systems," in *26th Int. Conf. Plast. Opt. Fibres (POF 2017)*, 2017, pp. 2–5.

[80] ——, "WiFi, Multiband Clipped LTE-A and Gbps 4-PAM Simultaneous Transmission over 50m Thick-core POF and Wireless Link for Home Area Networks," in *43rd Eur. Conf. Opt. Commun.*, 2017.

[81] F. Forni, N. C. Tran, H. P. A. V. D. Boom, E. Tangdiongga, and A. M. J. Koonen, "Simultaneous Multiband WSN, WLAN, LTE-A, and Gb/s 4-PAM Signals Transmission over 50 m 1mmCore Diameter POF for Home Area Network F." in *OFC/NFOEC 2018- Opt. Fiber Commun. Natl. Fiber Opt. Eng. Conf. 2018*, 2018, pp. 1–4.

[82] Cisco, "The Zettabyte Era : Trends and Analysis," Tech. Rep., 2017.

[83] F. Giannini and G. Leuzzi, *Nonlinear Microwave Circuit Design.* Wiley, 2004.

[84] X. N. Fernando, "DSP Modeling of the ROF Link Nonlinearity," in *Radio over fiber Wirel. Commun. from Fundam. to Adv. Top.*, wiley-ieee ed. Wiley, 2014, ch. 8, pp. 129–137.

[85] V. J. Urick, J. D. McKinney, J. F. Diehl, and K. J. Williams, "Fiber-optic links with all-photonic RF gain and low RF noise figure," *IEEE MTT-S Int. Microw. Symp. Dig.*, 2011.

[86] V. J. Urick, J. D. McKinney, and K. J. Williams, *Fundamentals of Microwave Photonics*, wiley ed., 2015.

[87] D. Visani, C. Okonkwo, S. Loquai, H. Yang, Y. Shi, H. Van Den Boom, T. Ditewig, G. Tartarini, B. Schmauss, J. Lee, T. Koonen, and E. Tangdiongga, "Beyond 1 Gbit/s transmission over 1 mm diameter plastic optical fiber employing DMT for in-home communication systems," *J. Light. Technol.*, vol. 29, no. 4, pp. 622–628, 2011.

[88] I.-S. S. Board and Authorized, *Specific requirements Part 11 : Wireless LAN Medium Access Control (MAC) and Physical Layer (PHY) Specifications Amendment 4 : Enhancements for Very High Throughput for Operation in Bands below 6 GHz IEEE Computer Society*, New York, NY, 2013.

[89] Y. Rahmatallah and S. Mohan, "Peak-To-Average Power Ratio Reduction in OFDM Systems: A Survey And Taxonomy," *Commun. Surv. Tutorials, IEEE*, vol. 15, no. 4, pp. 1567–1592, 2013.

[90] "Understanding PAPR in OFDM systems," https://www.nutaq.com/blog/understanding-papr-ofdm-systems, 2018, January.

[91] T. Li, R. V. Penty, and I. H. White, "Novel digital radio over fibre for 4G-LTE," *2015 IEEE Int. Conf. Commun. Work. ICCW 2015*, pp. 312–317, 2015.

[92] R. van Nee and A. de Wild, "Reducing the peak-to-average power ratio of OFDM," in *Vehicular Technology Conference, 1998. VTC 98. 48th IEEE*, vol. 3, May 1998, pp. 2072–2076 vol.3.

[93] "Fresnel zone calculator," http://afar.net/fresnel-zone-calculator/, 24-11-2017.

[94] H. A. Mahmoud and H. Arslan, "Error vector magnitude to SNR conversion for nondata-aided receivers," *IEEE Trans. Wirel. Commun.*, vol. 8, no. 5, pp. 2694–2704, 2009.

[95] L. A. N. Man, S. Committee, and I. Computer, "Part 11 : Wireless LAN Medium Access Control (MAC) and Physical Layer (PHY) S pecifications IEEE Computer Society," Tech. Rep. March, 2012.

[96] Agilent Technologies, "Fundamentals of RF and Microwave Noise Figure Measurements," Tech. Rep., 2010.

[97] Nokia, "LTE evolution for IoT connectivity," Tech. Rep.

[98] IEEE, "IEEE Std 802.15.4-2015 - IEEE Standard for Low-Rate Wireless Networks," IEEE, New York, NY, Tech. Rep. April 2016, 2016.

[99] R. Yoshizawa and H. Ochiai, "Effect of clipping and filtering with distortionless PAPR reduction for OFDM systems," *2015 IEEE 82nd Veh. Technol. Conf. VTC Fall 2015 - Proc.*, no. 3, 2016.

[100] K. Kim, D. S. Shin, Y. D. Chung, K. S. Choi, J. S. Sim, and J. Kim, "Improving the noise figure of the 60-GHz radio-over-fiber system using a system-on-package EAM module with two-stage LNAs," in *MWP 2007 - 2007 IEEE Int. Top. Meet. Microw. Photonics*, 2007, pp. 124–126.

[101] C. Bouras and G. Diles, "Interference Management Strategy for 5G Femtocell Clusters," *Wirel. Pers. Commun.*, vol. 96, no. 1, pp. 323–339, 2017.

[102] P. Torres, S. Straullu, S. Abrate, and R. Gaudino, "Alternative Solutions for Fronthauling Based on DSP-Assisted Radio-over-Fiber," in *19th Int. Conf. Transparent Opt. Networks (ict. 2017)*, 2017, pp. 2–5.

[103] J. S. Zou, H. Chen, F. Huijskens, Z. Cao, E. Tangdiongga, and T. Koonen, "Demonstration of Fully Functional MIMO Wireless LAN Transmission over GI-MMF for In-building Networks," in *OFC/NFOEC 2013 - Opt. Fiber Commun. Natl. Fiber Opt. Eng. Conf. 2013*, no. Ld, 2013, pp. 8–10.

[104] A. Koonen, H. P. a. V. D. Boom, E. O. Martinez, P. Guignard, and E. Tangdiongga, "Cost optimization of optical in-building networks," in *37th Eur. Conf. Exhib. Opt. Commun.*, vol. 19, no. 26, COBRA Institute, Eindhoven

Univ. of Technology, P.O. Box 513, NL 5600MB Eindhoven, The Netherlands. Ieee, 2011, pp. 1–3.

[105] S. Loquai, F. Winkler, S. Wabra, E. Hartl, and B. Schmauss, "High-Speed , Large-Area POF Receivers for Fiber Characterization and Data Transmission 10-Gb / s Based on MSM-Photodetectors," *J. Light. Technol.*, vol. 31, no. 7, pp. 1132–1137, 2013.

List of Symbols

3GPP 3rd Generation Partnership Project.
4-PAM 4 level pulse amplitude modulation.

ADC analog-to-digital converter.
A-RoF analog radio over fiber.
AP access point.
APD avalanche photodiode.
AWG arbitrary waveform generator.

BBoF baseband over fiber.
BER bit error rate.
BPF band-pass filter.

CAP carrierless amplitude phase.
CapEx capital expenditure.
CCDF complementary cumulative distribution function.
CDR_1 1 dB compression dynamic range.
CR coding rate.

DAC digital-to-analog converter.
DC direct current.
DPO digital phosphor oscilloscope.
D-RoF digitized radio over fiber.
DAS distributed antenna system.
DMT discrete multitone.
DSL digital subscriber line.

DSP digital signal processing.
DSSS direct sequence spread spectrum.

eB2B electrical back-to-back.
EPC evolved packet core.
E-TM evolved test model.
EE-LD edge-emitting laser diode.
EMI electromagnetic interference.
E-UTRA evolved universal terrestrial radio access.
EVM error vector magnitude.

FDD frequency division duplex.
FDM frequency division multiplexing.
FEC forward error correction.
FIR finite impulse response.
FP Fabry-Pérot.
FTTH Fiber-to-the-Home.

GI graded index.

HAN home area network.
HPF high-pass filter.

IDFT inverse discrete Fourier transform.
IEEE Institute of Electrical and Electronics Engineers.
IF intermediate frequency.
IFFT inverse fast Fourier transform.
IFoF IF over fiber.
IIP3 3rd order input intercept point.
IMD intermodulation distortion.
IM-DD intensity modulated direct detection.
IMT international mobile telecommunications.
IoT Internet of Things.
IP Internet protocol.
IP3 3rd order intercept point.
ISI inter-symbol interference.
ISM industrial, scientific and medical.

ITU-T international telecommunication union telecommunication standardization sector.

LD laser diode.
LED light-emitting diode.
LIA low-impedance amplifier.
LOS line-of-sight.
LPF low-pass filter.
LTE long-term evolution.
LTE-A long-term evolution - advanced.

MIMO multiple-input and multiple-output.
MMF multi-mode optical fiber.
MMIC monolithic microwave integrated circuit.
MOST media oriented systems transport.
M-RAT multi radio access technology.
M2M machine-to-machine.
MSM metal-semiconductor-metal.

NA numerical aperture.
NF noise figure.
NLOS non-line-of-sight.
NRZ non-return-to-zero.

oB2B optical back-to-back.
OFDM orthogonal frequency-division multiplexing.
OFDMA orthogonal frequency-division multiple access.
OIP3 3rd order output intercept point.
OpEx operational expenditure.
OQPSK offset quadrature phase-shift keying.
OS operating system.

PAM pulse amplitude modulation.
PAPR peak-to-average power ratio.
PC personal computer.
PDSCH physical downlink shared channel.
PLC power-line communication.

PMMA Poly(methyl methacrylate).
POF plastic optical fiber.
POF-AC POF Application Center.
PON passive optical network.
PRBS pseudorandom binary sequence.

QAM quadrature amplitude modulation.
QPSK quadrature phase-shift keying.

RAN radio access network.
RAT radio access technology.
RB resource block.
RC-LED resonant-cavity LED.
RE resource element.
RF radio frequency.
RoF radio over fiber.
RRU radio resource unit.

SDR software-defined radio.
$SFDR_3$ 3rd order spurious free dynamic range.
Si Silicon.
SI step index.
SINR signal-to-interference-plus-noise ratio.
SMF single-mode optical fiber.
SNR signal-to-noise ratio.

TDD time division duplex.
TIA transimpedance amplifier.
TNO Netherlands Organisation for Applied Scientific Research.

UE user equipment.

VCSEL vertical-cavity surface-emitting laser.
VSA vector signal analyzer.
VSG vector signal generator.

WDM wavelength division multiplexing.
WLAN wireless local area network.
WSN wireless sensor network.

List of Publications

Peer-reviewd journals:

1. **F. Forni**, Y. Shi, N. Tran, H.P.A. van den Boom, E. Tangdiongga, A.M.J. Koonen, "Multi-Format Wired and Wireless Signals over Large-Core Plastic Fibers for In-home Network", in *J. Light. Technol.* (to be published).

2. **F. Forni**, Y. Shi, H.P.A. van den Boom, E. Tangdiongga, A.M.J. Koonen, "Multiband LTE-A and 4-PAM signals over large-core plastic fibers for in-home networks", in *IEEE PTL*, vol. 28, no. 20, pp. 2281-2284, Oct. 2016.

3. **F. Forni**, Y. Shi, H.P.A. van den Boom, E. Tangdiongga, A.M.J. Koonen, "LTE-A compliant multi-band radio and gigabit/s baseband transmission over 50m of 1mm core diameter GI-POF for in-home networks", in *Electronics Letters*, vol. 52, no. 9, pp. 738-740, Apr. 2016.

Peer-reviewed conferences:

1. **F. Forni**, N.C. Tran, H.P.A. van den Boom, E. Tangdiongga, A.M.J. Koonen, "Simultaneous Multiband WSN, WLAN, LTE-A, and Gb/s 4-PAM Signals Transmission over 50 m 1 mm Core Diameter POF for Home Area Network", in *Optical Fiber Communication Conference*, San Diego, CA, 2018, paper Th2A.57.

2. **F. Forni**, Y. Shi, H.P.A. van den Boom, E. Tangdiongga, A.M.J. Koonen, "WiFi, Multiband Clipped LTE-A and Gbps 4-PAM Simultaneous Transmission over 50m Thick-core POF and Wireless Link for Home Area Networks", in *43rd European Conference on Optical Communication*, Gothenburg, Sweden, 2017, paper Th.2.B.5.

3. **F. Forni**, Y. Shi, H.P.A. van den Boom, E. Tangdiongga, A.M.J. Koonen, "WLAN and Multiband LTE-A Simultaneous Transmission over 50 m Thick-core GI-POF for In-home Distributed Antenna Systems", in *26th International Conference on Plastic Optical Fibres*, Aveiro, Portugal, 2017.

4. **F. Forni**, Y. Shi, H.P.A. van den Boom, E. Tangdiongga, A.M.J. Koonen, "Multiband LTE-A, WiFi ac, and 4-PAM Baseband Simultaneous Transmission over 50m Thick-core POF for In-home Network", in *19th International Conference on Transparent Optical Networks*, Girona, Spain, 2017.

5. **F. Forni**, Y. Shi, H.P.A. van den Boom, E. Tangdiongga, A.M.J. Koonen, "SINR-based equalization for multiband LTE-A and Gbps 4-PAM transmission over 50m thick-core POF and wireless link", in *Optical Fiber Communication Conference*, Los Angeles, CA, 2017, paper W2A.35.

6. **F. Forni**, Y. Shi, H.P.A. van den Boom, E. Tangdiongga, A.M.J. Koonen, "LTE-A multiband and ethernet over large-core diameter GI-POF for wired and wireless in-home networks", in *42nd European Conference on Optical Communication*, Dsseldorf, Germany, 2016, pp. 1253-1255.

7. **F. Forni**, Y. Shi, H.P.A. van den Boom, E. Tangdiongga, A.M.J. Koonen, "Experimental comparison of simultaneous transmission of LTE-A multiband and gigabit/s 4-PAM signals up to 50 m of large-core graded-index POF", in *18th International Conference on Transparent Optical Networks*, Trento, Italy, 2016, doi: 10.1109/ICTON.2016.7550692.

8. **F. Forni**, Y. Shi, H.P.A. van den Boom, E. Tangdiongga, A.M.J. Koonen, "Multiband 4G and gigabit/s baseband transmission over large-core GI and SI POF for In-Home Networks", in *25th International Conference on Plastic Optical Fibers*, Birmingham, United Kingdom, 2016.

9. **F. Forni**, H.P.A. van den Boom, Y. Shi, E. Tangdiongga, A.M.J. Koonen, "Full-service home area networks using plastic optical fibers", in *24th International Conference on Plastic Optical Fibers*, Nuremberg, Germany, 2015, pp. 223-226.

10. Y. Shi, **F. Forni**, A. Dieteren, G.N. van den Hoven, "Plastic optical fibre based in-home optical networks", in *24th International Conference on Plastic Optical Fibers*, Nuremberg, Germany, 2015, pp. 223-226.

Regional conferences:

1. **F. Forni**, Y. Shi, H.P.A. van den Boom, E. Tangdiongga, A.M.J. Koonen, "Long term evolution-advanced multiband wired and wireless transmission over thick-core plastic optical fiber for short distance communications", in *21st Annual Symposium of the IEEE Photonics Society Benelux Chapter*, Gent, Belgium, 2016, pp. 147-150.

2. **F. Forni**, H.P.A. van den Boom, Y. Shi, E. Tangdiongga, A.M.J. Koonen, "Suitability of thick-core plastic optical fibers for long-term evolution multiband transmission", in *20th Annual Symposium of the IEEE Photonics Society Benelux Chapter*, Brussels, Belgium, 2015, pp. 257-260.

3. **F. Forni**, Y. Shi, H.P.A. van den Boom, E. Tangdiongga, A.M.J. Koonen, "Suitability of thick-core plastic optical fibers to broadband in-home communication", in *19th Annual Symposium of the IEEE Photonics Benelux Chapter*, Enschede, The Netherlands, 2014.

Acknowledgments

I would like to acknowledge all the people that in different ways supported me during my PhD.
I am particularly grateful to my promoter prof. Ton Koonen for offering me the opportunity to start this PhD project in July 2014, for his inspiring guidance and valuable support. Many thanks also to my co-promoter dr. Eduward Tangdiongga for his supervision for my work. I appreciate his dedication in giving me the feedback at all times. Next, I would like to thank dr. Yan Shi for her daily guidance during the project, her suggestions have helped me to fit in the PhD position, to think bigger, and to see the big picture of each challenge I have been facing. I also would like to acknowledge dr. Karl Tran for taking over as supervisor in the last year. I am also grateful to all the members of my PhD committee for reviewing, commenting, and approving this work. I appreciate your time and kind considerations.
Next, I would like to thank Genexis B.V. for actively contributing and investing in the project, in particular dr. Gerlas van den Hoven, Ben Eman, and Maarten Egmond for the fruitful discussions and meetings. I would like to acknowledge TNO, in particular Teun van der Veen and Wieger Ijntema for the productive collaboration. The same goes also for the other companies involved in the project.
Furthermore, I would like to express my gratitude to dr. Giovanni Tartarini for giving the opportunity to perform the master thesis project at ECO group, which set me on the path to pursuing the doctoral title.
Many thanks to all ECO (ex-) colleagues, my dear office, and lunch mates for the (non-) technical conversations but also for funny moments, which made these four years a very enjoyable experience. Especially, I am grateful to Henrie van den Boom for the invaluable discussions on POF technology and countless suggestions.
I would like to thank my friends wherever they are that directly and indirectly

helped me through these years.
Finally, I would like to dedicate this thesis to my beloved parents, brother, and family that have been loving, spurring, and encouraging me throughout years and to my dear Laura for the faithful support and encouragement.

Curriculum Vitae

Federico Forni was born in Bologna, Italy, in 1989. He received the bachelor degree in electronic and telecommunication engineering from the Alma Mater Studiorum, Bologna, Italy, in 2011. He performed his master thesis project on automated optical test of photonic integrated chips at the COBRA research institute (later renamed IPI research institute) at Eindhoven University of Technology, Eindhoven, The Netherlands, in 2013. He returned to Bologna and received the master degree (cum laude) in telecommunication engineering from the Alma Mater Studiorum, in 2014.
The same year, he joined again IPI research institute working toward the Ph.D. degree at the Electro-Optical Communication group of the Eindhoven University of Technology. His work is part of the NWO-TTW Flexible Broadband Communication project. His research focuses on optical access networks, home area networks, plastic optical fibers, radio-over-fiber techniques, and 5G radio access technology. He also served as a reviewer for IEEE/OSA Journal of Lightwave Technology, IEEE International Conference on Communications, IEEE Photonics Technology Letters, IEEE Communications Magazine, and Photonic Network Communications.

This work is part of the research programme NWO-TTW Perspectief MEMPHIS II (Merging Electronics and Micro and nano-Photonics in Integrated Systems) with project number 13530 (Flexible Broadband Communication), which is (partly) financed by the Netherlands Organisation for Scientific Research (NWO).